Chiral Symmetry Breaking in the Fractional Quantum Hall Effect in Graphene

by

Sujit Narayanan

M.Sc., Indian Insitute of Technology, Madras, 2015
B.Sc., Delhi University, 2013

Thesis Submitted in Partial Fulfillment of the
Requirements for the Degree of
Doctor of Philosophy

in the
Department of Physics
Faculty of Science

© Sujit Narayanan 2023
SIMON FRASER UNIVERSITY
Summer 2023

Copyright in this work is held by the author. Please ensure that any reproduction or re-use is done in accordance with the relevant national copyright legislation.

Declaration of Committee

Name: **Sujit Narayanan**

Degree: **Doctor of Philosophy**

Thesis title: **Chiral Symmetry Breaking in the Fractional Quantum Hall Effect in Graphene**

Committee:

Chair: Eldon Emberley
Professor, Physics

Malcolm P. Kennett
Supervisor
Professor, Physics

Igor Herbut
Committee Member
Professor, Physics

Levon Pogosian
Committee Member
Professor, Physics

David Broun
Examiner
Associate Professor, Physics

Claudio Chamon
External Examiner
Professor
Physics, Material Science and Engineering
Boston University

Abstract

Quantum Hall states for non-interacting electrons on graphene's honeycomb lattice are predicted to occur for filling fractions $\nu = \pm(4n+2)$, for integer n. Integer and fractional quantum Hall states in graphene are observed in the zeroth Landau level with $-2 < \nu < 2$ and arise from electron-electron interactions. It is generally agreed that there is symmetry breaking in these states, and for the integer quantum Hall state at $\nu = 0$ there has been considerable debate as to whether this arises from quantum Hall ferromagnetism or chiral symmetry breaking (CSB) via magnetic catalysis. There has been relatively little exploration of the orders associated with fractional quantum Hall states in graphene with $0 < |\nu| < 1$. In this thesis we study the fractional quantum Hall effect in graphene in the presence of CSB orders; in particular charge density wave order (C), easy-axis Neél anti-ferromagnetic order (N) and ferromagnetic order (F).

A feature of incompressible fractional quantum Hall states in e.g. GaAs is that they usually have odd denominators while even denominator states such as $\nu = 1/2$ are compressible. Even denominator fractional quantum Hall states (EDFQH) were recently observed in graphene in a small range of magnetic fields at $\nu = \pm 1/2$ and $\pm 1/4$. The existence of these states is a consequence of degeneracies in the electronic spectrum of graphene that lead to a multicomponent fractional quantum Hall effect. We use a Chern-Simons description of multicomponent fractional quantum Hall states in graphene to investigate the properties of these states and suggest variational wavefunctions that may describe them. We find that the experimentally observed even denominator fractions and standard odd fractions (such as $\nu = 1/3$, $2/5$, etc.) can be accommodated within the same flux attachment scheme and argue that they may arise from sublattice or chiral symmetry breaking orders (such as charge-density-wave and antiferromagnetism) of composite Dirac fermions, a phenomenon unifying integer and fractional quantum Hall physics for relativistic fermions in the zeroth Landau level.

With the aim of finding ways to discriminate between different classes of symmetry breaking we study the collective excitations of fractional quantum Hall states in graphene. We focus on states which allow for chiral symmetry breaking orders. We investigate numerically how the collective excitation spectra depend on filling and the flux attachment scheme for two classes of variational states, the Töke-Jain sequence and the Modak-Mandal-Sengupta sequence. We find qualitative similarities between our results and previous work. We propose a hierarchy of stability of states with different flux attachment schemes. We focus on several different $\nu = 1/3$, $1/2$ and $2/5$ states and compare with their observed order of stability in experiments. We find that the stability is largely dominated by the flux attachment and that order parameters play a more minor role. We comment on limitations of our approach.

Keywords: graphene; fractional quantum Hall effect ; chiral symmetry breaking; even denominator states; collective excitations

Dedication

To Amma, Acha, Pappu, Priya and Advik

Acknowledgements

There are a number of people I would like to thank who have contributed directly or indirectly to this thesis. First of all I am grateful to have Malcolm as my supervisor. His way of accommodating the working style of his students rather than imposing his own has definitely changed my outlook. With me he has been patient in answering my incessant questions and his words of encouragement instilled in me hope, on several occasions, when things seemed bleak and hopeless. I wish to express my gratitude to Igor for being on my committee, for his courses which I have thoroughly enjoyed discussing inside and outside the classroom, for all the discussions we have had outside of physics and for his words of encouragement and support. I appreciate George for being on my committee in the beginning and providing helpful comments. I am grateful to Levon for being on my committee and for his courses both as a student and as a TA and for his calm and composed demeanor.

Within the physics department I have been lucky to have had friends and colleagues who have enriched my experience. Settling in Vancouver would not have been as easy as it was if it were not for Lavisha, Matthew and Cristina for which I will be forever grateful. Kola, Laleh, Farnaz, Aria, Alex Fang and Meldon made me feel at home in Vancouver when I was new here and I thank them. I would also like to thank Subrata, Leya, Tushar, Koushik, Prithviraj, Jibin, Elham, Sreeparna and the Indian group for the food and discussions. I want to thank Florian, Jeonghun, Obinna, Hamid, Ali Nezhad and Mehdi for discussions about physics amongst other things and Joseph for all his help with numerical stuff. I am grateful to Dave Broun and Jeff Sonier for their courses. I am grateful to Rose, Ayako, Stephen, Vinisha and Ben for their help with everything. Ulas has been a friend and a movie companion since almost the first day of school and continues to be so. I am thankful to Shayan and Ali for their friendship and always being open to talk about anything without any judgement. I thank Shayan for recommending books and Ali for always being able to point out the issue when I was stuck on my project. I am thankful to Avinash for the discussions we have had and for his friendship.

Outside the department a number of people have had a significant influence on me and helped broaden my worldview. I want to thank the people I have met through TSSU and Contract Workers Justice. Especially I want to thank Derek, Abhi, Amal, Vince, Ben, Katie, Sabrina, Lillian, Kayla and comrade Catherine, my newfound movie buddy. Nick for his chats about organizing, Ed for being cool and Jade who has been a close friend and mentor who has taught me a lot about organizing, education and kindness among other things for which I am extremely grateful.

I am grateful to Kulvinder-ji for her love and kindness and for taking time out of her hectic life to cook for me. I am thankful to Taslin-ji, Ranjit-ji, Surinder-ji, Kulbir-ji, Mohinder-ji, Amarjit-ji and all the other workers I met through contract workers justice for their their trust and their love. I am grateful Rajarshi decided to move to Vancouver and for teaching and helping me so much with the numerical calculations, for forcing me to travel in BC and discover places which I would not have otherwise and to Richa and Jacob for all the food they cooked for me. I thank Raghav, Aara, Janice and Lucy for their kindness and for making life in Malibu Drive an enjoyable experience.

Outside of Vancouver I want to thank Aniket, Niles and Madhu for their calls and texts. I also want to thanks Sooraj and Pradhan for their long friendship and many calls and wonderful conversations reminiscing about the past. I am thankful to Rinu for getting married in France and giving me a reason to travel and to Lipsa for letting me stay with her and her friendship for the last twelve years. I want to thank Anjishnu for checking up on me every weekend and for his friendship. I am grateful to Shifa for being in touch with me constantly, the many phone calls and for being so easy to talk to. Shravya has always been someone I admired and looked up to and I am grateful for her friendship and for shaping the way I think about the world.

Lastly I want to thank my family whose support was foundational in everything I have done. I thank Priya for her love and kindness, Acha for showing me there is more to a person than meets the eye, Amma for her love and for being so witty and my brother for being a mentor, for always having supported me in every way possible and for inculcating in me a curiosity for the world around me.

Table of Contents

List of Tables

List of Figures

Quotation

The Wheel of Time turns, and Ages come and pass, leaving memories that become legend. Legend fades to myth, and even myth is long forgotten when the Age that gave it birth comes again. In one Age, called the Third Age by some, an Age yet to come, an Age long past, a wind rose in the $\cdots$[1]*. The wind was not the beginning. There are neither beginnings nor endings to the turning of the Wheel of Time. But it was a beginning*. -Robert Jordan, Wheel of Time

[1]Every book in the Wheel of Time series begins with this paragraph. The only difference is the location of where the wind rises, represented here by $\cdots$.

Chapter 1

Introduction

Carbon's ability to catenate, i.e. form chains with other atoms, makes it the essential ingredient in forming millions of organic compounds and hence for life itself. Physical properties may vary widely depending on the dimensionality of the carbon system. Graphene is a two dimensional allotrope of carbon. In graphene the carbon atoms are arranged in a honeycomb structure made out of hexagons, Fig. 1.1. Some other higher (or lower) dimensional allotropes of carbon can be constructed out of graphene. Graphite is a three-dimensional (3D) allotrope of carbon, Fig. 1.1, that is a stack of graphene layers held together by weak van der Waals forces and is well known for its use as pencil lead. Carbon nanotubes can be constructed out of graphene by folding a graphene strip in a particular direction and reconnecting the carbon atoms along the edges that meet. Hence carbon nanotubes can be thought of as one-dimensional systems [2, 3]. Fullerenes can be constructed out of graphene wrapped into a sphere and by introducing positive curvature defects via pentagons [4].

Novoselov *et al.* in 2004 [5] were able to isolate and study graphene, a one-atom thick layer of carbon atoms. The graphene films were prepared by repeated peeling of a graphite sample using scotch tape and were spotted by their optical effects on a SiO_2 substrate [5, 6]. For their work Konstantin Novoselov and Andre Geim were awarded the Nobel prize in Physics in 2010.

In graphene the carbon atoms are sp^2 hybridized which leads to a σ bond (overlap of orbitals in an end to end fashion) between the carbon atoms with a separation of 1.42 Å. This gives rise to a trigonal planar structure for the carbon atoms in graphene. The remaining p orbital is perpendicular to the plane of the carbon atoms and has an extra valence electron. The out of plane p orbital can bond covalently with another p orbital to give rise to a π-bond. Since there is only one electron in the p orbital the π bands are only half filled [7]. This is illustrated in Fig 1.2.

The unique and unusual properties of graphene arise from its two dimensionality and hexagonal lattice. In reciprocal space the lattice is also hexagonal and the valence

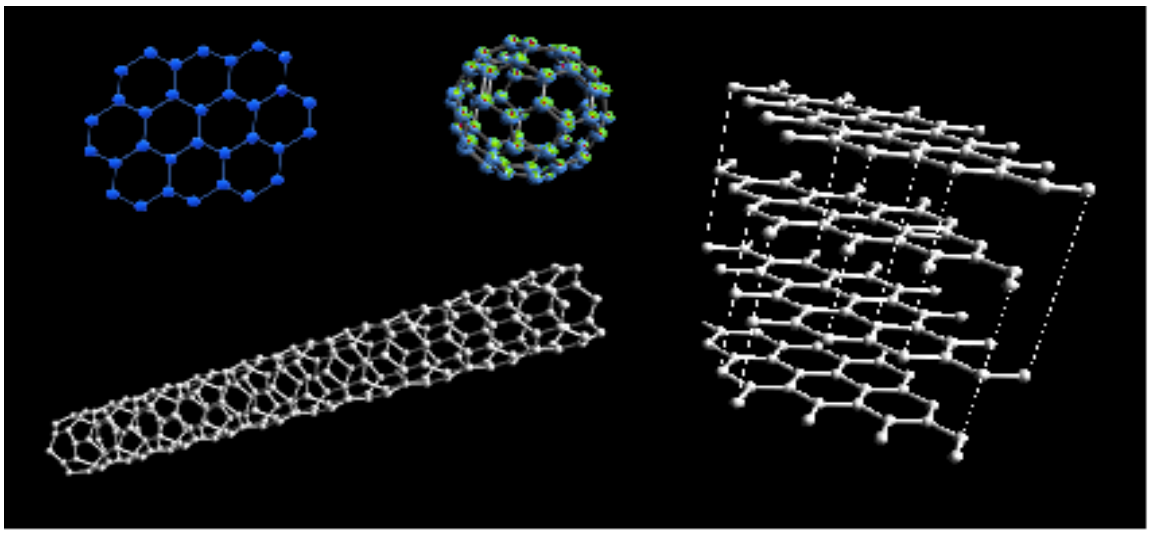

Figure 1.1: Graphene (top-left) is a two dimensional layer of carbon atoms comprised of hexagons. Graphite (right) is composed of layers of graphene held together by weak van der Waals forces. Carbon nanotubes (bottom) can be thought of as rolled up graphene strips. Fullerene, C_{60}, (top-center) can be made from graphene by introducing pentagons on a hexagonal-lattice. Adapted from [1].

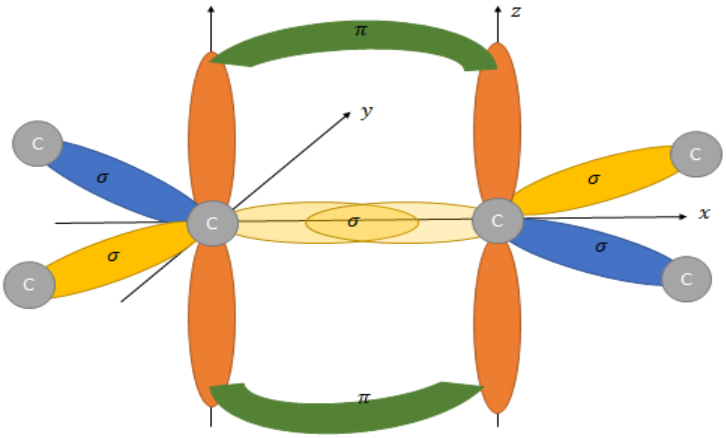

Figure 1.2: sp^2 hybridization of carbon atoms in graphene showing the σ and π bonds.

and conduction band touch each other at the corners of the Brillouin zone. These special points are known as Dirac points. At half-filling, when there is one electron per carbon atom on the lattice in the π band, the valence band is completely filled while the conduction band is completely empty. The chemical potential thus intercepts at these Dirac points. The electronic dispersion at the Dirac points is linear at low energies. This indicates that the low energy excitations in graphene behave as massless Dirac fermions. As a consequence, graphene mimics quantum electrodynamics (QED) for Dirac fermions albeit with role of the speed of light, c, played by the Fermi velocity, $v_F \sim 10^6$m/s which is about 300 times smaller than the speed of light in vacuum [1, 8, 9].

The remarkable properties of graphene have led to its usefulness in a number of applications. High electron mobility in graphene makes it ideal for semiconductor device applications that require fast response times [10]. High conductivity and high optical transparency combined has led to proposals for transparent conductive layer for photonic devices [11]. Other uses of graphene and graphene based compounds are in biomedical engineering in the form of graphene oxide in drug/gene delivery and tissue engineering [12] and in electronics in the form of graphene based metal-air batteries [13], graphene woven fabrics used as sensors in wearable technology [14], supercapacitors [15], the formulation and deposition of conductive cotton fabric [16], in printing technology in the form of graphene functional inks [17] and as nanoscale coating for aerospace applications [18].

Two sheets of graphene stacked with a relative twist in their orientation generated much recent excitement due to the discovery of interaction-induced insulating states and superconductivity in these twisted bilayer graphene (TBG) systems at certain specific values of the twist angle known as magic angles [19–25]. Low-temperature electrical transport measurements on high-quality tear-and-stack magic angle twisted bilayer graphene (MATBG) revealed interaction-induced insulating states with nearby superconducting dome [19, 21]. The similarity between the phase diagram and phenomenology of this relatively simple system and that of the high-temperature superconductors (HTS) has led to exploration of the consequences and the possibility of answering long standing problems in HTS [26–37].

A hallmark of Dirac fermion behaviour in graphene is the integer quantum Hall effect. The quantum Hall effect refers to the phenomenon when a two dimensional gas of electron is subjected to a high magnetic field, at low temperatures and the Hall conductivity/Hall resistance (Eq. 1.2) becomes quantized and develops a series of plateaux and simultaneously the transverse/diagonal conductivity/resistance goes to zero (Fig. 1.3). Experiments performed by Wakabayashi and Kawaji [38] with Si-MOSFET (Metal-Oxide Semiconductor Field Effect Transistor) samples employing a Corbino disk geometry observed the diagonal conductivity (Eq. 1.2) approaching very

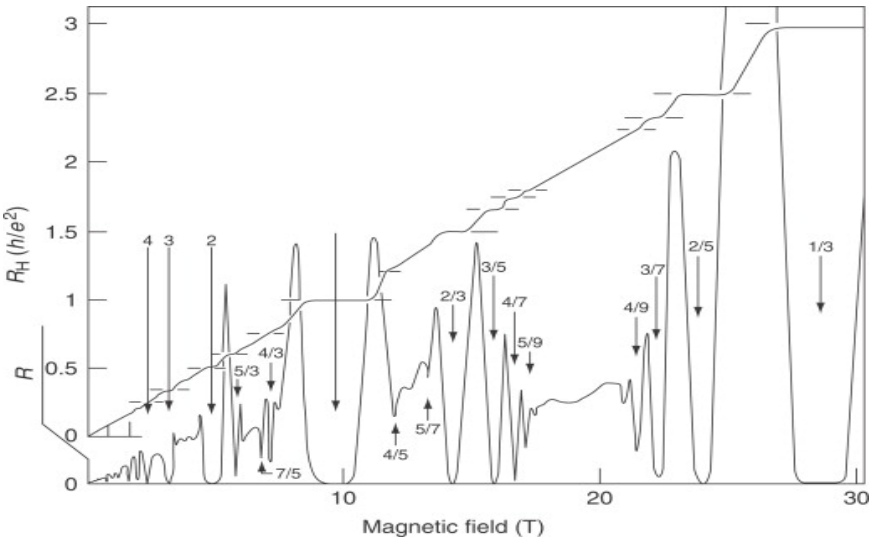

Figure 1.3: The Hall resistance (R_H) develops a series of plateaus concurrent with a minimum in longitudnal resistance (R). Reproduced with permission from Ref. [42]

small values at high magnetic fields and at low temperature similar to predictions by Ando *et. al.* [39] but it was not until the experiments perfomred by von Klitzing using silicon-based MOSFET samples developed by Dorda and Pepper that the Hall resistance was found to be exactly quantized [40] leading to the discovery of the integer quantum Hall effect (IQHE). von Klitzing won the Nobel prize in Physics in 1985 for his discovery. For a two dimensional electron gas placed under a strong magnetic field, at low temperatures, the conductivity and resistivity tensor on the Hall plateaux have the form:

$$\sigma = \begin{bmatrix} 0 & -\frac{\nu e^2}{h} \\ \frac{\nu e^2}{h} & 0 \end{bmatrix}; \quad \rho = \begin{bmatrix} 0 & \frac{h}{\nu e^2} \\ -\frac{h}{\nu e^2} & 0 \end{bmatrix}, \tag{1.1}$$

where h is the Planck's constant and e is the charge of the electron and ν is an integer known as the filling fraction and is related to the density of electrons and the magnetic field. In terms of fundamental constants

$$\sigma_{xy} = \sigma_H = \frac{\nu e^2}{h}; \quad \sigma_{xx} = 0; \quad \rho_{xx} = 0; \quad \rho_{xy} = \rho_H = \frac{h}{\nu e^2}. \tag{1.2}$$

The quantization condition in Eq. 1.2 is exact up to one part in 10^9 and is indifferent to impurities or geometric details of the two-dimensional system [41].

Soon after the discovery of the IQHE, Tsui *et al.* [43] observed the fractional quantum Hall effect (FQHE) in GaAs-AlGaAs heterostructures of high quality (i.e. with low disorder). They discovered a plateau in the Hall resistivity at $\rho_{xy} = \frac{3h}{e^2}$ and a vanishing longitudinal resistivity ρ_{xx} for a partially filled Landau level ($\nu = 1/3$). Subsequently

other fractional quantum Hall (FQH) states have been discovered such as $\nu = 2/3$ [44–46], $\nu = 4/3$ [44, 47] and $\nu = 5/3$ [47]. The temperature dependence of the FQH states was found to have an activated behaviour in the diagonal resistivity (ρ_{xx}) and Hall resistivity (ρ_{xy}) present over some temperature ranges, corresponding to a gap in the excitation spectrum [46]. The FQHE (Fig 1.3) does not fit into the non-interacting electron picture. The theoretical breakthrough on the problem of FQHE came from Laughlin, who wrote down a trial wavefunction for the FQH states at $\nu = 1/m$, where m is an odd integer [48]. Laughlin's theory was able to show that in a FQH state the system behaves like an incompressible fluid [48] and hence has a gap in the excitation spectrum as observed in experiments. Laughlin, Tsui and Störmer were awarded the Nobel prize in Physics in 1998 for their work.

In the presence of strong magnetic fields, at low temperatures, the IQHE is also observed in graphene. The IQHE is qualitatively different from that observed in semiconductor heterostructures because the behaviour of Dirac fermions in a magnetic field is different from that of non-relativistic fermions [49–52]. The fractional quantum Hall effect has also been observed in graphene [53–59] and is the primary subject of this thesis.

1.1 Outline

The first part of the thesis is a review of experiment and theory for quantum Hall effects, integer and fractional in semiconductor heterostructures and in graphene. In Chapter 2 we give an overview of the quantum Hall effect in semiconductor heterostructures. After a brief overview of the experiments we describe the quantum mechanical version of the IQHE theory in the Landau gauge. The role of disorder and edge modes are also touched upon. We then describe the FQHE along with Laughlin's theory of FQHE, the quasiparticles in the FQHE. We then describe Haldane's pseudopotential method for higher Landau levels. This naturally leads to the hierarchical schemes of which the composite fermion (CF) approach to the problem of FQHE is an example. The Chern-Simons (CS) theory is then introduced as a field theory that describes the FQHE. In Chapter 3 we begin with a description of the bandstructure of graphene and the symmetries of the low energy theory of electrons in graphene and then move onto the nature of the IQHE in graphene and its differences from the IQHE in traditional 2DEGs. We focus mainly on the interaction-induced IQHE in the lowest Landau level in graphene. In particular we focus on how electron-electron interactions in graphene lead to the breaking of chiral symmetry through the mechanism of magnetic catalysis and we briefly touch upon the FQHE in graphene, noting its similarities and differences from the FQHE in traditional 2DEGs.

The second part of the thesis is based on extending the ideas described in the first part and applying it to explain experimental observations of FQHE in graphene. In Chapter 4 we begin with a brief introduction to the nature of even-denominator fractional quantum Hall (EDFQH) states that have been studied, both theoretically and experimentally, in semiconductor heterostructures. On the theory side we briefly touch upon the theory of composite Dirac fermions (CDFs) and the Halperin-Lee-Read (HLR) theory of EDFQH states. Following a brief overview of the experimental observation of EDFQH states in graphene we describe an extension of the CF picture (multi-component flux attachment scheme) to include the four-fold symmetry in graphene's Landau levels. We employ a multi-component flux attachment scheme to explain the experimental observation of EDFQH states in graphene in the presence of chiral symmetry breaking (CSB) orders. We provide a list of possible variational wavefunctions that could be ground states of the system at these EDFQH states along with the CSB orders that would be present in the system for these ground states. Using this method we are unable to distinguish between the states with different order parameters. Chapter 4 is based on the publication S. Narayanan, B. Roy and M. P. Kennett, Phys. Rev. B **98**, 235411 (2018).

The final part of the thesis aims to attempt to answer the question raised in the previous chapter of how to distinguish CSB orders in FQH states in graphene and eventually lead to a theory that leads to experimentally verifiable results. To this end we develop a field theory of composite fermions in graphene and employing the Schwinger Keldysh formalism we write down an effective action in Chapter 5. Using the effective action we are able to calculate the electromagnetic response of the system. We study the collective excitations of the system in the presence of CSB orders combined with the flux attachment scheme described in Chapter 4. We observe a variation in the spectrum of collective excitations for different flux attachment and compare the excitation spectra of different FQH states. Chapter 5. is based on the publication S. Narayanan and M. P. Kennett, Phys. Rev. B **106**, 165119 (2022).

Chapter 2

The Quantum Hall Effect

When two dimensional electron systems are placed in a strong magnetic field, at low temperatures, quantum Hall states are observed [40, 43]. The signature of the quantum Hall effect (QHE) is the appearance of plateaux in the Hall conductivity/resistivity (Fig. 1.3). The quantization of the Hall resistance is extremely accurate and is insensitive to geometry of the sample or the amount of disorder present in the sample. The accuracy of the quantization of the Hall resistance has been used to determine the value of the fine structure constant α [40]. The fine structure constant in terms of the Hall resistance R_H is

$$\alpha = \frac{1}{2}\mu_0 c \frac{e^2}{h} = \frac{1}{2}\mu_0 c (R_K)^{-1}, \tag{2.1}$$

where μ_0 is the permeability of vacuum, c is the speed of light and $R_K = h/e^2$ is defined as the *von Klitzing* constant with $R_K = 25812.807 \pm 0.05\Omega$.

The high density electron systems which are required to observe the QHE are present in Si-MOSFETs and semiconductor heterostructures with almost perfect lattice matched semiconductor-semiconductor interfaces like GaAs/$Al_xGa_{1-x}As$ $(0 < x \leq 1)$ heterostructures. Fig 2.1 shows the energy level diagram of a n-channel Si-MOSFET device. It consists of a semiconductor p-Si which shares a planar interface with a thin layer of SiO_2 (an insulator). On the other end is a metal gate electrode. A gate voltage (V_G) is applied between the gate and the Si/SiO_2 interface which results in the energy bands being bent as shown in Fig 2.1. For strong electric fields the conduction band falls below the Fermi level and electrons can accumulate inside a small pocket in the form of a two-dimensional well [60]. The width of the well is small ($\sim$ 50 Å) which allows the electrons to move freely in the plane of the interface but restricts their motion perpendicular to the interface and hence motion along the perpendicular is quantized. The system is referred to as an inversion layer owing to the charge carriers being electrons while the semiconductor is p-type [41].

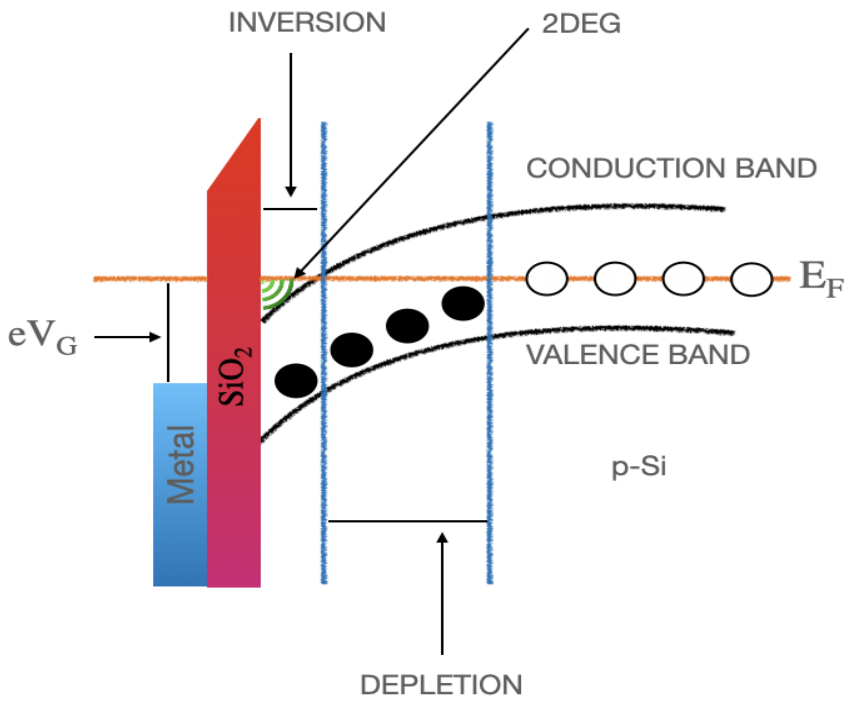

Figure 2.1: Energy level diagram of a n-channel Si-MOSFET.

The gallium arsenide system is similar to the Si-MOSFET system. GaAs is a weak *p*-type semiconductor whereas AlAs, which has a wider energy gap, acts as an insulator. The two materials have nearly the same lattice and dielectric constants. The band gap of the AlGaAs alloy is much wider than that of the GaAs and it increases with the aluminium concentration. Near the interface the carriers in the doped alloy transfer through the interface into the low lying conduction bands of GaAs. The electric field due to the charge transfer gives rise to bending of the bands at the interface as shown in Fig. 2.2. As with the Si-MOSFET a well is formed on the GaAs side, which owing to its width ($\sim$ 100 Å) acts as a two-dimensional plane for the electrons to move in.

After von Klitzing's initial experiment [40] integral quantization of Hall resistance was demonstrated in a variety of systems such as GaAs-heterostructures [61–63], GaAs/InP heterostructures [64–66], HgTe/CdTe heterostructures [67], InAs/GaSb heterostructures [68] and in Si/Ge systems [69].

2.0.1 Classical Theory of Electrons in a Magnetic Field

Consider the motion of an electron restricted to moving in the *xy*-plane with velocity $\mathbf{v} = v_x\hat{\mathbf{x}} + v_y\hat{\mathbf{y}}$ and subjected to a magnetic field, $\mathbf{B} = B\hat{\mathbf{z}}$. The classical equation of motion

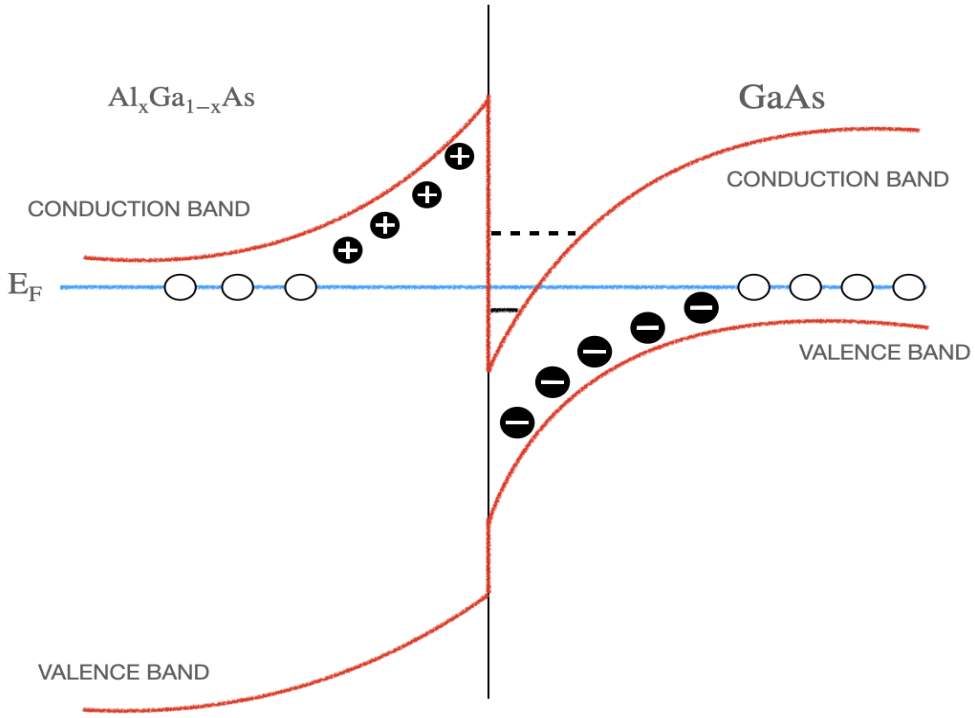

Figure 2.2: Energy level diagram of a GaAs-AlGaAs heterostructure device.

is

$$m_e \frac{d\mathbf{v}}{dt} = -e\mathbf{v} \times \mathbf{B}. \tag{2.2}$$

The force on the electron is always perpendicular to its velocity and hence the electron undergoes a uniform circular motion with an angular frequency, $\omega_c = eB/m_e$, known as the cyclotron frequency.

If we now add an electric field, $\mathbf{E}$, and a linear (in velocity) friction term which mimics the effect of electrons colliding with impurities, then the resulting equation of motion becomes

$$m_e \frac{d\mathbf{v}}{dt} = -e\mathbf{v} \times \mathbf{B} - \frac{m_e \mathbf{v}}{\tau} - e\mathbf{E}, \tag{2.3}$$

where τ is the average time between collisions also known as the scattering time.

In equilibrium ($d\mathbf{v}/dt = 0$) the equation of motion takes the form

$$\frac{e\tau}{m_e}\mathbf{v} \times \mathbf{B} + \mathbf{v} = -\frac{e\tau}{m_e}\mathbf{E}. \tag{2.4}$$

In terms of the current density ($\mathbf{J} = -n_e e\mathbf{v}$, where n_e is the density of electrons) the equation of motion takes the form

$$\begin{pmatrix} 1 & \omega_c\tau \\ -\omega_c\tau & 1 \end{pmatrix}\mathbf{J} = \frac{e^2 n_e \tau}{m_e}\mathbf{E}. \tag{2.5}$$

The current density is related to the applied electric field through Ohm's law, $\mathbf{J} = \sigma\mathbf{E}$, where σ is the conductivity tensor. From Eq. 2.5 the conductivity tensor has the form

$$\sigma = \begin{pmatrix} \sigma_{xx} & \sigma_{xy} \\ -\sigma_{xy} & \sigma_{xx} \end{pmatrix} = \frac{n_e e^2 \tau}{m_e}\frac{1}{1+\omega_c^2\tau^2}\begin{pmatrix} 1 & -\omega_c\tau \\ \omega_c\tau & 1 \end{pmatrix}. \tag{2.6}$$

The resistivity tensor is defined as the inverse of the conductivity tensor (Eq. 2.6) and has the form

$$\rho = \sigma^{-1} = \begin{pmatrix} \rho_{xx} & \rho_{xy} \\ -\rho_{xy} & \rho_{xx} \end{pmatrix} = \begin{pmatrix} m_e/n_e e^2\tau & B/n_e e \\ -B/n_e e & m_e/n_e e^2\tau \end{pmatrix}. \tag{2.7}$$

The diagonal components, $\rho_{xx} = \rho_{yy} = m_e/n_e e^2\tau$, correspond to the longitudinal resistance and the off-diagonal component, $\rho_{xy} = B/n_e e$, corresponds to the Hall resistance. The Hall resistance is independent of the details of scattering (encoded by the scattering time τ) and only depends on the applied magnetic field, B, electron density, n_e, and the sign of the charge carriers.[1]

In two dimensions resistivity and resistance have the same units and measurements of resistance in Hall experiments are actually measuring the resistivity which is an intrinsic property of the material itself. In a typical Hall experiment setup a current passes through the sample, in say the x-direction, and a magnetic field is applied perpendicualr to the plane of the sample, in the z-direction. In the presence of the magnetic field the charged particles are deflected and an electric field E_H is induced in the y-direction and in equilibrium the force due to the induced field balances the Lorentz force due to the magnetic field. Mathematically this is expressed as

$$eE_H = ev_x B. \tag{2.8}$$

The Hall coefficient is defined as the ratio of the induced electric field, E_H, to the Hall resistivity, ρ_{xy}:

$$R_H = \frac{E_H}{\rho_{xy}} = \frac{1}{n_e e}. \tag{2.9}$$

[1]Here we have assumed the charged particles are electrons with a charge, $-e$. We could have started with an arbitrary charge, q and the Hall resistance would then be $\rho_{xy} = -B/n_e q$

The Hall coefficient characterizes the material and indicates the sign of the majority charge carriers and is also a measure of their density.

2.0.2 Quantum Theory of Electrons in a magnetic field

The IQHE can be understood from a picture of non-interacting electrons. The quantum mechanical problem is that of independent two-dimensional spinless electrons in a perpendicular magnetic field. The Hamiltonian for a single electron is[2] [70]

$$H = \frac{1}{2m}(\mathbf{p} + e\mathbf{A})^2. \tag{2.10}$$

Choosing the two dimensional plane as the xy-plane the magnetic field $\mathbf{B} = B\hat{\mathbf{z}} = \nabla \times \mathbf{A}$. Define operators

$$\boldsymbol{\pi} = \mathbf{p} + e\mathbf{A} = m\dot{\mathbf{x}}, \tag{2.11}$$

with $\mathbf{x} = (x, y)$. The operators π_i $(i = x, y)$ satisfy the commutation relations

$$\left[\pi_x, \pi_y\right] = -ie\hbar B. \tag{2.12}$$

Define raising ($a^\dagger$) and lowering (a) operators

$$a = \frac{1}{\sqrt{2e\hbar B}}(\pi_x - i\pi_y); \quad a^\dagger = \frac{1}{\sqrt{2e\hbar B}}(\pi_x + i\pi_y), \tag{2.13}$$

which satisfy $[a, a^\dagger] = 1$. In terms of these operators the Hamiltonian becomes

$$H = \hbar\omega_c(a^\dagger a + 1/2), \tag{2.14}$$

where $\omega_c = eB/m$ is the cyclotron frequency (and takes the same value as in the classical case). The eigenstates, $\{|n\rangle\}$, are labelled by integers, n, and they satisfy

$$a^\dagger |n\rangle = \sqrt{n+1}\,|n+1\rangle\,; \quad a\,|n\rangle = \sqrt{n}\,|n-1\rangle\,. \tag{2.15}$$

The state $|n\rangle$ has energy

$$E_n = \hbar\omega_c(n + 1/2), \quad n \in N. \tag{2.16}$$

The energy levels are called *Landau levels* and they are equally spaced by energy $\hbar\omega_c$ which is proportional to the magnetic field B. In order to specify the eigenfunction a

[2]The magnetic field is assumed to be strong enough that we are dealing with spin polarized electrons and hence the Zeeman term can be ignored.

choice of gauge has to be made. One such choice is the Landau gauge [3]

$$\mathbf{A} = xB\hat{\mathbf{y}}. \tag{2.17}$$

The Landau gauge breaks translation symmetry in the x-direction but the physical magnetic field $\mathbf{B}$ preserves it. In the Landau gauge the Hamiltonian in Eq. 2.10 becomes

$$H = \frac{1}{2m}\left[p_x^2 + (p_y + eBx)^2\right]. \tag{2.18}$$

Due to translation invariance in the y-direction the wavefunctions are plane waves in that direction and we can use the ansatz [70]

$$\psi_k(x, y) = e^{iky} f_k(x). \tag{2.19}$$

When the Hamiltonian acts on this wavefunction, p_y gets replaced with $\hbar k$ i.e. $H\psi_k = H_k\psi_k$, where H_k is given by

$$H_k = \frac{1}{2m}p_x^2 + \frac{m\omega_c^2}{2}(x + kl_B^2)^2, \tag{2.20}$$

where l_B is the magnetic length. The magnetic length is a characteristic length scale in quantum phenomena involving magnetic fields

$$l_B = \sqrt{\frac{\hbar}{eB}}. \tag{2.21}$$

Equation 2.20 is the Hamiltonian for a harmonic oscillator centered at $x = -kl_B^2$. The energy eigenvalues are those given in Eq. 2.16. The explicit wavefunction is

$$\psi_{n,k}(x, y) = \mathcal{N} e^{iky} H_n(x + kl_B^2) e^{-(x+kl_B^2)^2/2l_B^2} \tag{2.22}$$

where $\mathcal{N}$ is a normalization constant. Here H_n is the n^{th} Hermite polynomial. The wavefunction depends on two quantum numbers, $n \in \mathbf{N}$ the Landau level index and $k \in \mathbf{R}$ the momentum.

Landau levels have a large degeneracy. The energy levels depend on the Landau level index n whereas the wavefunction depends on both n and k. Suppose we have a system of finite size in the xy-plane with side lengths L_x and L_y. In the y-direction the momentum will be quantized in units of $2\pi/L_y$. In the x-direction, for our choice of gauge, there is no manifest translational invariance. The wavefunctions in Eq. 2.22 are

[3] See Appendix A for a description of the symmetric gauge.

localised exponentially around $x = -kl_B^2$ and since $0 \leq x \leq L_x$ the allowed values of k are $-L_x/l_B^2 \leq k \leq 0$. The number of allowed states then becomes

$$N_B = \frac{L_y}{2\pi}\int_{-L_x/l_B^2}^{0} dk_x = \frac{L_x L_y}{2\pi l_B^2} = \frac{eBA}{2\pi\hbar}, \tag{2.23}$$

where A is the area of the sample. Thus each Landau level has a macroscopic degeneracy. For a fixed magnetic field we can define the fraction of Landau level filled up by electrons as the filling fraction, ν. The filling fraction, ν, is given by

$$\nu = 2\pi l_B^2 n_e, \tag{2.24}$$

where n_e is the density of electrons. When ν is an integer, k, then Landau levels $n = 0, 1, ..., k$ are all completely filled. Filling fraction, ν, can alternatively be defined in terms of the density of flux quanta, $\Phi_0 = 2\pi\hbar/e$ present in the system. The density of flux quanta present in the system is given by

$$n_\Phi = \frac{1}{A}\left(\frac{\Phi}{\Phi_0}\right) = \frac{B}{\Phi_0} = \frac{1}{2\pi l_B^2}, \tag{2.25}$$

where A is the area. From Eqs. 2.24 and 2.25 we find that

$$\nu = \frac{n_e}{n_\Phi}. \tag{2.26}$$

Thus the filling fraction is the ratio of the density of electrons to the density of the flux quantum present in the system.

At low temperatures and high magnetic field the integer quantum Hall effect (IQHE) is observed [40, 43]. The IQHE is characterized by the appearance of plateaux in the Hall conductivity/resistivity (implying the Hall conductivity/resistivity is quantized) and concomitantly the longitudinal conductivity/resistivity vanishes. These features can be seen in the plot of resistance (longitudinal and Hall resistance) versus the magnetic field in Fig. 1.3. In the limit of high magnetic field and low temperatures the dimensionless parameter, $\omega_c\tau$, becomes large and from Eqs. 2.7 and 2.24, the resistivity tensor has the form

$$\rho = \begin{pmatrix} 0 & \frac{h}{\nu e^2} \\ \frac{h}{\nu e^2} & 0 \end{pmatrix}. \tag{2.27}$$

This expression suggests that the Hall resitivity, $\rho_H = h/\nu e^2$ varies continuously with ν or alternatively the magnetic field, B. In experiments instead what is seen are broad plateaux as the magnetic field is varied.

The presence of plateaux can be explained once disorder is taken into account. Dis-

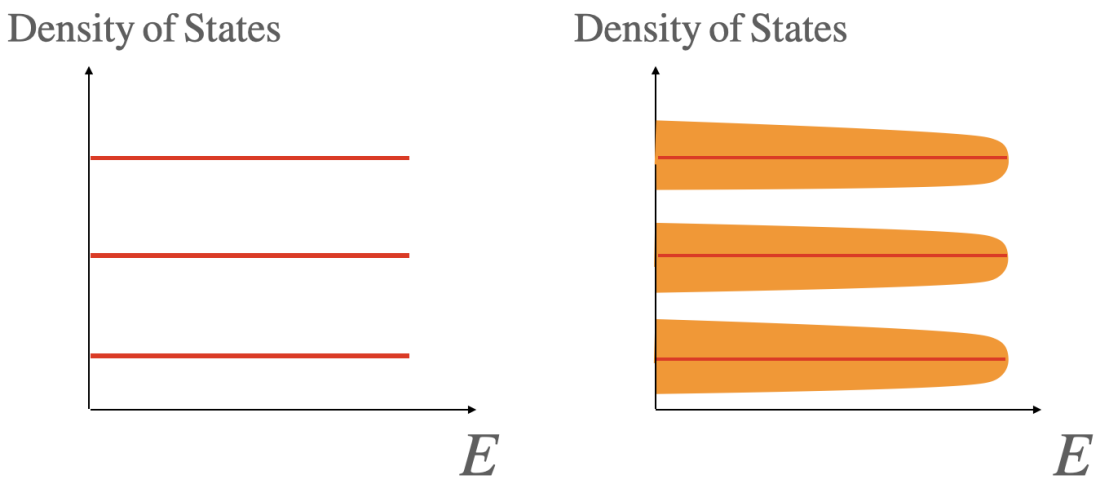

Figure 2.3: Schematic density of states without disorder (left) and in the presence of disorder (right). The localized states are represented by the orange shaded area and the extended states are represented by the sharp red lines in the presence of disorder.

order in the system lifts the degeneracy of the Landau levels. As long as the disorder strength is small compared to the energy gap between the Landau levels

$$V_{\text{dis}} \ll \hbar\omega_c, \tag{2.28}$$

the effect of the disorder is to broaden the energy spectrum as illustrated in Fig. 2.3. Disorder also turns extended states into localized states. Extended states are present at the centre of each Landau level band of the broadened spectrum while states beyond the centre are localized. It is the extended states that are responsible for conduction of electrons in the system. If all the extended states in a given Landau level are filled and the magnetic field is varied, keeping the electron density fixed, then the electrons start occupying the empty localized states but since localized states do not contribute to the conduction the conductivity remains the same even if the magnetic field is varied. This explains the observation of plateaux in the experiments.

The vanishing of the longitudinal conductivity/resistivity and non-zero Hall resisitivity together implies that there is a current flowing at the edges of the system. Figure 2.4 shows the semi-classical orbits of an electron is a two-dimensional sample of finite size. The orbits in the bulk are clockwise if the magnetic field points into the plane (out of the plane). At the edge of the sample the electrons cannot complete their orbits and instead skip along the boundary. In Fig. 2.4 this means that the only direction the electrons on the left can go is up and on the right, down. Hence the motion is one where the particles move along a one-dimensional boundary in a single direction.

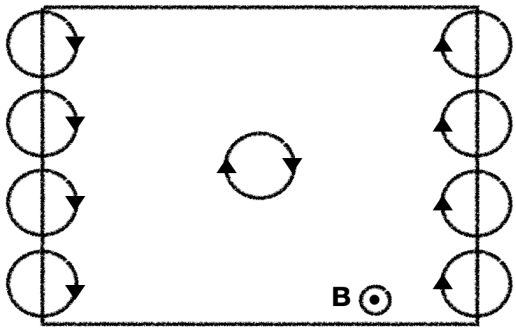

Figure 2.4: Edge Modes in a two-dimensional sample.

2.1 The Fractional Quantum Hall Effect

The discovery of IQHE by von Klitzing was soon followed by the discovery of the fractional quantum Hall effect by Tsui *et al.*[43]. The FQHE was observed in very clean (less disorder/impurities) samples and at higher magnetic fields ($B \sim 10T$) than the IQHE. The experimental signature of the FQHE is the appearance of plateaux in the Hall resistivity at rational fractions i.e., $\rho_{xy} = h/\nu e^2$ with $\nu = p/q$ where p and q are both integers. Although the experimental signatures of the IQHE and the FQHE are associated with the appearance of Hall plateaus and the vanishing of the longitudinal resistivity the physics behind each effect is quite different. The IQHE is observed when a Landau level is completely filled and hence the Fermi energy lies in the gap between the filled Landau level and the next empty one. In the case of FQHE the Fermi energy lies inside the partially filled Landau level and electrons can be added within the same Landau level implying the absence of a single particle gap [71]. The gap in the spectrum, Δ, is a consequence of Coulomb interactions between the electrons and hence is a many-body gap:

$$\Delta \simeq \frac{e^2}{\sqrt{n_d}\epsilon}, \tag{2.29}$$

where $\sqrt{n_d}$ is the average interparticle distance and ϵ is the dielectric constant of the medium. Clearly the Coulomb interaction energy should be greater than any disorder potential present in the system if the energy gap is to be robust and thus there is a hierarchy of energy scales

$$V_{dis} \ll \Delta \ll \hbar\omega_c. \tag{2.30}$$

The effect of interaction is to lift the degeneracy of the Landau levels. Since the degeneracy of the Landau levels is huge the problem of identifying the ground state of a FQH state cannot be solved using degenerate perturbation theory. The explanation of

the FQHE was provided by Laughlin [48] for which he was awarded the Nobel prize in 1998.

Laughlin's Theory

Laughlin treated the fractional quantum Hall state at $\nu = 1/m$ as an incompressible fluid and proposed a class of trial wavefunctions, in the symmetric gauge (cf. Eq. A.8), describing the FQH liquid that have the form

$$\Psi(z_1, ..., z_N) = \left(\prod_{i<j} f(z_i - z_j) \right) e^{-\frac{\sum_{i=1}^{N} |z_i|^2}{4l_B^2}}, \tag{2.31}$$

where $f(z)$ is an analytic function of the complex coordinates of the particles, $z_i = x_i + iy_i$; $i = 1, ..., N$. Fermi statistics demands that $f(z_i - z_j)$ be odd under exchange of pair of particles and that it vanishes when $z_i \to z_j$. These requirements along with requiring that Ψ be an eigenstate of the total angular momentum [4] is met by $f(z)$ having the form $f(z) \sim z^m$, where m is an odd integer. Thus the Laughlin wavefunction is

$$\Psi(z_1, ..., z_N) = \prod_{i<j} (z_i - z_j)^m \; e^{-\frac{\sum_{i=1}^{N} |z_i|^2}{4l_B^2}}. \tag{2.32}$$

The trial wavefunction proposed by Laughlin is quite remarkable. Laughlin computed [48] the overlap between the trial wavefunction, Ψ and the exact wavefunction for a small number ($N \leq 3$) of electrons interacting through pair potentials $u(r)$ of the form $u(r) \sim 1/r, -\ln(r), \exp(-r^2/2)$ and found the overlap to be almost 99%. Trugman and Kivelson [72] showed that Ψ is the exact ground-state wavefunction, for all m, for an interaction potential of the form $u(r) = u_0 \nabla^2 \delta(r)$. Haldane [73] constructed a class of Hamiltonians for which Laughlin-like wavefunctions are the exact ground state.[5] The Laughlin states have been generalized to describe filling fractions other than $\nu = 1/m$. These hierarchical constructions were considered by Halperin [74] and Haldane [73].

The Laughlin wavefunction has no variational parameters in it. The ground state is determined by values of m that minimize the energy but m is determined by the total angular momentum. It is amazing that Ψ in Eq. 2.32 works so well! Laughlin determined the optimal value of m which minimizes the energy by mapping the wavefunctions to a classical plasma in two dimensions [48]. The probability density (setting $l_B = 1$)

[4] See Eq. A.12.

[5] See Sec. 2.1.1

associated with the Laughlin wavefunction has the form

$$P(z_i) = \prod_{i<j}(z_i - z_j)^{2m} e^{\sum_{i=1}^{N}|z_i|^2/2}. \tag{2.33}$$

We can write this in the form of a Boltzmann distribution function

$$P(z_i) = e^{-\beta U(z_i)}, \tag{2.34}$$

with

$$\beta U(z_i) = -2m\sum_{i<j}\log(|z_i - z_j|) + \sum_{i=1}^{N}|z_i|^2. \tag{2.35}$$

If we further assume $\beta = 1/m$ the potential $U(z_i)$ has the form

$$U(z_i) = -2m^2\sum_{i<j}\log(|z_i - z_j|) + m\sum_{i=1}^{N}|z_i|^2. \tag{2.36}$$

The first term is the same as a Coulomb potential between two particles carrying charge $q = m$ each and restricted to two dimensions.

A constant charge density creates an electric potential of the form $-\nabla^2\phi = 2\pi\rho_0$ and the second term in the potential in Eq. 2.36 satisfies

$$-\nabla^2(|z_i|^2) = -4, \tag{2.37}$$

and hence each electron feels a background charge density

$$\rho = -\frac{1}{2\pi l_B^2}, \tag{2.38}$$

where we have put back the magnetic length to make sense of the result physically. The plasma will try to neutralise the background charge density and the density of particles carrying charge m required to do so satisfies the condition

$$nm = \rho_0 \Rightarrow n = \frac{1}{2\pi l_B^2 m}, \tag{2.39}$$

which is the density of electrons for a state at filling fraction $\nu = 1/m$. Hence we see that the Laughlin wavefunction describes the FQHE state at $\nu = 1/m$.

Quasiparticles

Charged excitations of the quantum Hall state are either quasi-holes or quasi-particles. Mathematically they can be generated by introducing an infinitely thin solenoid at some point η in the quantum Hall fluid and then passing a flux quantum through it adiabatically. For the single particle wavefunction this amounts to a change from m to $m+1$

$$(z-\eta)^m e^{-|z|^2/4} \rightarrow (z-\eta)^{m+1} e^{-|z|^2/4}. \tag{2.40}$$

For the quasi-hole the wavefunction has the form

$$\psi_{\text{hole}} = \prod_{i=1}^{N}(z_i-\eta)\prod_{j<k}(z_j-z_k)^m e^{\sum_{j=1}^{N}-|z_j|^2/4}. \tag{2.41}$$

The electronic wavefunction now vanishes at $z=\eta$ and hence a hole has been introduced into the system. Consider introducing m such holes in the system at the same position η; then the m-hole wavefunction is

$$\psi_{\text{m-hole}} = \prod_{i=1}^{N}(z_i-\eta_l)^m\prod_{j<k}(z_j-z_k)^m e^{\sum_{j=1}^{N}-|z_j|^2/4}. \tag{2.42}$$

Once again if we associate a Boltzmann distribution with the probability density of the m-hole wavefunction the potential in Eq. 2.36 is modified to

$$U(z_i) = -m^2\sum_{i<j}\log(|z_i-z_j|) - m\sum_i \log(|z_i-\eta|) + m\sum_{i=1}^{N}|z_i|^2. \tag{2.43}$$

Now, the second term in the expression looks like an impurity in the plasma with a net charge of $+1$. Given there are m holes introduced in the system the charge of each of these quasi-holes is $+1/m$. Hence quasi-holes are charged excitations of the FQH liquid which carry fractional charge.

The other type of charged exciations are quasi-particles. Quasi-particles ought to carry a charge $e^* = -1/m$ with the same sign as that of an electronic charge. Measurements of shot noise are consistent with the charge carriers of the state $\nu = 1/3$ having fractional charge $-e/3$ [75].

2.1.1 Haldane Pseudopotentials

When the magnetic field is strong, in the fractional quantum Hall regime, the Landau level separation, $\hbar\omega_c$, is large enough that the degrees of freedom are restricted to a single Landau level, i.e. $\hbar\omega_c \gg E_{other}$ where E_{other} are other energy scales in the

problem. Thus, excitations between Landau levels can be considered to be high energy degrees of freedom and low energy excitations are those within the same Landau level. Within a single Landau level the kinetic energy is quenched and hence the Hamiltonian of the system can be described solely in terms of interactions between particles within the Landau level.

Haldane [73, 76] showed that a translationally and rotationally invariant two-body interaction, within a single Landau level, can be decomposed in terms of pseudopotential parameters (V_m, $m \geq 0$). The pseudopotential parameters describe the cost of having a pair of particles in a state with relative angular momentum, m, which is an odd number for electrons. The pseudopotential also leads to a description of the fractional quantum Hall state within the Landau level.

The Hamiltonian projected to a single Landau level is described solely in terms of the interaction term

$$H = \sum_{i<j} V(\mathbf{r}_i - \mathbf{r}_j). \tag{2.44}$$

The Hamiltonian acts on two particles at a time and the two-particle wavefunction can be decomposed in terms of the center of mass and relative degrees of freedom [77]

$$\Psi(\mathbf{r}_i, \mathbf{r}_j) = \sum_{\alpha,\beta} A_{\alpha,\beta} \Psi^{c.o.m.}_{\alpha} \Psi^{rel}_{\beta}(\mathbf{r}_i - \mathbf{r}_j). \tag{2.45}$$

Translational invariance implies that the Hamiltonian only acts on the relative degrees of freedom. In the lowest Landau level the single particle wavefunction is given by Eq. A.8 and hence for the two-particle case the product of the center of mass and the relative wavefunctions in Eq. 2.45 can be written as (setting $l_B = 1$)

$$\Psi^{c.o.m.}\left(\frac{z_i + z_j}{2}\right) \Psi^{rel}(z_i - z_j) e^{-\frac{1}{4}(|z_i|^2 + |z_j|^2)}. \tag{2.46}$$

The interaction and hence the Hamiltonian is diagonal in a basis of the center of mass degrees of freedom. Hence the Hamiltonian can be expanded in terms of a complete basis of relative wavefunctions as

$$H = \sum_{i<j} \sum_{m,m'} |m; ij\rangle \langle m; ij| V(\mathbf{r}_i - \mathbf{r}_j) |m', ij\rangle \langle m'; ij|, \tag{2.47}$$

where

$$|m; ij\rangle = C_m (z_i - z_j)^m, \tag{2.48}$$

where m is the relative angular momentum between the particles and C_m are normalization constants. As a consequence of rotational invariance of the interaction the Hamil-

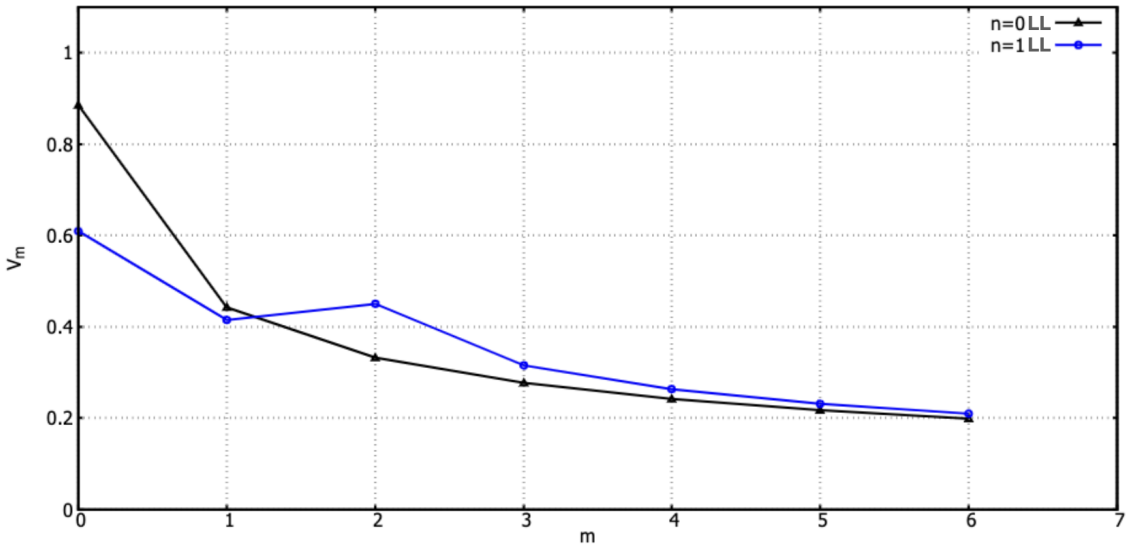

Figure 2.5: Pseudopotential parameters V_m plotted as a function of relative angular momentum m for the Coulomb interaction $V(\mathbf{q}) = e^2/4\pi\epsilon|\mathbf{q}|$, for the $n = 0$ Landau level (in black) and $n = 1$ Landau level (in blue).

tonian is diagonal in the relative angular momentum m,

$$H = \sum_{i<j} \sum_{m} V_m P_{ij}^m, \tag{2.49}$$

where V_m are the pseudopotential parameters given by

$$V_m = \langle m; ij | V(\mathbf{r}_i - \mathbf{r}_j) | m; ij \rangle , \tag{2.50}$$

and P_{ij}^m is the projection onto a two-particle state with relative angular momentum, m

$$P_{ij}^m = |m; ij\rangle \langle m; ij| . \tag{2.51}$$

The $\nu = 1/3$ state is the ground state for the Hamiltonian obtained by setting $V_1 > 0$ and all the other $V_{m\geq 3} = 0$. This ensures that a pair wavefunction of the form $(z_i - z_j)$ is assigned a positive energy cost whereas a wavefunction that has the form $(z_i - z_j)^3$ is formed without any energy cost. The latter wavefunction is the Laughlin wavefunction for the $\nu = 1/3$ state.

The pseudopotential approach can be generalized to higher Landau levels by mapping the system in a single Landau level to another system with a modified interaction [41, 78–80]. In the n^{th} Landau level the Hamiltonian in momentum space takes the

form [6]

$$H^n = \int d^2q V(\mathbf{q})\rho_n(-\mathbf{q})\rho_n(\mathbf{q}), \tag{2.52}$$

where ρ_n is the projected density describing electrons in the n^{th} Landau level [81] and is given by

$$\rho_n(\mathbf{q}) = F_n(\mathbf{q})\hat{\rho}_n(\mathbf{q}), \tag{2.53}$$

with $\hat{\rho}(\mathbf{q})$ the bare density and $F_n(\mathbf{q})$ the Landau level form factor

$$F_n(\mathbf{q}) = L_n(q^2/2)e^{-q^2/4}. \tag{2.54}$$

With this the Hamiltonian becomes

$$H^n = V(\mathbf{q})[F_n(\mathbf{q})]^2\hat{\rho}_n(-\mathbf{q})\hat{\rho}_n(\mathbf{q}). \tag{2.55}$$

Expanding the interaction potential in a series of Laguerre polynomials

$$V(\mathbf{q})[F_n(\mathbf{q})]^2 = \sum_m V_m L_m(q^2)e^{-q^2/2}, \tag{2.56}$$

we can identify V_m as the pseudopotential parameters and these are then given by

$$V_m = \int_0^\infty q dq V(\mathbf{q})[L_n(q^2/2)]^2 L_m(q^2)e^{-q^2}. \tag{2.57}$$

The first few pseudopotential parameters for the Coulomb interaction $V(\mathbf{q}) = e^2/4\pi\epsilon|\mathbf{q}|$ for the $n = 0$ and $n = 1$ Landau levels are shown in Fig. 2.5.

2.1.2 Composite Fermion Approach to FQHE

FQH states with $\nu = 1/m$ are described in terms of Laughlin's wavefunctions. The other fractions observed in experiments have been obtained in various hierarchical schemes [73, 74, 82].

The composite fermion (CF) picture seeks to unify the FQHE and the IQHE while providing a scheme for the hierarchy of FQH states observed in experiments [83, 84]. Consider the IQH state $\nu = p$. This corresponds to Φ_0/p flux per electron on average. The many body wavefunction for this state, Ψ_p, is rigid and is not affected by the interactions between electrons and the IQH state's characteristics follow from the electrons being fermions and obeying Fermi statistics. To each electron we attach an infinitely thin

[6] See Appendix B for details.

solenoid carrying a flux $\theta\Phi_0$ pointed in the direction opposite to the magnetic field. Such an object is referred to as a composite particle. The composite particles are known to obey fractional statistics [85] and under an exchange the phase is known to be $(-1)^{1+\theta}$ [86]. When $\theta = 2m$ i.e., an even number of flux is attached to each electron, the phase factor is the same as the situation where there are no flux tubes attached to the electron, $\theta = 0$. The state thus obtained can be labelled as Ψ_p^{2m}. Hence composite particles where an even number of flux are attached to the electrons behave like fermions and hence have Fermi statistics. Thus we can expect that if a system of electrons is rigid and exhibits the IQHE then a system of composite fermions made up of electrons with an even number of flux quanta attached to them is also rigid and hence exhibits the IQHE [83].

The CFs are electrons bound to an even number of flux quanta, $2m$. Because of the additional flux the CFs experience an effective magnetic field

$$B_{\text{eff}} = B - 2m\Phi_0\rho_0, \tag{2.58}$$

where ρ_0 is the density of electrons and $B = \Phi_0\rho_0/\nu$ is the magnetic field giving rise to the FQHE state. The CFs are in a IQHE state with $\nu_{CF} = p$ and hence the effective magnetic field is

$$B_{\text{eff}} = \Phi_0\rho_0/p. \tag{2.59}$$

The filling fraction of electrons can be expressed as

$$\nu = \frac{p}{2mp+1}. \tag{2.60}$$

The CF method hence relates the IQHE of composite fermions to the FQHE of electrons. The assumptions made here work if the original electron liquid is itself incompressible. The arguments of gauge invariance introduced before [87, 88] still hold. For the $\nu = p$ IQHE state p electrons are transferred, in a Corbino geometry, from the inner edge to the outer one as the flux through the center is increased by one flux quanta. For the Ψ_p^{2m} state an additonal $2mp$ flux quanta has to be supplied to transfer p electrons. The Hall resistivity hence becomes $R_{xy} = h/\nu e^2$ with $\nu = p/(2mp+1)$.

The fractions obtained using the CF method all have odd denominator with the exception of $\nu = 1/2m$ states which are obtained when $p \to \infty$. The order of stability of the fractions can be seen if we assume that due to the likelihood of flux unbinding being higher in states with larger m the gap is also likely to be less stable for larger m. Hence if a state with filling fraction $\nu = p/(2mp+1)$ exists then a state with $\nu = p/(2m'p+1)$ will exist provided $m' < m$.

Wavefunctions of IQHE states at filling fraction $\nu = p$ can be constructed starting from a picture of non-interacting electrons in a magnetic field. The Hamiltonian for this system is given by Eq. 2.10 and the wavefunctions are Ψ_p. At the mean field level the CFs, for the FQHE state at $\nu = p/(2mp+1)$, experience an effective magnetic field as given in Eq. 2.58. Additionally the CFs are described by electrons with $2m$ flux quanta attached to them. The binding of flux tubes to electrons is generated by a singular gauge potential of the form [83, 85, 86]

$$\mathbf{a}(\mathbf{r}_i) = \frac{2m}{2\pi}\Phi_0 \sum_{j\neq i} \nabla_i \theta_{ij}, \tag{2.61}$$

with

$$\theta_{ij} = -i\ln\frac{z_i - z_j}{|z_i - z_j|}, \tag{2.62}$$

the relative angle between particles i and j in the complex plane. The potential $\mathbf{a}(\mathbf{r}_i)$ generates a magnetic field given by

$$\mathbf{b_i} = \nabla \times \mathbf{a}(\mathbf{r}_i) = 2m\Phi_0 \sum_{i\neq j} \delta^2(\mathbf{r_i} - \mathbf{r_j}). \tag{2.63}$$

Each electron thus sees $2m$ flux attached to every other electron.

The mean field Hamiltonian for the composite fermions then becomes

$$H_{CF} = \frac{1}{2m_e}\sum_i \left[\mathbf{p}_i + e\mathbf{A}'(\mathbf{r}_i) + \mathbf{a}(\mathbf{r}_i)\right]^2, \tag{2.64}$$

where the gauge field $\mathbf{A}'(\mathbf{r}_i)$ generates the effective magnetic field B_{eff}.

For large magnetic fields the gap between Landau levels is also large and only the lowest Landau level (LLL) becomes important. Eliminating the gauge field, $\mathbf{a}(\mathbf{r}_i)$, from Eq. 2.64 and requiring that at $\nu = 1/m$ the wavefunction should correspond to Laughlin wavefunction leads to the wavefunction being [83, 89],

$$\Psi_\nu = \mathscr{P}_{LLL}\Phi e^{-i2m\sum_{i<j}\theta_{ij}} = \Phi\prod_{j<k}\left(z_i - z_j\right)^{2m}, \tag{2.65}$$

where Φ satisfies Schrödinger's equation for $\nu^* = m$ and $\nu^* = B_{\text{eff}}\rho_0$. Experimental evidence for composite fermions will be discussed in Chapter 4, where we discuss even denominator fractional quantum Hall effects (EDFQHs). The theory of CFs can be extended to include spin and other degrees of freedom. We discuss these "multi-component" CF theories in the context of graphene in Chapter 4.

2.2 Chern-Simons Theory

An alternative to the wavefunction approach is an effective field theory which tries to capture the response of the low energy excited state just above the ground state. The effective theory that describes the quantum Hall effect is known as Chern Simons theory. [7]

Building on ideas of Girvin and Macdonald [92] and Read [93], Zhang *et al.* proposed a theory of the FQHE using a Chern Simons effective field theoretic description in terms of a bosonic superfluid. Lopez and Fradkin [94] used fermionic Chern-Simons field theory to describe the fractional quantum Hall system, motivated by the composite fermion wavefunction approach of Jain [83]. This was further extended by Halperin, Lee and Read [95], Murthy and Shankar [96] and others.

The Chern-Simons term is defined through the action

$$S_{CS}[A] = \frac{k}{4\pi}\int d^3x \;\; \epsilon^{\mu\nu\rho} A_\mu \partial_\nu A_\rho, \tag{2.66}$$

where A_μ is a fixed field that does not have any fluctuations and $x = (x^0, x^1, x^2)$ is the space-time coordinate in 2+1 dimensions. The lack of fluctuations is related to the assumption that at low energies there are no low lying excitations in response to perturbations to the system. This is true for the IQHE where there is a gap to the first excited state. Typically we are interested in writing down a partition function of the form

$$Z[A_\mu] = \int \mathscr{D}c \;\; e^{iS[c;A_\mu]}, \tag{2.67}$$

where $S[c;A_\mu]$ is the action and c are fermionic operators. The action S is arbitrary aside from the requirement that it has to include a coupling to the field A_μ through a current J_μ as

$$S_A = \int d^3x \;\; J_\mu A^\mu. \tag{2.68}$$

Once we integrate out the fields c, we have a low energy effective theory given by

$$Z[A_\mu] = e^{iS_{\text{eff}}[A_\mu]}, \tag{2.69}$$

where $S_{\text{eff}}[A_\mu]$ is the effective action which turns out to be the Chern-Simons action.

---

[7] The discussion in this section is primarily based on Refs. [70, 90, 91].

Varying the effective action with respect to the field A_μ leads to

$$\frac{\delta S_{\text{eff}}}{\delta A_\mu(x)} = \langle J_\mu(x) \rangle, \tag{2.70}$$

where for the spatial components

$$J_i = \sigma_{ij} E_j; \quad E_j = \partial_0 A_j. \tag{2.71}$$

The presence of a non-zero Hall conductivity, σ_{xy}, implies the existence of a term in the action of the form $\sim A_x \sigma_{xy} \partial_0 A_y$. This can be made gauge invariant and we get the form of the effective action as the Chern-Simons term

$$S_{\text{eff}} = S_{CS}[A] = \frac{k}{4\pi} \int d^3x \;\; \epsilon^{\mu\nu\rho} A_\mu \partial_\nu A_\rho. \tag{2.72}$$

The Chern-Simons term is gauge invariant up to a boundary term i.e., if we make a gauge transformation $A_\mu \to A_\mu + \partial_\mu \lambda$, then the effective action becomes

$$S_{CS} \to S_{CS} + \frac{k}{4\pi} \int d^3x \;\; \partial_\mu (\lambda \epsilon^{\mu\nu\rho} \partial_\nu A_\rho), \tag{2.73}$$

which is a total derivative. Given the Chern-Simons action in Eq. 2.72 we can compute the current as

$$J_i = \frac{\delta S_{CS}[A]}{\delta A_i} = -\frac{k}{2\pi} \epsilon_{ij} E_i, \tag{2.74}$$

and we can obtain the Hall conductivity as

$$\sigma_{xy} = \frac{k}{2\pi}. \tag{2.75}$$

If we compare Eq. 1.2 and Eq. 2.75 we see that the Hall conductivity of ν filled Landau levels is related to the level of the Chern-Simons term k via

$$k = \frac{\nu e^2}{\hbar}. \tag{2.76}$$

Quantization of Chern-Simons Theory

If Eq. 2.76 has to hold, then the level of the Chern-Simons term, k, can only take integer values. In order to see the quantization of the Chern-Simons theory we make time periodic or Euclidean, parameterised by τ. This is equivalent to formulating the theory

such that the time variable lives on a circle $\mathbf{S}^1$ and obeys the periodicity condition

$$\tau \equiv \tau + \beta. \tag{2.77}$$

Under a gauge transformation, a field that carries a charge, e, transforms as

$$\psi \to e^{ie\lambda/\hbar}\psi. \tag{2.78}$$

Usually the function λ is taken to be single valued but the actual requirement is that $e^{ie\lambda\hbar}$ is single valued and hence we need to consider λ modulo 2π

$$e\lambda\hbar \cong e\lambda/\hbar + 2\pi. \tag{2.79}$$

This allows for gauge transformations that can wind around the circle $\mathbf{S}^1$

$$\lambda = \frac{2\pi\hbar\tau}{e\beta}, \tag{2.80}$$

which leads to the temporal component of the gauge field A_0 transforming as

$$A_0 \to A_0 + \frac{2\pi\hbar}{e\beta}, \tag{2.81}$$

which is a constant shift. We consider the two dimensional system to form a sphere $\mathbf{S}^2$ instead of a plane and then thread a magnetic flux through the sphere given by

$$\frac{1}{2\pi}\int_{\mathbf{S}^2} F_{12} = \frac{\hbar}{e}, \tag{2.82}$$

where $F_{\mu\nu}$ is the field strength [90]. This is equivalent to placing a magnetic monopole inside of the sphere. With a constant $A_0 = s$ the Chern-Simons term in Eq. 2.72 becomes

$$S_{CS} = \frac{k}{4\pi}\int d^3x\,[A_0F_{12} + A_1F_{20} + A_2F_{10}]. \tag{2.83}$$

Integration by parts of the second and third terms gives a factor of 2 and with a constant flux the result is

$$S_{CS} = \beta s\frac{\hbar k}{e}, \tag{2.84}$$

where the factor of β comes from the time integral in Eq. 2.83. Thus, under a gauge transformation of the form in Eq. 2.80 the temporal component of the gauge field A_0 is changed according to Eq. 2.81 and the Chern-Simons term is not gauge invariant and

instead transforms as

$$S_{CS} \to S_{CS} + \beta s \frac{\hbar^2 k}{e^2}. \tag{2.85}$$

Even though the Chern-Simons action is not gauge invariant, the partition function in Eq. 2.69 is gauge invariant provided

$$\frac{\hbar k}{e^2} \in \mathbf{Z}. \tag{2.86}$$

Again if we make the association $k = \frac{\nu e^2}{\hbar}$ then we can see that indeed k takes integer values.

Chern-Simons Theory for the Fractional Quantum Hall Effect

The argument for the level of the Chern-Simons term taking integer values shows why the Hall conductivity is quantized for the IQHE. For the FQHE the argument above seemingly does not hold. The issue is with the assumption that at low energies there is a energy gap in the system and hence there are no low lying excitations in the system. For the FQHE while it is true that there is an energy gap in the system there can be topological excitations that affect the system at low energies. Moreover these excitations can be described by an emergent U(1) gauge field a_μ that propagates only inside the material [90].

Consider the $\nu = 1/m$ state. For this state there is a single emergent U(1) gauge field a_μ. After integrating out the dynamical fields corresponding to the fermions the partition function is

$$Z[A_\mu] = \int Da_\mu e^{iS_{\text{eff}}[a;A]/\hbar}. \tag{2.87}$$

The aim is to find a suitable effective action $S_{\text{eff}}[a;A]$ that describes the FQHE. To this end there has to be a coupling between the gauge fields A_μ and a_μ. The field A_μ couples to the electron current J_μ which is given by [70, 90]

$$J^\mu = \frac{e^2}{2\pi\hbar} \epsilon^{\mu\nu\rho} \partial_\nu a_\rho. \tag{2.88}$$

If we look at the electron density $J_0 = \rho$ it is given by

$$\rho = \frac{e^2}{2\pi\hbar} \mathscr{B}, \tag{2.89}$$

where

$$\mathscr{B} = \partial_1 a_2 - \partial_2 a_1, \tag{2.90}$$

is the magnetic field generated by the gauge field, a_μ, which is different from the physical external magnetic field, B. Hence it is the magnetic flux of a_μ that couples to the field A_μ. This magnetic flux can also be interpreted as the charge of the field a_μ.

Thus, at low energies the action can be postulated to be

$$S_{\text{eff}} = \frac{e^2}{\hbar}\int d^3x\left[\frac{1}{2\pi}\epsilon^{\mu\nu\rho}A_\mu\partial_\nu a_\rho - \frac{m}{4\pi}\epsilon^{\mu\nu\rho}a_\mu\partial_\nu a_\rho\right]. \tag{2.91}$$

The effective action has a term which couples the field A_μ to a current which is a mixed Chern-Simons term and a Chern-Simons term involving a_μ . Terms with higher derivatives of a_μ are omitted since at low energies and large wavelength, these terms become unimportant. A Chern-Simons term for the field A_μ could be added to the effective action in Eq. 2.91 but such a term would just be describing the integer contribution to the Hall conductivity.

Since the field a_μ appears in Eq. 2.91 quadratically we can integrate it out from the equations of motion to obtain a

$$f_{\mu\nu} = \frac{1}{m}F_{\mu\nu}, \tag{2.92}$$

where $f_{\mu\nu} = \partial_\mu a_\nu - \partial_\nu a_\mu$ and $F_{\mu\nu} = \partial_\nu A_\mu - \partial_\nu A_\mu$. This indicates that up to a gauge transformation a is related to A by $a = A/m$. Substituting this back into Eq. 2.91 we arrive at the effective action

$$S_{\text{eff}} = \frac{e^2}{\hbar}\int d^3x\frac{1}{4\pi m}\epsilon^{\mu\nu\rho}A_\mu\partial_\nu\ A_\rho. \tag{2.93}$$

Comparing this with Eq. 2.72 we read off the level of the Chern-Simons term as being $k = e^2/\hbar m$ and hence the Hall conducitivity is

$$\sigma_{xy} = \frac{e^2}{2\pi\hbar m}, \tag{2.94}$$

which is the required conductivity for the Laughlin state.

Although the expression in Eq. 2.94 is the correct form of the Hall conductivity the form of the action in Eq. 2.93 violates gauge invariance [70, 90] as can be seen by following the arguments that led to the condition given in Eq. 2.86. The problem lies with integrating out the gauge field a_μ. The system has properties like fractionally charged quasiparticles and topological degeneracies that can only be understood in a theory which includes both A and a fields. The reason integrating out the field a_μ gives the correct Hall conductivity is that it is valid locally since the action is gauge invariant locally as long as we are far away from the boundary and this is enough to determine the Hall conductivity [70, 90].

2.2.1 Quasiparticles and Fractional Statistics

We can add a term to the action Eq. 2.91 that describes the gauge field a_μ that is coupled to its own current j_μ. Switching off the background field A_μ leads to the equations of motion for a_μ

$$\frac{e^2}{2\pi\hbar} f_{\mu\nu} = \frac{1}{m}\epsilon_{\mu\nu\rho} j^\rho. \tag{2.95}$$

The charge density can be read off as

$$j_0 = \frac{e^2}{2\pi\hbar} m\mathscr{B}. \tag{2.96}$$

If we consider a static point charge at the origin for which $j_0 = e\delta^2(\mathbf{x})$ then

$$\mathscr{B} = \frac{\Phi_0}{m}\delta^2(\mathbf{x}), \tag{2.97}$$

which implies that the effect of the Chern-Simons term is to bind a flux $\frac{\Phi_0}{m}$ to each particle of charge e. In this case the only non-zero component of the current, j_μ, is j_0 which from Eq. 2.74 becomes

$$j_0 = \frac{e^2}{2\pi\hbar}\mathscr{B} = \frac{e}{m}\delta^2(\mathbf{x}). \tag{2.98}$$

This is the charge density of a stationary particle which carries a charge $\frac{e}{m}$. We can generalize the result to include N such particles carrying a charge e at positions $\mathbf{x}_a$. In this case the charge density and current densities are given by

$$j_0(\mathbf{x}) = e\sum_{a=1}^{N}\delta^2(\mathbf{x}-\mathbf{x}_a(t)) \quad \text{and} \quad \mathbf{j} = e\sum_{a=1}^{N}\dot{\mathbf{x}}_a\delta^2(\mathbf{x}-\mathbf{x}_a(t)). \tag{2.99}$$

We can fix the gauge by imposing $a_0 = 0$ and $\partial_i a_i = 0$ and solve the equation of motion Eq. 2.95 to get [91]

$$a_i(\mathbf{x},t) = \frac{\hbar}{em}\sum_{a=1}^{N}\epsilon_{ij}\frac{x^j - x_a^j(t)}{|\mathbf{x}-\mathbf{x}_a(t)|^2}, \tag{2.100}$$

where we used the Green's function for the two dimensional Laplacian,

$$\nabla^2 \log|\mathbf{x}-\mathbf{y}| = 2\pi\delta(\mathbf{x}-\mathbf{y}). \tag{2.101}$$

Using the identity $\partial_i \arg(\mathbf{x}) = -\epsilon_{ij}\frac{x^j}{|x|}$ we can rewrite Eq. 2.100 as

$$a_i(\mathbf{x},t) = \frac{\hbar}{em}\sum_{a=1}^{N}\partial_i \arg(\mathbf{x}-\mathbf{x_a}). \tag{2.102}$$

Under such a gauge transformation a particle represented by a field $\psi(\mathbf{x})$ transforms as [91]

$$\psi(\mathbf{x}) \to \tilde{\psi}(\mathbf{x}) = \exp\left(-i\sum_{a=1}^{N}\partial_i \arg(\mathbf{x}-\mathbf{x_a})\right)\psi(\mathbf{x}). \tag{2.103}$$

As each particle carries a flux $\frac{\hbar}{em}$, when one particle is moved in a closed curve C around another it picks up an Aharonov-Bohm phase given by [91]

$$\exp\left(i\frac{e}{\hbar}\oint_C \mathbf{a}\cdot d\mathbf{x}_a\right) = \exp\left(\frac{2\pi i}{m}\right). \tag{2.104}$$

Taking one particle around the other is equivalent to a double exchange of particles and hence we find that the statistical exchange phase, α, of these quasiparticles are [91]

$$\alpha = \frac{1}{m}. \tag{2.105}$$

Heirarchy of states and $\mathscr{K}$-matrices

The Chern-Simons formalism can be extended to include fractions other than the Laughlin fractions. The most natural way to extend the formalism is by introducing a set of emergent gauge fields a_I. In terms of these fields the low energy effective theory (in units of $\hbar = e = 1$) of a FQH liquid can be written in the form [8]

$$\mathscr{L} = \frac{1}{4\pi}\mathscr{K}_{\alpha\beta}\epsilon^{\mu\nu\rho}a_{\alpha\mu}\partial_\nu a_{\beta\rho} - t_\alpha\epsilon^{\mu\nu\rho}A_\mu\partial_\nu a_{\alpha\rho}, \tag{2.106}$$

where the $\mathscr{K}$ matrix is a symmetric integer matrix and t is known as the charge vector [97]. Properties like statistics of exchange, ground state degeneracy etc. can be obtained from both $\mathscr{K}$ and t. Integrating out the gauge fields we can get the Hall conductivity [98] as

$$\sigma_{xy} = (\mathscr{K}^{-1})_{\alpha\beta}t_\alpha t_\beta. \tag{2.107}$$

[8] The indices α and β, unlike the indices μ ,ν and ρ, are not space-time indices so we do not worry about whether they are up or down.

The charges of the quasiparticles are given by

$$(e^*)_\alpha = (\mathscr{K}^{-1})_{\alpha\beta} t_\beta, \tag{2.108}$$

and the statistics of quasiparticles that couple to a_α with that which couple to a_β are

$$\alpha_{\alpha\beta} = (\mathscr{K}^{-1})_{\alpha\beta}. \tag{2.109}$$

In these units, the Hall conductivity, σ_{xy}, and the filling fraction, ν, are the same and hence the filling fraction is also given by

$$\nu = (\mathscr{K}^{-1})_{\alpha\beta} t_\alpha t_\beta. \tag{2.110}$$

The parametrization of $\mathscr{K}$ matrix and t-vector that gives rise to the hierarchical scheme [73] is

$$\mathscr{K} = \begin{pmatrix} m & \pm 1 & 0 & \cdots \\ \pm 1 & 2p_1 & \pm 1 & \\ 0 & \pm 1 & 2p_2 & \\ \vdots & & & \ddots \end{pmatrix} \quad \text{and} \quad t = (1, 0, 0, \cdots). \tag{2.111}$$

The benefit of using the $\mathscr{K}$ matrix is that it can be used to describe multicomponent FQH states such as multi-layer systems, systems with spin or systems with other degrees of freedom. In the context of multi-layer systems an element of the matrix, $\mathscr{K}_{\alpha\beta}$, has the physical interpretation of being the number of flux quanta attached to particles in layer α as seen by those in layer β. The $\mathscr{K}$ matrix formalism will be important in the discussion of the FQHE in graphene. In the next chapter we will give a brief introduction to graphene and its properties followed by an introduction to the IQHE and the FQHE in graphene.

Chapter 3

Quantum Hall Effects in Graphene

Graphene is composed of carbon atoms arranged in a honeycomb lattice as shown in Fig. 3.1. The lattice structure is comprised of two inter-penetrating triangular sublattices, A and B. The sublattice A is generated by the vectors [99, 100]

$$\mathbf{a_1} = (\sqrt{3}, -1)\, a; \quad \mathbf{a_2} = (0, 1)\, a; \tag{3.1}$$

where $a = 1.42$ Å is the lattice spacing. The sublattice B is then given by $\mathbf{B} = \mathbf{A} + \mathbf{b_i}$, $i = 1, 2, 3$, with the $\mathbf{b_i}$ being

$$\mathbf{b_1} = \left(\frac{1}{\sqrt{3}}, 1\right)\frac{a}{2}; \quad \mathbf{b_2} = \left(\frac{1}{\sqrt{3}}, -1\right)\frac{a}{2}; \quad \mathbf{b_3} = \left(\frac{-1}{\sqrt{3}}, 0\right)a. \tag{3.2}$$

The reciprocal lattice is also hexagonal and is generated by the vectors

$$\mathbf{R_1} = \frac{4\pi}{\sqrt{3}a}\left(\frac{1}{2}, \frac{\sqrt{3}}{2}\right); \quad \mathbf{R_2} = \frac{4\pi}{\sqrt{3}a}\left(\frac{1}{2}, -\frac{\sqrt{3}}{2}\right). \tag{3.3}$$

The inequivalent Dirac points $\mathbf{K}$ and $\mathbf{K}'$ at the corners of the Brillouin zone in Fig. 3.1, are of particular importance to the physics of graphene and are given by

$$\mathbf{K} = \frac{4\pi}{\sqrt{3}}a\left(\frac{1}{2}, \frac{1}{2\sqrt{3}}\right); \quad \mathbf{K}' = \frac{4\pi}{\sqrt{3}}a\left(\frac{1}{2}, -\frac{1}{2\sqrt{3}}\right). \tag{3.4}$$

As described in Fig. 1.2, the carbon atoms are sp^2 hybridized with an extra electron in the p-orbital perpendicular to the plane of the carbon atoms. The overlap of neighbouring p-orbitals gives rise to a hopping amplitude of $t \sim 2.7$eV in graphene [7]. Including the nearest-neighbour hopping, the tight-binding Hamiltonian for graphene

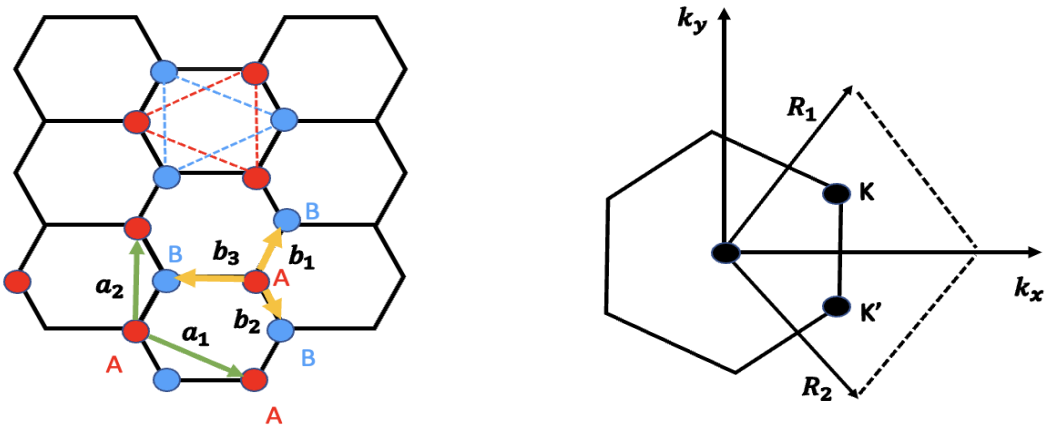

Figure 3.1: Right: Hexagonal lattice structure of graphene showing the inter-penetrating triangular sublattices A (red) and B (blue) with dashed lines. The lattice vectors $\mathbf{a_1}$, $\mathbf{a_2}$ generate the A (red) sublattice and the B (blue) sublattice is generated by $\mathbf{B} = \mathbf{A} + \mathbf{b_i}$ with i=1, 2, 3. Left: The reciprocal lattice of graphene is also hexagonal and generated by lattice vectors $\mathbf{R_1}$ and $\mathbf{R_2}$. The points $\mathbf{K}$ and $\mathbf{K}'$ are inequivalent Dirac points where the Dirac cones are located.

can be written as [100, 101]

$$H_t = -t \sum_{\mathbf{A},i,\sigma=\pm1} [u_\sigma(\mathbf{A}) v_\sigma(\mathbf{A}+\mathbf{b_i}) + H.c.] + \beta \sum_{\mathbf{A},\sigma=\pm1} \left[u^\dagger_\sigma(\mathbf{A}) u_\sigma(\mathbf{A}) - v^\dagger_\sigma(\mathbf{A}+\mathbf{b_i}) v_\sigma(\mathbf{A}+\mathbf{b_i})\right], \tag{3.5}$$

where $u^\dagger_\sigma$ ($v^\dagger_\sigma$) and u_σ (v_σ) are the creation and annihilation operators for an electron with spin, σ, on the sublattice A (B) with $\mathbf{A} + \mathbf{b_i} = \mathbf{B}$. The first term is the nearest neighbour hopping term and the second term measures the difference in onsite energy between the two sublattices. In terms of Fourier modes (supressing the spin index)

$$u(\mathbf{A}) = \int \frac{d^2k}{(2\pi)^2} e^{i\mathbf{k}\cdot\mathbf{A}} u(\mathbf{k}); \quad v(\mathbf{B}) = \int \frac{d^2k}{(2\pi)^2} e^{i\mathbf{k}\cdot\mathbf{B}} v(\mathbf{k}). \tag{3.6}$$

The Hamiltonian in momentum-space is

$$H_t = \int \frac{d^2k}{(2\pi)^2} \left[u^\dagger(\mathbf{k}), v^\dagger(\mathbf{k})\right] \begin{bmatrix} \beta & -t\left(e^{i\mathbf{k}\cdot\mathbf{b}_1} + e^{i\mathbf{k}\cdot\mathbf{b}_2} + e^{i\mathbf{k}\cdot\mathbf{b}_3}\right) \\ -t\left(e^{i\mathbf{k}\cdot\mathbf{b}_1} + e^{i\mathbf{k}\cdot\mathbf{b}_2} + e^{i\mathbf{k}\cdot\mathbf{b}_3}\right) & -\beta \end{bmatrix} \begin{bmatrix} u(\mathbf{k}) \\ v(\mathbf{k}) \end{bmatrix}. \tag{3.7}$$

The energy eigenvalues of the tight-binding Hamiltonian are given by [100, 101]

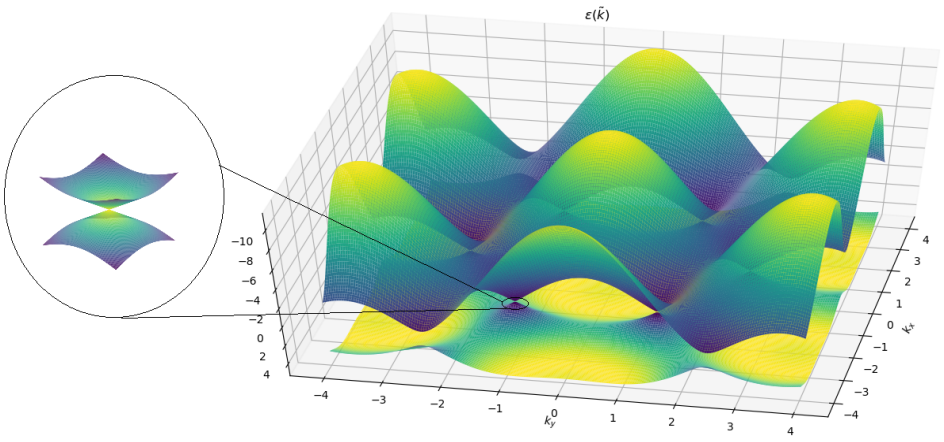

Figure 3.2: Energy dispersion of graphene. Right: Energy spectrum (in units of t). Left: Enlarged view of energy band near one of the Dirac points showing the linear dispersion at low energies.

$$E(\mathbf{k}) = \pm\left(\beta^2 + t^2|e^{i\mathbf{k}\cdot\mathbf{b_1}} + e^{i\mathbf{k}\cdot\mathbf{b_2}} + e^{i\mathbf{k}\cdot\mathbf{b_3}}|^2\right)^{1/2}. \tag{3.8}$$

The energy eigenvalues can be either positive or negative and at half-filling, when there is one electron per site on the lattice, the negative-energy states (valence band) are completely filled and the positive-energy (conduction band) states are completely empty. The separation between the conduction and valence band is minimal when the function $f(\mathbf{k}) = e^{i\mathbf{k}\cdot\mathbf{b_1}} + e^{i\mathbf{k}\cdot\mathbf{b_2}} + e^{i\mathbf{k}\cdot\mathbf{b_3}}$ goes to zero. The zeros of $f(\mathbf{k})$ define the Dirac points located at the six vertices of the Brillouin zone. Out of the six points only two are inequivalent and they are given in Eq. 3.4. $\mathbf{K}' = -\mathbf{K}$ is also equivalent to the choice in Eq. 3.4 [100]. At the Dirac points there is a band gap of $2|\beta|$ for $\beta \neq 0$. When $\beta = 0$ the band gap goes to zero at the Dirac points and thus the conduction and valence band touch. For graphene, $\beta = 0$ since both the sublattices are composed of carbon atoms and hence there is no difference in energies between the two sublattices. Hence neutral graphene is a semi-metal. Hexagonal boron nitride (hBN) has the same structure as graphene but since it has a mixture of boron and nitrogen atoms in the hexagon, $\beta \neq 0$ and thus boron nitride is an insulator [102]. Graphene on a hBN substrate can also end up with $\beta \neq 0$. With $\beta = 0$ we can expand the function $f(\mathbf{k})$ around one of the Dirac points, e.g. $\mathbf{K}$, with $\mathbf{k} = \mathbf{K} + \mathbf{q}$ and $|\mathbf{q}| \ll |\mathbf{K}|$

$$f(\mathbf{K}+\mathbf{q}) \simeq -i\frac{t\sqrt{3}}{2}e^{-i\frac{2\pi}{3}}q_x\hat{k_x} + i\frac{t}{2}\left(e^{i\frac{2\pi}{3}} - 1\right)q_y\hat{k_y}. \tag{3.9}$$

The energy dispersion near the Dirac points then becomes

$$E(\mathbf{k}) = \lambda v_F |\mathbf{q}| + O\left[\left(\frac{q}{K}\right)^2\right], \tag{3.10}$$

where $v_F = 3ta/2$ is the Fermi velocity [7, 99]. $\lambda = \pm$ is the band index with $\lambda = +$ corresponding to the conduction band and $\lambda = -$ corresponding to valence band. The energy dispersion, including a small next nearest neighbour hopping contribution, is shown in Fig. 3.2 with a blow up of the dispersion near one of the Dirac points. As opposed to a quadratic dispersion, $E(\mathbf{k}) = k^2/2m$, the dispersion in Eq. 3.10 is linear in momentum and the Fermi velocity does not depend on the mass or the momentum and is a constant.[1] Including the spin degrees of freedom it is possible to rewrite the low energy Hamiltonian around the points $\mathbf{K}$ and $\mathbf{K}' = -\mathbf{K}$ as [100, 101]

$$\begin{aligned} H_t = &-\frac{t\sqrt{3}}{2}\sum_{\sigma=\pm}\int_{\mathbf{K}+\mathbf{q}}^{\Lambda}\frac{d^2q}{(2\pi a)^2}\left[u_\sigma^\dagger(\mathbf{K}+\mathbf{q}), v_\sigma^\dagger(\mathbf{K}+\mathbf{q})\right]\mathscr{P}_+\begin{bmatrix} u(\mathbf{K}+\mathbf{q}) \\ v(\mathbf{K}+\mathbf{q})\end{bmatrix} \\ &-\frac{t\sqrt{3}}{2}\sum_{\sigma=\pm}\int_{\mathbf{K}'+\mathbf{q}}^{\Lambda}\frac{d^2q}{(2\pi a)^2}\left[u_\sigma^\dagger(\mathbf{K}'+\mathbf{q}), v_\sigma^\dagger(\mathbf{K}'+\mathbf{q})\right]\mathscr{P}_-\begin{bmatrix} u(\mathbf{K}'+\mathbf{q}) \\ v(\mathbf{K}'+\mathbf{q})\end{bmatrix}, \end{aligned} \tag{3.11}$$

where $\mathscr{P}_\pm = \pm q_x\sigma_x - q_y\sigma_y$ with σ_x, σ_y being Pauli matrices and Λ an ultraviolet (long wavelength) cutoff marking the limit where the linear dispersion approximation holds. The reference frame here has been rotated to $q_x = \mathbf{q}\cdot\mathbf{K}/q$ and $q_y = (\mathbf{K}\times\mathbf{q})\times\mathbf{K}/K^2$. The low energy Hamiltonian can be recast in a condensed form as a Dirac Hamiltonian

$$H_t = \sum_{\sigma=\pm}\Psi_\sigma^\dagger(\mathbf{x})(i\gamma_0\gamma_i q_i)\Psi_\sigma(\mathbf{x}), \tag{3.12}$$

with

$$\Psi_\sigma^\dagger(\mathbf{x}) = \int^{\Lambda}\frac{d^2q}{(2\pi a)^2}e^{i\mathbf{q}\cdot\mathbf{x}}\left[u_\sigma^\dagger(\mathbf{K}+\mathbf{q}), v_\sigma^\dagger(\mathbf{K}+\mathbf{q}), u_\sigma^\dagger(-\mathbf{K}+\mathbf{q}), v_\sigma^\dagger(-\mathbf{K}+\mathbf{q})\right], \tag{3.13}$$

where we have introduced gamma matrices which are 4×4 Hermitian matrices. They are defined as [105]

$$\gamma_0 = I_2\otimes\sigma_3; \quad \gamma_1 = \sigma_3\otimes\sigma_2; \quad \gamma_2 = I_2\otimes\sigma_1. \tag{3.14}$$

[1] Interactions do renormalize v_F [103, 104].

We can define two more anticommuting gamma matrices that close the Clifford algebra as

$$\gamma_3 = \sigma_1 \otimes \sigma_2; \quad \gamma_5 = \sigma_2 \otimes \sigma_2, \tag{3.15}$$

and the 5 gamma matrices satisfy the algebra $\{\gamma_\mu, \gamma_\nu\} = 2\delta_{\mu\nu}$ with $\mu, \nu = 0, 1, 2, 3, 5$ [105].

Using the representation of the gamma matrices in Eqs. 3.14 and 3.15 we can rewrite the Hamiltonian in Eq. 3.12 after a unitary transformation as [106]

$$H_t^\xi = \xi v_F (q_x \sigma_x + q_y \sigma_y), \tag{3.16}$$

with $v_F = -3ta/2$. Here the 4×4 Hamiltonian has been split into two 2×2 matrices. $\xi = \pm$ is referred to as the "valley pseudospin". $\xi = +$ corresponds to the point K at $+\mathbf{K}$ and $\xi = -$ corresponds to the point K' at $-\mathbf{K}$. The energy in Eq. 3.10 is independent of the valley pseudospin. In the Hamiltonian Eq. 3.16 the Pauli matrices, σ_i; $i = x, y$, act on the "sublattice pseudospin". Pseudospin up corresponds to one of the sublattices, say A, and pseudospin down to the other sublattice, B. The Hamiltonian acts on spinor components given by

$$\Psi_{\xi=+} = \begin{pmatrix} \psi_+^A \\ \psi_+^B \end{pmatrix}; \qquad \Psi_{\xi=-} = \begin{pmatrix} \psi_-^B \\ \psi_-^A \end{pmatrix}. \tag{3.17}$$

The role of the sublattices are inverted for the two valleys.

3.1 Quantum Hall Effect in Graphene

As mentioned in the introduction one of the key pieces of experimental evidence confirming the underlying relativistic nature of electrons in graphene was the discovery of the quantum Hall effects in graphene [51, 107]. In order to understand the phenomenon of the quantum Hall effect in graphene we first discuss relativistic massless 2D fermions in a strong perpendicular magnetic field. The Hamiltonian in the presence of magnetic field can be obtained from the Hamiltonian in Eq. 3.16, by substituting $\mathbf{p} \to \mathbf{p} + e\mathbf{A} = \mathbf{\Pi}$ to obtain

$$H_B^\xi = \xi \sqrt{2} \frac{v_F}{l_B} \begin{pmatrix} 0 & a \\ a^\dagger & 0 \end{pmatrix}, \tag{3.18}$$

where the expressions for a, $a^\dagger$ in the symmetric gauge can be obtained from Eq. 2.13, l_B is the magnetic length, v_F is the Fermi velocity and ξ is the valley index. From Eq. 3.18

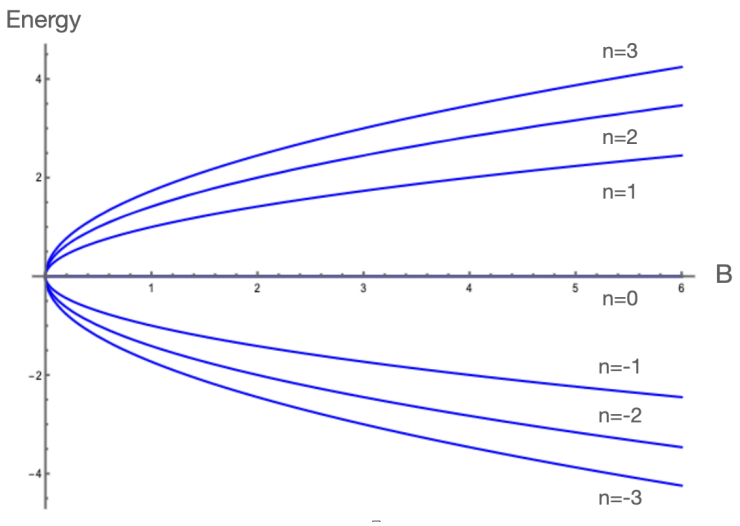

Figure 3.3: Relativistic Landau level as a function of magnetic field.

we obtain the cyclotron frequency

$$\omega_c = \sqrt{2}\frac{v_F}{l_B}. \tag{3.19}$$

Unlike the cyclotron frequency in the non-relativistic case, $\omega_c = eB/m$, the cyclotron frequency given in Eq. 3.19 does not depend on the mass, which is to be expected since the band mass in graphene is zero.

The eigenvalues of the Hamiltonian can be obtained by solving the eigenvalue equation, $H_B^{\xi}\psi_n = \epsilon_n\psi_n$ where the meaning of the subscript n will be made explicit later. The spinor has two components and is of the form [106]

$$\psi_n = \begin{pmatrix} u_n \\ v_n \end{pmatrix}. \tag{3.20}$$

Solving the eigenvalue equation yields

$$a^{\dagger}av_n = \left(\frac{\epsilon_n}{\omega_c}\right)^2 v_n, \tag{3.21}$$

for the second spinor component. Thus, up to a constant, we can identify the second spinor component, v_n, with an eigenstate, $|n\rangle$, of a quantum harmonic oscillator number operator $a^{\dagger}a$ which satisfies $a^{\dagger}a\,|n\rangle = n\,|n\rangle$ for $n \geq 0$ and n labels the Landau level.

Hence, from Eq. 3.21, we find that the energy of the eigenstate is given by

$$\left(\frac{\epsilon_n}{\omega_c}\right)^2 = n \Rightarrow \epsilon_{\lambda,n} = \lambda\omega_c\sqrt{n}, \tag{3.22}$$

where $\lambda = \pm$. Thus there are states with both positive and negative energies. We previously defined λ to be the band index with $\lambda = +$ for the conduction band and $\lambda = -$ for the valence band in the absence of the magnetic field. Expressing the energy in terms of the magnetic field we obtain

$$\epsilon_{\lambda,n} \propto \lambda\sqrt{2nB}. \tag{3.23}$$

The relativistic Landau levels disperse as $\lambda\sqrt{nB}$, Fig. 3.3, as opposed to nB in the non-relativistic case, Fig. 2.3. The first component of the spinor can be obtained by noting that $u_n \sim a v_n \sim a\,|n\rangle \sim |n-1\rangle$. The zeroth Landau level (ZLL), $n = 0$, is special since $a\,|n=0\rangle = 0$ and hence $u_n = 0$ and hence the spinor is given by

$$\psi_0 = \begin{pmatrix} 0 \\ |0\rangle \end{pmatrix}. \tag{3.24}$$

For higher Landau levels, $n \neq 0$, the spinor is given by

$$\psi^{\xi}_{\lambda,n\neq 0} = \begin{pmatrix} |n-1\rangle \\ \xi\lambda\,|n\rangle \end{pmatrix}. \tag{3.25}$$

For the $n = 0$ Landau level, only one of the components is non-zero. From Eq. 3.17 this component corresponds to the K valley ($\xi = +$) for the B sublattice and to the K' valley ($\xi = -$) for the A sublattice. Thus the valley pseudospin and sublattice pseudospin coincide for the ZLL.

Electrons in graphene have not only a twofold spin degeneracy but also a twofold valley degeneracy as a consequence of there being two inequivalent points, K and K', which determine the low energy properties of electrons. Hence for the IQHE in graphene the filling fraction changes in steps of 4 between Hall plateaux. The Hall resistance is quantized at filling fractions [49, 50]

$$\nu = \pm 4\left(n + \frac{1}{2}\right) = \pm(4n+2). \tag{3.26}$$

The shift of 2 can be explained as follows: in the non-relativistic case for the zeroth Landau level, in the absence of charge-carriers, $\nu = 0$ corresponds to a completely empty Landau level. In the case of graphene, at charge neutrality $\nu = 0$, the lowest Landau level is only half filled. The Fermi level lies inside the lowest Landau level rather than in between two Landau levels which is the criterion for the IQHE. The condition for the IQHE is that the zeroth Landau level is either completely filled, $\nu = 2$, or that it is completely empty, $\nu = -2$. The sequence of IQHE states given by Eq. 3.26 has been demonstrated experimentally [51, 52].

Interaction Induced Integer Quantum Hall Effect

The sequence of IQHE states in graphene given in Eq. 3.26 occur at low magnetic fields ($\lesssim 10\,\mathrm{T}$) and can be understood solely in terms of a picture of noninteracting fermions. As the magnetic field is increased, additional plateaux are observed at $\nu = 0, \pm 1, \pm 4$ [108, 109] which are not compatible with a non-interacting picture. Graphene on a $h-$BN substrate also showed Hall states at $\nu = \pm 3$ [55]. For the $\nu = \pm 4$ state the energy gap was found to scale linearly with the total magnetic field, implying that the spin degeneracy of the $n = \pm 1$ Landau level is lifted by the Zeeman coupling while for $\nu = 0, \pm 1$ the gap was seen to be independent of the parallel component of the applied magnetic field for small parallel field [108]. The presence of a quantum Hall state at $\nu = 0, \pm 1$ implies that the four fold spin-valley degeneracy of the lowest Landau level has been lifted (breaking of symmetry). Such a lifting of degeneracy cannot be explained without the inclusion of electron-electron interactions.[2]

Several mechanisms have been proposed for the breaking of symmetry [105, 110–124]. These symmetry breaking proposals fall into three general categories. One set of proposals take the broken symmetry broken to be the chiral (sublattice) symmetry, leading to the presence of chiral symmetry breaking (CSB) orders like charge-density wave (C) and anti-ferromagnetism (N) [105, 110–112, 116, 118, 119, 125, 126]. Another proposal corresponds to valley-odd quantum Hall ferromagnetism (QHFM) [113, 114, 117, 122, 124, 127]. A third set of proposals showed that the magnetic catalysis orders and the QHFM orders necessarily coexist indicating that the two sets of orders have a common dynamical origin. This proposal goes under the broad category of generalized magnetic catalysis [121, 125, 126, 128].

Quantum Hall Ferromagnetism

The QHFM state minimizes the Coulomb energy within a single Landau level. The way to achieve this is by making the electrons stay as far apart as possible to lower the interaction energy which in turn implies that the wavefunction be spatially antisymmetric. In the zeroth Landau level this leads to the spin and valley parts of the wavefunction being symmetric at commensurate fillings. Thus, within the zeroth Landau level in the QHFM picture there is a SU(4) symmetry in the spin + valley indices at integer fillings listed in Eq. 3.27. At quarter-filling ($\nu = -1$), half-filling ($\nu = 0$), and three-quarters-filling ($\nu = 1$) the SU(4) symmetry is spontaneously broken by a SU(4) ferromagnetic state. Symmetry breaking within the zeroth Landau level leads to the splitting of the four-fold

[2] Although the presence of a substrate, like hBN, might also be able to lift the degeneracy, $\nu = 0, \pm 1$ have been observed in suspended graphene where there are no substrate effects [56].

degenerate levels into either two two-fold degenerate levels or four non-degenerate levels. In order to get a better understanding of how this comes about it is useful to define a reduced filling factor for the highest filled Landau level, with index n, that is completely filled, ν_G as [127],

$$\nu_G = \nu - 4n + 2 \leq 4. \tag{3.27}$$

Thus for the sequence in Eq. 3.26 a completely filled Landau level, for any n, corresponds to $\nu_G = 4$ and for $\nu_G = 1, 2, 3$ the Landau level is partially filled. QHFM occurs at these partial fillings of the Landau level.

Given that the system has an SU(4) symmetry, the wavefunction that describes the system at these partial fillings is [113, 127]

$$|\Psi_0\rangle = \prod_{1\leq\sigma\leq\nu_G} \prod_k c^\dagger_{k,\sigma} |0\rangle\,, \tag{3.28}$$

where σ labels the internal states and runs from 1 to 4 and k labels an intra Landau level orbital index. For the Landau gauge, k is the wave-vector in the direction of the plane wave propagation and for the symmetric gauge, k labels the angular momentum. $|0\rangle$ is the vacuum state and $c^\dagger_{k,\sigma}$ is the electron creation operator. As an example, in Ref. [124] the $\nu = \pm 1$ state was proposed to be a spin-polarized charge density wave state with a larger electron density on one of the sublattices. For this state the wavefunction in Eq. 3.28 can be written as

$$|\,\nu = \pm 1\rangle = \prod_m c^\dagger_{\uparrow A,m} |0\rangle\,, \tag{3.29}$$

where the electron creation operator $c^\dagger_{\uparrow A,m}$, creates an electron in the $n = 0$ Landau level with spin up and angular momentum m that lies on the A sublattice of the honeycomb lattice.

The state in Eq. 3.28 was proposed to be the exact ground state for a broad class of repulsive interactions, especially for $\nu_G = 1$ [113]. Electrons added to the system occupy the empty internal state and thereby lose exchange energy [127] which results in an energy cost leading to the incompressibility of the state.

The result of the presence of a QHFM order, Δ_Q, is to split the energy levels and lower the energy by such a splitting. Thus at half-filling when all the negative energy Landau levels are completely filled we have, from Eq. 3.23,

$$\epsilon_{-;n} = -\sqrt{2nB} \pm \Delta_Q. \tag{3.30}$$

This is to be contrasted to the chiral symmetry breaking (CSB) picture, discussed below, where the effect of the presence of the chiral symmetry breaking order, Δ_{CSB} is to push

down all of the filled energy levels [129, 130] and thus

$$\epsilon_{-,n} = -\sqrt{2nB + \Delta_{CSB}^2}. \tag{3.31}$$

The CSB picture of quantum Hall states at $\nu = 0, \pm 1$ arises out of interaction driven CSB orders that are induced by the process of magnetic catalysis which we briefly review.

Magnetic catalysis

Magnetic catalysis refers to the enhancement of dynamical symmetry breaking in the presence of an external magnetic field [129]. The essence of magnetic catalysis lies in the dimensional reduction that occurs in the presence of an external magnetic field and the formation of fermion-antifermion condensates that are associated with spontaneous symmetry breaking leading to the dynamical generation of a mass/energy gap in the energy spectrum. For a system of Dirac fermions in 2+1 dimensions in the presence of an external magnetic field the energy is found to be [129]

$$\epsilon_{\lambda,n} = \lambda\sqrt{2nB + m^2}, \tag{3.32}$$

where m is the mass and $\lambda = \pm$ labels the conduction (+) or the valence (−) band. Importantly we note that for all the Landau levels with $n > 0$, the energy is shifted up ($\lambda = +$) or down ($\lambda = -$) with the exception of the $n = 0$ Landau level which is now split into two with one sublevel having positive energy $\epsilon = m$ and the other sublevel having negative energy $\epsilon = -m$. The degeneracy of states for the $n = 0$ level is $eB/2\pi$ while that for $n > 0$ is eB/π. The factor of two difference in the degeneracies comes from half-filled vs filled LLs [129]. When the mass term is much smaller than the magnetic energy term, $m \ll \sqrt{eB}$, the low energy theory is completely described by the zeroth Landau level. There is no dependence on momentum, which is not surprising, since the magnetic field quenches the kinetic energy completely in two-dimensions.

For Dirac fermions placed in a magnetic field in 2+1 dimensions there is a spontaneous symmetry breaking which leads to a nonzero chiral condensate which in the limit of a vanishing mass $m \to 0$ is [129]

$$\langle\bar{\Psi}\Psi\rangle = -\frac{eB}{2\pi}. \tag{3.33}$$

The term on the right hand side is exactly the degeneracy of states in the lowest Landau level. Thus even when the mass term is zero, in the presence of a magnetic field there is spontaneous breaking of chiral symmetry. In [129] it was further shown that in the presence of weak interactions there is a dynamical mass that is generated by the magnetic field.

3.1.1 Magnetic catalysis in Graphene

At strong magnetic fields there are additional plateaux at $\nu = 0, \pm 1$ in graphene. The presence of these states cannot be explained in a picture of non-interacting electrons. It is necessary to include interactions. In the case of the zeroth Landau level in graphene the four fold degeneracy of the Landau level can be removed when there is dynamical generation of a Dirac mass [110, 116, 118, 119, 131]. The mechanism of magnetic catalysis at half filling leads to pushing of the filled Landau levels down below the chemical potential, opening up a gap in the quasiparticle spectrum. Within this framework it is the sublattice degeneracy that is lifted in the zeroth Landau level with the symmetry breaking being equal or opposite for the two spin projections depending on the interaction strength. A charge density wave would correspond to the former and antiferromagnetism to the latter. Here we follow the mechanism proposed in [118, 119].

We begin by defining the extended Hubbard model [119] as $H = H_0 + H_1$

$$H_0 = -t \sum_{A,i,\sigma=\pm} u^\dagger_\sigma(A) v_\sigma(B) + H.c., \tag{3.34}$$

$$H_1 = U \sum_{X \in A,B} n_+(X) n_-(X) + \frac{V}{2} \sum_{A,i,\sigma,\sigma'} n_\sigma(A) n_{\sigma'}(B), \tag{3.35}$$

where H_0 is a non-interacting tight binding Hamiltonian for graphene in the low energy limit. $n_\sigma(A) = u^\dagger_\sigma u_\sigma$ and $n_\sigma(B) = v^\dagger_\sigma v_\sigma$ with $\sigma = \pm 1$. H_1 contains two terms. The first term corresponds to the on-site interaction and the second to the nearest neighbour interaction. The nearest neighbour repulsive interaction can be thought of as arising from the short range part of a Coulomb interaction between the electrons. In the presence of a magnetic field perpendicular to the plane of graphene sheet, H_0 can be rewritten in the form

$$H_0 = \int d\mathbf{x} \sum_\sigma \Psi^\dagger_\sigma(\mathbf{x}) i\gamma_0\gamma_i D_i \Psi_\sigma(\mathbf{x}), \tag{3.36}$$

where Ψ_σ was defined in Eq. 3.13 and $D_i = i\partial_i - A_i$ and the magnetic field $B = \partial_1 A_1 - \partial_2 A_2$. Consider an auxiliary Hamiltonian [119] of the form

$$H = mM + i\gamma_0\gamma_i D_i, \tag{3.37}$$

with M being a 4×4 Hermitian matrix. Clearly when $m = 0$ then $H = H_0$. If the matrix M satisfies $\{H_0, M\} = \{\gamma_0\gamma_i, M\} = 0$ and $M^2 = 1$ then squaring the Hamiltonian gives

$$H^2 = D_i^2 + B(\sigma_z \otimes \sigma_z) + m^2. \tag{3.38}$$

One of the possible forms the matrix M can have is [119]

$$M = a(I_2 \otimes \sigma_z) + b(\sigma_x \otimes \sigma_x) + c(\sigma_y \otimes \sigma_x), \tag{3.39}$$

with real coeffcients a, b, c which satisfy $a^2 + b^2 + c^2 = 1$.

The eigenvalues of H^2 are $2nB + m^2$ for $n = 0, 1, 2, \ldots$. When $n > 0$ this implies that the eigenvalues of H are $\pm\sqrt{2nB + m^2}$ with a degeneracy of B/π per unit area. This is the same as when $m = 0$. For $n = 0$ the eigenvalues of H for any choice of (a, b, c) in M are $\epsilon = \pm|m|$ and the degeneracy is halved, $B/2\pi$ per unit area.

The spectrum of H is invariant under rotations of the combination (a, b, c). This is a consequence of the SU(2) chiral symmetry of H_0. Any particular choice of of M in H breaks this SU(2) symmetry and it leads to the same eigenvalues. Such a chiral-symmetry breaking gap and further splitting of the Landau levels by a Zeeman effect can lead to IQH states at $\nu = 0, \pm 1$. We can add the Zeeman term explicitly to the non-interacting part, H_0, and we get

$$H_D = \sigma_0 \otimes i\gamma_0\gamma_i D_i + \lambda(\sigma_3 \otimes I_4), \tag{3.40}$$

where $\lambda = g\mu_B B$ is the Zeeman coupling. Here we have enlarged the degrees of freedom considered by including the spin degrees of freedom with the 2×2 matrices acting on spin index on top of the valley + sublattice degree of freedom with the 4×4 γ matrices acting on valley + sublattice indices. The effect of mass generation is to split the $n = 0$ Landau level (LL) whereas for $n \neq 0$ LLs the negative energy states are all pushed down and the positive energy states are all pushed up. In non-relativistic systems, like GaAs heterostructures, there is a lowest Landau level (LLL), $n = 0$, and the quantum Hall states appear within the first few LLs. In graphene the $n = 0$ LL is in the middle rather than the bottom of the spectrum as a result of the relativistic spectrum with all the negative energy states completely filled at half-filling of the $n = 0$ LL. Hence the total energy of the filled LLs is maximally lowered by formation of CSB orders.

When there is chiral-symmetry breaking leading to mass generation it is natural to ask what kind of order parameters are present in the IQH states at $\nu = 0, \pm 1$. Starting from the interaction part of the extended Hubbard Hamiltonian, Eq. 3.35, we can define the easy-axis Neél (N), ferromagnetic (F) and charge-density wave (C) order parameters as

$$\mathbf{N} = \langle \mathbf{m}(A) - \mathbf{m}(B) \rangle; \quad \mathbf{F} = \langle \mathbf{m}(A) + \mathbf{m}(B) \rangle; \quad C = \langle n(A) - n(B) \rangle, \tag{3.41}$$

where $\mathbf{m}(A) = u^\dagger_\sigma \boldsymbol{\sigma}_{\sigma\sigma'} u_{\sigma'}$ is the magnetization on sublattice A. Similarly $\mathbf{m}(B) = v^\dagger_\sigma \boldsymbol{\sigma}_{\sigma\sigma'} v_{\sigma'}$ is the magnetization for sublattice B. Setting the magnetization to be parallel to the

magnetic field, $\mathbf{F} \rightarrow F_3 = F$ we finally have the full single particle effective Hamiltonian in the presence of a magnetic field :

$$H = \sigma_0 \otimes i\gamma_0\gamma_i D_i + (\lambda + F)(\sigma_3 \otimes I_4) + (\mathbf{N}\cdot\boldsymbol{\sigma} + CI_2) \otimes \gamma_0. \tag{3.42}$$

Using compressibility [132], capacitance [133] and transport [134] the dependence of the gaps at $\nu = 0, \pm 1$ on the magnetic field has been studied extensively. The results of these experiments showed a crossover from a linear dependence [134] on magnetic field, B, to sublinear [133] to almost a $\sqrt{B}$ dependence [132] with increasing field strength. This type of crossover of scaling of the gap with the magnetic field cannot be captured by a simple estimate of $\sqrt{B}$ scaling due to the long-range Coulomb interaction, necessitating the inclusion of the finite-range components of Coulomb interaction. In pristine graphene in the presence of even weak on-site interactions the $\nu = 0$ state has an underlying antiferromagnetic order (N) [118, 119] and the inclusion of the Zeeman term, (λ), projects the anti-ferromagnetic order to be easy-plane and perpendicular to the magnetic along with the simultaneous appearance of a ferromagnetic order parallel to the magnetic field (F) [118].

The magnetic field dependence of the gaps arising from CSB orders for quantum Hall states at $\nu = 0, \pm 1$ was compared with experiments in Ref. [130], finding good agreement. Edge states in the presence of chiral symmetry breaking orders were also studied in Ref. [135] and were found to be in agreement with experimental results in Ref. [136]. In particular comparison of numerical studies in Ref. [130] with experiments [132–134] lead to the pciture that $\nu = 0$ has an underlying easy-plane antiferromagnetic order $N_\perp$ with a weak ferromagnetic order F when a Zeeman term is included. The $\nu = 1$ state on the other hand was found in Ref. [130] to be consistent with a charge density wave order, C, with an easy-axis antiferromagnetic order, N_3.

There have been some more recent experimental [137–139] and theoretical [140, 141] papers that suggest the true nature of states in the ZLL may be more complicated than the picture put forward in the CSB scenario.

3.1.2 Fractional Quantum Hall Effect In Graphene

The fractional quantum Hall effect has also been observed in graphene [53–59]. Fig. 3.4 shows incompressible states at fractional filling in graphene [56]. Theoretical interest in the FQHE in graphene has also been considerable [142–156]. The IQHE in graphene differs from the IQHE in other two-dimensional electron gases (2DEG) due to the relativistic dispersion and the underlying SU(4) symmetry of electrons in graphene when placed in a magnetic field. Naturally we would like to compare the FQHE in graphene and other 2DEG. In Sec. 2.1.1 we saw how the pseudopotential description

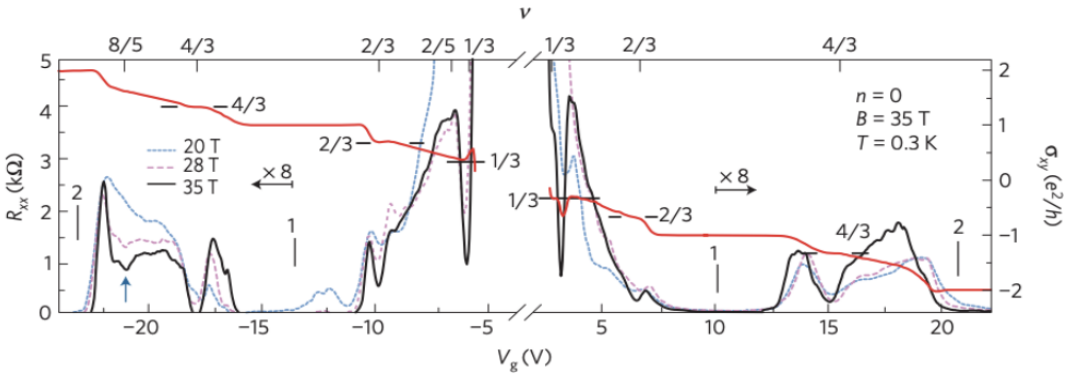

Figure 3.4: FQHE in graphene: , Magnetoresistance, R_{xx}, (left axis) and Hall conductivity, σ_{xy}, (right axis) in the $n = 0$ and $n = 1$ Landau levels in graphene plotted as a function of applied gate voltage, V_g. Reprinted with permission from Ref. [55].

is well suited to describe FQHE in not only the lowest but also higher Landau levels in terms of an effective interaction. The Landau level form factors for the case of 2DEG were found to be

$$F_n^{2DEG}(\mathbf{q}) = L_n(q^2 l_B^2/2) e^{-q^2 l_B^2/4}. \tag{3.43}$$

The form factors for graphene have the form [157]

$$F^G_{n=0}(\mathbf{q}) = e^{-q^2 l_B^2/4}; \quad F^G_{n\neq 0}(\mathbf{q}) = \frac{1}{2}[L_{n-1}(q^2 l_B^2/2) + L_n(q^2 l_B^2/2)] e^{-q^2 l_B^2/4}. \tag{3.44}$$

As mentioned earlier, within a partially filled Landau level that is well separated from other Landau levels the kinetic energy of the particles is quenched and the Hamiltonian of the system is solely determined by the interactions between particles within the Landau level. For electrons in the n^{th} Landau level, considering only Coulomb interactions, the effective interaction potential is given by

$$V^D_{\text{eff}}(\mathbf{q}) \sim \frac{1}{\epsilon(\mathbf{q})|\mathbf{q}|}[F^D_n(\mathbf{q})]^2 \quad D = G, 2DEG\,. \tag{3.45}$$

We see that the effective interaction potential is dependent on the Landau level form factor. We can also calculate the pseudopotential parameters given in Eq. 2.57 with the form factors given in Eq. 3.44. A comparison of the pseudopotential parameters for the $n = 0$ and $n = 1$ Landau level in a "non-relativistic" system and graphene is shown in Fig. 3.5. In the zeroth Landau level the form factor, and hence the effective potential, is the same for both graphene and other 2DEGs and hence within the pseudopotential formalism there is no difference between the two systems. For $n = 1$ we see that the

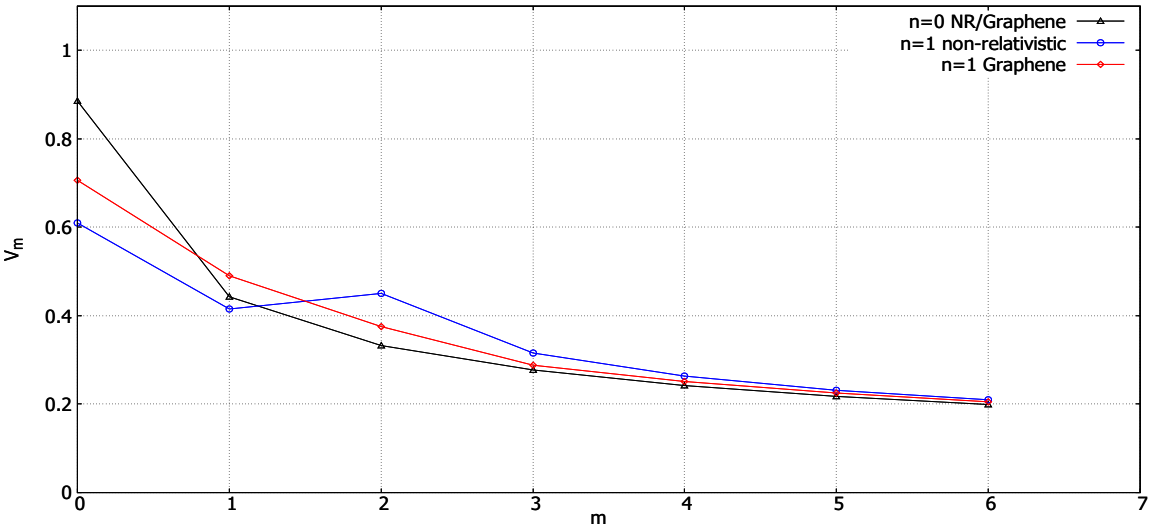

Figure 3.5: Pseudopotential V_m as a function of relative angular momentum m. Pseudopotentials for $n = 0$ for graphene/non-relativistic system (black), for $n = 1$ in graphene (red) and $n = 1$ in non-relativistic system (blue).

effective interaction is different and hence we expect there to be a difference in the FQH states in the $n = 1$ Landau level of non-relativistic 2DEG and the $n = 1$ FQH state of graphene. The same is true for higher Landau levels too.

From the above discussion it seems clear that FQHE in graphene and 2DEG are not different due to the underlying form of the Landau level i.e. relativistic or non-relativistic energy spectrum. The major difference (for $n \neq 0$) arises from the difference in effective interaction potential which in turn is a consequence of different wavefunctions that describe the system. The other key difference is the underlying SU(4) symmetry of the Landau levels in graphene. In this thesis we primarily focus on the $n = 0$ Landau level of graphene and hence we will focus on the underlying SU(4) symmetry of the Landau levels and describe the FQHE in graphene in the presence of the chiral symmetry breaking orders described in the previous section.

In the next chapter we will develop the theory of FQHE in graphene in terms of a multi-component flux attachment scheme which is a generalization of the composite fermion picture described in Sec. 2.1.2.

Chapter 4

Even Denominator Fractional Quantum Hall Effect in Graphene

The fractions ν initially observed in experiments on the FQHE had odd denominators. The absence of experimental observation of even denominator fractional quantum Hall (EDFQH) states remained a puzzle. Laughlin's many particle wavefunction [48], due to its anti-symmetry, was mainly applied to odd denominator, $\nu = 1/m$, FQH states. The hierarchical schemes also inherited the anti-symmetry feature and thus were used to explain the other odd denominator fractions [73, 74]. No symmetry based arguments could be given for the apparent absence of EDFQH states. Theoretical studies predicted a state at $\nu = 1/2$ [158, 159] without the formation of a FQH state. A minimum in the longitudinal resistivity, ρ_{xx}, was observed at even denominator fractions in higher LLs, $n \neq 0$, [47, 160] and a plateau in the Hall resistivity, ρ_{xy}, was observed for the $\nu = 2+1/2 = 5/2$ state in the $n = 2$ LL [161]. EDFQH states were observed for $\nu = 1/2$ [162–164] and $\nu = 1/4$ [165, 166] in the $n = 0$ LL of multicomponent systems (in semiconductors) but no incompressible states have been observed in the lowest Landau level of a single component system. [1]

Halperin, Lee and Read (HLR) [95] and Zhang and Kalmeyer [167] independently proposed theories for the $\nu = 1/2$ state. The HLR theory was based on the the Chern-Simons composite Fermion (CS-CF) theory proposed by Fradkin and Lopez [168] to explain the "Jain" sequence [83] of FQH states given by

$$\nu = \frac{p}{2mp+1}. \tag{4.1}$$

[1] In this context single and multicomponent refers to the internal degrees of freedom of the electrons in the system. Unpolarized electrons, electrons confined to two spatially separated layers or electrons confined to two electronic subbands all would constitute two-component systems. Graphene with spin and valley and sublattice pseudospin all considered would correspond to an eight-component system. Completely spin polarized electrons on the other hand would be an example of a single component system.

To recapitulate, in the composite fermion picture, a system of electrons in a FQH state with filling fraction given by Eq. 4.1 is mathematically equivalent to a system of composite fermions (electrons bound to an even number of flux quanta $2m$) that are in an IQH state with m composite fermion Landau levels filled. In field theoretic terms a system of electrons in the FQH state with $\nu = p/(2mp+1)$ is equivalent to a system of composite fermions interacting with a Chern-Simons gauge field in a magnetic field different from the external applied field (Eq. 2.58).

The sequence of fractions (setting $m = 1$, i.e. attaching 2 flux quanta per electron) given in Eq. 4.1 leads to even denominator fraction, $\nu = 1/2$ in the limit $p \to \infty$. The effective field (Eq. 2.59) that the CFs experience in this limit becomes zero

$$B_{\text{eff}} = B - B_{1/2} = \frac{\Phi_0 \rho_0}{p} \xrightarrow[p\to\infty]{} 0, \tag{4.2}$$

where we have defined $B_{1/2} = 2\Phi_0\rho_0$.

The limit $p \to \infty$ also describes a situation with an infinite number of CF Landau levels filled. For 2DEGs at zero magnetic field there is a well defined Fermi surface. If the density of fermions is held constant, the system exhibits IQH states at filling fractions given by Eq. 2.25 as the magnetic field is changed. Similarly for CFs when the effective magnetic field is zero (corresponding to a half filled Landau level of electrons, $\nu = 1/2$) there is a well defined Fermi surface and as the effective magnetic field is tuned the CFs exhibit IQH states at "filling fractions" $\nu_{CF} = p$ which correspond to an FQH state for electrons given by (with $m = 1$) Eq. 4.1.

The Fermi surface comes associated with a well defined Fermi wave-vector given by [95]

$$k_F = (4\pi\rho_0)^{1/2}. \tag{4.3}$$

Away from $\nu = 1/2$ the fermions are expected to exhibit cyclotron motion with

$$R_C = \frac{\hbar k_F}{eB_{\text{eff}}}, \tag{4.4}$$

in the effective magnetic field [95, 169]. Using surface acoustic waves Willett *et al.* [170], were able to observe a geometric resonance with cyclotron orbits of the charge carriers thus solidifying not only the theory proposed by HLR but also giving physical confirmation to the existence of the composite fermions.

Even denominator FQH states were observed in graphene recently [171]. As was mentioned in Sec. 3.1.2 the spatial wavefunctions for FQH states in the $n = 0$ Landau level in graphene are expected to be the same as in the non-relativistic case owing to the Landau level form factor (or the orbital wavefunctions), Eq. 2.54, being the same for

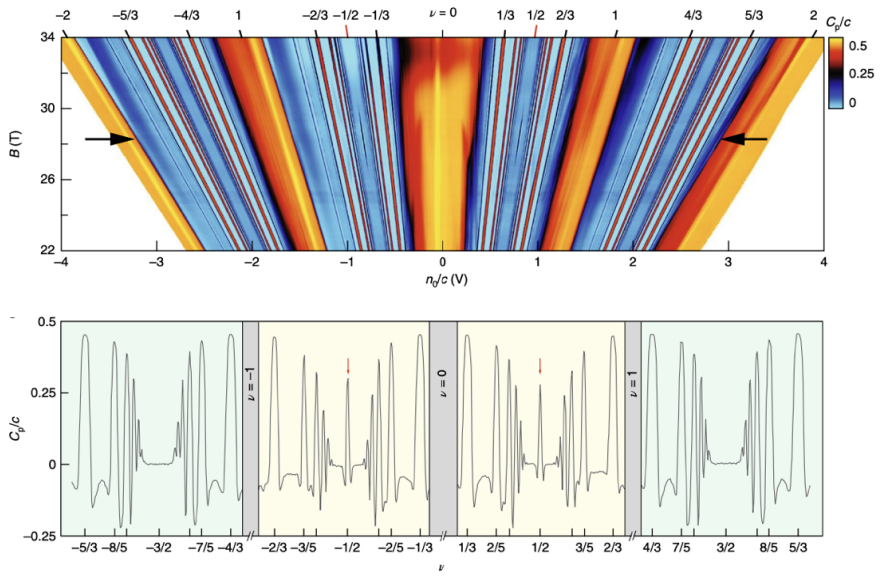

Figure 4.1: Top: Penetration field capacitance C_p/c plotted as a function of magnetic field, B and the charge density n_0/c where c is the average geometric capacitance of the two gates. Bottom: Incompressible states (indicated with red arrows) at even denominator fractions $\nu = \pm 1/2$ shown in a plot of C_P/c vs ν for $B = 28.3T$. Note that the $\nu = \pm 3/2$ states that are further away from the charge neutrality point remain compressible. Reprinted with permission from [171].

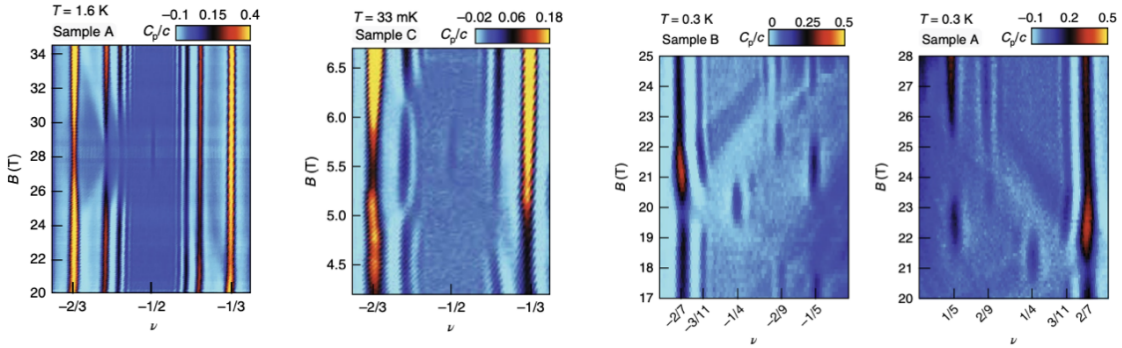

Figure 4.2: Left to right : C_P as a function of filling factor ν in the vicinity of $\nu = -1/2$, $\nu = 1/2$, $\nu = -1/4$ and $\nu = 1/4$ at different temperatures. Reprinted with permission from [171].

both the systems. As a consequence, single component EDFQH states are not expected to be seen. As also mentioned, in the introductory paragraph of the chapter, EDFQH states have been observed in multicomponent systems which implies that the EDFQH state likely has a multicomponent nature. The underlying spin and valley degrees of freedom of electrons in graphene play the role of layer/subband in the non-relativistic case. Before getting into a theoretical description of these states we give a brief overview of the experiment that observed the EDFQH state in graphene [171].

4.1 Experimental Observation of $\nu = 1/2, 1/4$ States in Graphene

The setup used by Zibrov *et al.* [171] consisted of a heterostructure of monolayer graphene sandwiched between layers of hexagonal boron nitride (hBN) and gate electrodes that were made up of graphite, on either side [171, 172]. They measured the penetration field capacitance, C_p, which is the differential capacitance between the top and bottom gates while the monolayer graphene is held at constant chemical potential. Penetration field capacitance is proportional to the inverse of the thermodynamic incompressibility ($\kappa^{-1} \propto d\mu/dn$) [171–174].

Figure 4.1(top) is a colour plot of the penetration field capacitance, C_p, divided by the average geometrical capacitance of the top and bottom gates, c, as a function of the magnetic field, B, and the charge density, $n_0/c = V_t + V_b - 2V_s$ where V_t, V_b and V_s are the voltages applied to the top gate, bottom gate and sample respectively. Incompressible states appear as high values of C_p. The quantized Hall conductance of gapped states at fixed filling factors is equal to the slope in the density-magnetic field ($n-B$) plane given by the Středa formula [175]. The bottom of Fig. 4.1 is a plot of C_p/c as a function of the filling factor ν at a fixed magnetic field, $B = 28.3$T. There are sharp peaks in C_p/c indicating incompressible states at $\nu = \pm 1/2$ whereas the states $\nu = \pm 3/2$ do not show a sharp peak in C_p/c indicating that the states are likely to be compressible. In Fig. 4.2 there is also a peak in the C_p/c value at $\nu = \pm 1/4$, again indicating an incompressible state.

The key features observed by Zibrov *et. al.* [171] are:

- Only the EDFQH states $\nu = \pm 1/2$ and $\nu = \pm 1/4$ are incompressible whereas other incompressible EDFQH states are absent (Fig. 4.1). This is most likely owing to the proximity of the observed incompressible state to the charge neutral state at $\nu = 0$.
- The EDFQH states appear for a small range of magnetic fields and then subsequently disappear (Fig. 4.2) at higher or lower magnetic fields

- At the magnetic fields at which these two EDFQH states are observed, some odd denominator fractions coexist with them ($\nu = 1/3, 1/5, 2/3, 2/7, 3/7, 4/9$), while other fractions disappear or weaken ($\nu = 2/9, 3/11$) (with some sample dependence).

Zibrov *et al.* proposed that the EDFQH states are associated with a phase transition from a partially sublattice polarized (PSP) to a canted antiferromagnet (CAF) phase [171]. Below we compare to their experimental observation using the framework of the Chern-Simons theory of multicomponent FQH states in graphene in the presence of symmetry breaking orders [145, 176].

4.2 Multicompnent Flux Attachment Scheme and Chern-Simons Theory

One[2] of the distinguishing features of the FQH effect in monolayer graphene is that there are four isospin components in the zeroth LL, corresponding to two valley and two spin degrees of freedom [142, 143, 145–149, 152, 153, 155, 156, 177]. In addition, due to strong electronic interactions (e.g. onsite Hubbard repulsion), these states cannot be assumed to be spin polarized. This allows for more degrees of freedom than in systems that have previously demonstrated EDFQH states at $\nu = \pm\frac{1}{2}$ and $\nu = \pm\frac{1}{4}$, and a wide variety of possible states need to be considered in composite fermion or Chern-Simons theories. Previous theoretical studies of the integer Quantum Hall states at $\nu = 0$ and $\nu = \pm 1$ that take into account filled LLs [130, 178, 179] have inferred a preference for CSB orders due to strong LL mixing. Calculations based on this idea have shown good agreement with experiment [130, 180]. Ref. [130] argued for the presence of a canted antiferromagnet for $\nu = 0$ and charge-density-wave (CDW) order with a small component of Neel antiferromagnetism (AFM) at $\nu = 1$. Hence we suggest that CSB may be operative for FQH states with $0 < |\nu| < 1$. We make use of the framework for the Chern-Simons theory of multi-component FQH states in graphene in the presence of symmetry breaking orders [145, 153, 181] to investigate possible composite fermion wavefunctions for the observed EDFQH states. In the $n = 0$ LL of graphene, sublattice and valley degrees of freedom are equivalent in the absence of sublattice-symmetry breaking orders. We start from a chirally symmetric theory and allow for the possibility of dynamical symmetry breaking in the FQH states.

The possibility of incompressible EDFQH states in monolayer graphene was noted in Ref. [145]. However, there are numerous ways to realize such fractions. Our approach

[2]The rest of the chapter is based on the publication S. Narayanan, B. Roy and M. P. Kennett, Phys. Rev. B **98**, 235411 (2018).

to identifying candidate variational states is as follows. First, we consider flux attachment schemes that give either $\nu = \frac{1}{2}$ or $\nu = \frac{1}{4}$. Second, we use the key features of the observations mentioned in the previous section to winnow out candidate states by postulating that for filling fractions close to the EDFQH the most likely states to be seen at the same magnetic field are those with the same flux attachment scheme. We also determine the other fractions that naturally arise from the flux attachments that give rise to EDFQH states and compare with the experimental observations to narrow down the possible states that might give rise to EDFQH effects.

We identify candidate variational wavefunctions for the observed EDFQH states which are summarized in Tables 4.1 and 4.5. We observe that the majority of these candidate states show CSB in the form of either a CDW or AFM. In light of this result and the role that chiral symmetry plays in the integer quantum Hall effect in the zeroth LL [130], we suggest that CSB is likely a unifying phenomenon for both regular and composite Dirac fermions in the zeroth LL in monolayer graphene. We discuss experiments that can be used to test this idea and to discriminate between potential orderings for a given flux attachment scheme.

4.2.1 Composite Fermions and Symmetry Breaking

The effective low energy Hamiltonian for graphene is $H = H_+ \oplus H_-$, which acts on eight component spinors $\Psi = [\Psi_{\mathbf{K}}, \Psi_{-\mathbf{K}}]^\top$, where for $\tau = \pm$, $\Psi^\top_{\tau\mathbf{K}} = [u_\uparrow, v_\uparrow, u_\downarrow, v_\downarrow](\tau\mathbf{K})$, $\pm\mathbf{K}$ label the two valleys and $u(v)$ is the amplitude on the $A(B)$ sublattice of graphene's honeycomb lattice. In the absence of symmetry breaking orders $H_\pm$ can be written as (setting $\hbar$, $v_F = 1$)

$$H_\pm \;=\; \pm I_2 \otimes \sigma_1 \, D_1 - I_2 \otimes \sigma_2 \, D_2, \tag{4.5}$$

where $D_i = -i\partial_i - eA_i$, $\mathbf{A}$ is the vector potential. We label the valley-spin configurations $(\mathbf{K}\uparrow), (\mathbf{K}\downarrow), (-\mathbf{K}\uparrow), (-\mathbf{K}\downarrow)$ by $\alpha = 1, 2, 3, 4$, respectively. We can thus write the kinetic part of the Hamiltonian as [145]

$$H = \sum_\alpha \Psi^\dagger_\alpha (\pm\sigma_1 D_1 - \sigma_2 D_2) \Psi_\alpha,$$

where $\Psi^\dagger_\alpha = \left(u^\dagger_\alpha, v^\dagger_\alpha\right)$. We introduce the transformation

$$\Psi_\alpha = e^{i\Phi_\alpha} \tilde{\psi}_\alpha, \tag{4.6}$$

where $\tilde{\psi}_\alpha$ is a composite fermion (CF) field and

$$\Phi_\alpha = \mathscr{K}_{\alpha\beta} \int d\mathbf{r}' \arg(\mathbf{r}-\mathbf{r}')\rho_\beta(\mathbf{r}').$$

Under this transformation

$$\Psi_\alpha^\dagger (\pm\sigma_1 D_1 - \sigma_2 D_2)\Psi_\alpha \longrightarrow \tilde{\psi}_\alpha^\dagger \left(\pm\sigma_1 \tilde{D}_1 - \sigma_2 \tilde{D}_2\right)\tilde{\psi}_\alpha,$$

where $\tilde{D}_{1,2} = D_{1,2} - a_{1,2}^\alpha$, with Chern-Simons field

$$\mathbf{a}^\alpha = \mathscr{K}_{\alpha\beta} \int d\mathbf{r}' g(\mathbf{r}-\mathbf{r}')\rho_\beta(\mathbf{r}'); \quad g(\mathbf{r}) = \frac{\hat{\mathbf{z}}\times\mathbf{r}}{r^2}.$$

Here $\mathscr{K}_{\alpha\beta}$ is called the flux attachment matrix. The form of the $\mathscr{K}$-matrix considered in Ref. [145] is given by

$$\mathscr{K} = \begin{pmatrix} 2k_1 & m_1 & n_1 & n_2 \\ m_1 & 2k_2 & n_3 & n_4 \\ n_1 & n_3 & 2k_3 & m_2 \\ n_2 & n_4 & m_2 & 2k_4 \end{pmatrix}. \tag{4.7}$$

It describes the amount of flux quanta attached to a CF species, labelled by α as seen by another CF species, labelled by β. In this particular instance $\mathscr{K}_{12} = m_1$, for example, would correspond to the flux attached to composite fermion species labelled by $\alpha = \mathbf{K}\uparrow$ as seen by the CF species labelled by $\beta = \mathbf{K}\downarrow$.

Requiring the $\tilde{\psi}_\alpha$ to be fermionic places contstraints on $\mathscr{K}$ [182]. Consider the following identity for fermions :

$$\left[\rho_\alpha(\mathbf{x}), \psi_\beta(\mathbf{x}')\right] = -\delta_{\alpha\beta}\psi_\alpha(\mathbf{x})\delta(\mathbf{x}-\mathbf{x}'), \tag{4.8}$$

where $\rho_\alpha(\mathbf{x}) = \psi_\alpha^\dagger(\mathbf{x})\psi_\alpha(\mathbf{x})$. Then from Eq. 4.7 we have the relation

$$\left[\Phi_\alpha(\mathbf{x}), \psi_\beta(\mathbf{x}')\right] = \mathscr{K}_{\alpha\beta}\arg(\mathbf{x}-\mathbf{x}')\psi_\beta(\mathbf{x}'). \tag{4.9}$$

From this we can obtain the following relations

$$\begin{aligned} e^{i\Phi_\alpha(\mathbf{x})}\psi_\beta(\mathbf{x}') &= e^{-i\mathscr{K}_{\alpha\beta}\arg(\mathbf{x}-\mathbf{x}')}\psi_\beta(\mathbf{x}')e^{i\Phi_\alpha(\mathbf{x})}, \\ \psi_\beta^\dagger(\mathbf{x}')e^{i\Phi_\alpha(\mathbf{x})} &= e^{-i\mathscr{K}_{\alpha\beta}\arg(\mathbf{x}-\mathbf{x}')}e^{i\Phi_\alpha}\psi_\beta^\dagger(\mathbf{x}'). \end{aligned} \tag{4.10}$$

For two CF operators then we have the following relation (using Eq. 4.6)

$$\tilde{\psi}^{\dagger}_{\alpha}\tilde{\psi}^{\dagger}_{\beta} = (-1)e^{i\mathcal{K}_{\alpha\beta}\arg(\mathbf{x}-\mathbf{x}')}\ e^{-i\mathcal{K}_{\beta\alpha}\arg(\mathbf{x}'-\mathbf{x})}\ \tilde{\psi}^{\dagger}_{\beta}\tilde{\psi}^{\dagger}_{\alpha}, \tag{4.11}$$

where

$$e^{i\arg(z)} = \frac{z}{|z|}, \tag{4.12}$$

and finally we get

$$\tilde{\psi}^{\dagger}_{\alpha}\tilde{\psi}^{\dagger}_{\beta} = (-1)^{1-\mathcal{K}_{\beta\alpha}}\left[\frac{z-z'}{|z-z'|}\right]^{\mathcal{K}_{\alpha\beta}-\mathcal{K}_{\beta\alpha}}\tilde{\psi}^{\dagger}_{\beta}\tilde{\psi}^{\dagger}_{\alpha}. \tag{4.13}$$

For the operators $\tilde{\psi}^{\dagger}_{\alpha}$ to be fermionic the constraints on $\mathcal{K}$ are

$$\begin{aligned} \mathcal{K}_{\alpha\beta} &= \mathcal{K}_{\beta\alpha} \\ \mathcal{K}_{\alpha\alpha} &= 2k; \quad k \in \mathbb{Z}. \end{aligned} \tag{4.14}$$

Hence the $\mathcal{K}$-matrix is a symmetric matrix with even integers as its diagonal elements. There is no constraint on the off diagonal elements although we do work with off-diagonal elements being integers. If they are odd integers then mutual statistics between the different species might be bosonic.

The magnetic field, $\mathbf{b}_{\alpha}$, generated by the Chern-Simons field, $\mathbf{a}^{\alpha}$, is given by [145, 176]

$$\mathbf{b}_{\alpha} = (1/e)\nabla \times \mathbf{a}^{\alpha} = -\Phi_0\mathcal{K}_{\alpha\beta}\rho_{\beta}. \tag{4.15}$$

The effective field thus experienced by CF species α, is then

$$B_{\alpha} = B - \Phi_0\mathcal{K}_{\alpha\beta}\rho_{\beta}. \tag{4.16}$$

The magnetic field, B, corresponds to the electrons being in a FQH state with filling fraction ν and the effective magnetic field, B_{α}, for CF species α, corresponds to the CF species being in an IQH state with filling fraction ν_{α}. If the density of CF species is $\rho_{\alpha} = \Psi^{\dagger}_{\alpha}\Psi_{\alpha} = \tilde{\psi}^{\dagger}_{\alpha}\tilde{\psi}_{\alpha}$ then Eq. 4.16 can be rewritten as:

$$\frac{\rho_{\alpha}}{\nu_{\alpha}} = \frac{\rho}{\nu} - \mathcal{K}_{\alpha\beta}\rho_{\beta}. \tag{4.17}$$

We can define the CSB order parameters by relating them to the CF densities as

$$\begin{aligned} 1 &= \frac{\rho_1+\rho_2+\rho_3+\rho_4}{\rho},\ C = \frac{\rho_1+\rho_2-\rho_3-\rho_4}{\rho}, \\ F &= \frac{\rho_1-\rho_2+\rho_3-\rho_4}{\rho},\ N = \frac{\rho_1-\rho_2-\rho_3+\rho_4}{\rho}, \end{aligned} \tag{4.18}$$

where C represents charge density wave (CDW) order, F ferromagnetism and N easy axis Neel order.

The Case of Order Parameters

In the spin $\otimes$ valley subspace the CDW order, C, enters the Hamiltonian (Eq. 3.42) through a term of the form $CI_2 \otimes \sigma_3$, the ferromagnetic order, F, through $F\sigma_3 \otimes I_2$ and the easy axis Neel order, N, through a term of the form $N\sigma_3 \otimes \sigma_3$. Hence the order parameters considered in Eq. 4.18 are all diagonal in the the spin $\otimes$ valley subspace.

It is natural to wonder why order parameters that are off-diagonal in the spin $\otimes$ valley subspace are not considered since we argued in Sec. 3.1.1 that an order parameter present in the $\nu = 0$ state, within the picture of magnetic catalysis, is the easy-plane antiferromagnetic order, $N_\perp$ that is present in the Hamiltonian in Eq. 3.42 as $N_1\sigma_1 \otimes \sigma_1 + N_2\sigma_2 \otimes \sigma_2$ which is clearly off diagonal in both spin and valley indices. Moreover Zibrov *et al.* [171] consider the EDFQH state as a consequence of a phase transition from a CAF to a PSP state, both of which are off diagonal orders in the spin-valley index.

The reason for this becomes clear when we consider the transformation that takes us from fermions to CFs in Eq. 4.6. Let us consider an order parameter, $\mathcal{O}$ that is off-diagonal in one or both of the indices is present in the Hamiltonian. Under the transformation in Eq. 4.6, the term in the Hamiltonian containing $\mathcal{O}$ transforms as

$$\Psi^\dagger_\alpha \mathcal{O}_{\alpha\beta} \Psi_\beta \to \tilde{\psi}^\dagger_\alpha \mathcal{O}_{\alpha\beta} \; e^{-i(\Phi_\alpha - \Phi_\beta)} \tilde{\psi}_\beta \quad \alpha \neq \beta. \tag{4.19}$$

If the order parameter were diagonal ($\alpha = \beta$) then the exponential phase factor would cancel out and all would be well. The phase field Φ_α is in general dependent on the density of the CF species, ρ_α and the $\mathcal{K}$-matrix elements (Eq. 4.7) and only under certain conditions is it true that the exponential term in the equation vanishes but there is no a priori reason to assume it will. The same issue arises if we have a multi-layer system and we include tunneling between the different layers. If we define a layer index and perform the transformation in Eq. 4.6 a tunneling term would be like an off diagonal term in the layer index and hence would run into the same problem. To our knowledge this issue has not been resolved. Since our work is based on the flux-attachment scheme we stick to CSB orders that are diagonal in the spin-valley index. We can now rewrite

the CF densities in terms of the order paramters

$$\frac{\rho_1}{\rho} = 1 + C + F + N, \tag{4.20}$$
$$\frac{\rho_2}{\rho} = 1 + C - F - N, \tag{4.21}$$
$$\frac{\rho_3}{\rho} = 1 - C + F - N, \tag{4.22}$$
$$\frac{\rho_4}{\rho} = 1 - C - F + N. \tag{4.23}$$

Now we can expand Eq. 4.17 (dividing throughout by ρ) explicitly as

$$\begin{aligned}
\left(\frac{1}{\nu_1} + 2k_1\right)(1 + C + F + N) &= \frac{4}{\nu} - m_1(1 + C - F - N) \\
&\quad - n_1(1 - C + F - N) - n_2(1 - C - F + N), \quad (4.24)\\
\left(\frac{1}{\nu_2} + 2k_2\right)(1 + C - F - N) &= \frac{4}{\nu} - m_1(1 + C + F + N) \\
&\quad - n_3(1 - C + F - N) - n_4(1 - C - F + N), \quad (4.25)\\
\left(\frac{1}{\nu_3} + 2k_3\right)(1 - C + F - N) &= \frac{4}{\nu} - n_1(1 + C + F + N) \\
&\quad - n_3(1 + C - F - N) - m_2(1 - C - F + N), \quad (4.26)\\
\left(\frac{1}{\nu_4} + 2k_4\right)(1 - C - F + N) &= \frac{4}{\nu} - n_2(1 + C + F + N) \\
&\quad - n_4(1 + C - F - N) - m_2(1 - C + F - N). \quad (4.27)
\end{aligned}$$

We consider the following simplification of the $\mathscr{K}$-matrix where $k_1 = k_2$, $k_3 = k_4$, $n = n_1 = n_2 = n_3 = n_4$, so that the flux attachment is the same within a valley (sublattice), but not necessarily the same as the other valley (sublattice). With this simplification we

can rewrite the set of equations in Eqs. 4.24- 4.27 as

$$\begin{aligned}
\frac{4\nu_*}{\nu} &= 4+[(2k_1+m_1+2n)(\nu_1+\nu_2)+(\nu_3+\nu_4)(2k_3+2n+m_2)] \\
&\quad +C[(\nu_1+\nu_2)(2k_1+m_1-2n)-(\nu_3+\nu_4)(2k_3+m_2-2n)] \\
&\quad +F[(\nu_1-\nu_2)(2k_1-m_1)-(\nu_3-\nu_4)(2k_3-m_2)] \\
&\quad +N[(\nu_1-\nu_2)(2k_1-m_1)-(\nu_3-\nu_4)(2k_3-m_2)], \qquad (4.28) \\
\frac{4\nu_C}{\nu} &= 4C+[(2k_1+m_1+2n)(\nu_1+\nu_2)-(\nu_3+\nu_4)(2k_3+2n+m_2)] \\
&\quad +C[(\nu_1+\nu_2)(2k_1+m_1-2n)+(\nu_3+\nu_4)(2k_3+m_2-2n)] \\
&\quad +F[(\nu_1-\nu_2)(2k_1-m_1)-(\nu_3-\nu_4)(2k_3-m_2)] \\
&\quad +N[(\nu_1-\nu_2)(2k_1-m_1)+(\nu_3-\nu_4)(2k_3-m_2)], \qquad (4.29) \\
\frac{4\nu_F}{\nu} &= 4F+[(2k_1+m_1+2n)(\nu_1-\nu_2)+(\nu_3-\nu_4)(2k_3+2n+m_2)] \\
&\quad +C[(\nu_1-\nu_2)(2k_1+m_1-2n)-(\nu_3-\nu_4)(2k_3+m_2-2n)] \\
&\quad +F[(\nu_1+\nu_2)(2k_1-m_1)+(\nu_3+\nu_4)(2k_3-m_2)] \\
&\quad +N[(\nu_1+\nu_2)(2k_1-m_1)-(\nu_3+\nu_4)(2k_3-m_2)], \qquad (4.30) \\
\frac{4\nu_N}{\nu} &= 4N+[(2k_1+m_1+2n)(\nu_1-\nu_2)-(\nu_3-\nu_4)(2k_3+2n+m_2)] \\
&\quad +C[(\nu_1-\nu_2)(2k_1+m_1-2n)+(\nu_3-\nu_4)(2k_3+m_2-2n)] \\
&\quad +F[(\nu_1+\nu_2)(2k_1-m_1)-(\nu_3+\nu_4)(2k_3-m_2)] \\
&\quad +N[(\nu_1+\nu_2)(2k_1-m_1)+(\nu_3+\nu_4)(2k_3-m_2)], \qquad (4.31)
\end{aligned}$$

where we introduce the following quantities:

$$\begin{aligned}
\nu_* &= \nu_1+\nu_2+\nu_3+\nu_4, \quad \nu_C = \nu_1+\nu_2-\nu_3-\nu_4, \\
\nu_F &= \nu_1-\nu_2+\nu_3-\nu_4, \quad \nu_N = \nu_1-\nu_2-\nu_3+\nu_4.
\end{aligned}$$

Finally the set of Eqs. 4.28-4.31 can be written in a condensed form as

$$M\begin{pmatrix} 1 \\ C \\ F \\ N \end{pmatrix} = \frac{1}{\nu}\begin{pmatrix} \nu_* \\ \nu_C \\ \nu_F \\ \nu_N \end{pmatrix}, \qquad (4.32)$$

where the matrix M can be read off from Eqs. 4.28-4.31. Assuming that M is non-singular we can take the inverse to obtain

$$\begin{pmatrix} 1 \\ C \\ F \\ N \end{pmatrix} = \frac{1}{\nu} M^{-1} \begin{pmatrix} \nu_* \\ \nu_C \\ \nu_F \\ \nu_N \end{pmatrix}, \tag{4.33}$$

with

$$M^{-1} = \frac{1}{\det(M)} \begin{pmatrix} b_{11} & b_{21} & b_{31} & b_{41} \\ b_{12} & b_{22} & b_{32} & b_{42} \\ b_{13} & b_{23} & b_{33} & b_{43} \\ b_{14} & b_{24} & b_{34} & b_{44} \end{pmatrix}, \tag{4.34}$$

where b_{ij} is the cofactor of M_{ij}. Expressions for the cofactors, b_{ij} and the determinant det(M) can be found in Appendix C.

Using the above relation we have

$$\begin{aligned} \nu &= \frac{b_{11}\nu_* + b_{21}\nu_C + b_{31}\nu_F + b_{41}\nu_N}{\det(\mathrm{M})}, \\ C &= \frac{1}{\nu}\frac{b_{12}\nu_* + b_{22}\nu_C + b_{32}\nu_F + b_{42}\nu_N}{\det(\mathrm{M})}, \\ F &= \frac{1}{\nu}\frac{b_{13}\nu_* + b_{23}\nu_C + b_{33}\nu_F + b_{43}\nu_N}{\det(\mathrm{M})}, \\ N &= \frac{1}{\nu}\frac{b_{14}\nu_* + b_{24}\nu_C + b_{34}\nu_F + b_{44}\nu_N}{\det(\mathrm{M})}. \end{aligned} \tag{4.35}$$

Solutions can always be obtained in this way but are not always amenable to a compact analytic expression.

The entries of the matrix $\mathscr{K}_{\alpha\beta}$ specify the flux attachment scheme. In the framework of Modak *et al.* this corresponds to a variational wavefunction of the form (omitting Gaussian factors) [145]

$$\Psi(\{z^\alpha\}) = \mathscr{P}_{\mathrm{ZLL}}\left[\prod_{\alpha=1}^{4}\Phi_{\nu_\alpha}\left(z_1^\alpha,\ldots,z_{N_\alpha}^\alpha\right)\right]\prod_{i<j}^{N_\alpha}\left(z_i^\alpha - z_j^\alpha\right)^{2k_\alpha}\prod_{i,j,\alpha,\beta;\alpha\neq\beta}^{N_\alpha,N_\beta}\left(z_i^\alpha - z_j^\beta\right)^{\mathscr{K}_{\alpha\beta}}, \tag{4.36}$$

where for the N_α particles of species α, $z_i^\alpha = x_i^\alpha - iy_i^\alpha$ are the complex coordinates for the i^{th} particle, Φ_{ν_α} is the wavefunction for ν_α filled Landau levels of species α and $\mathscr{P}_{\mathrm{ZLL}}$ indicates projection into the zeroth LL (ZLL). Different parameterizations of the $\mathscr{K}$ matrix correspond to different variational wavefunctions. We consider parameterizations

of the $\mathscr{K}$ matrix of increasing complexity and first search for solutions of Eq. 4.32 which have either $\nu = \frac{1}{2}$ or $\nu = \frac{1}{4}$.

We use the information about which fractions are seen at the same magnetic field as the EDFQH states to constrain flux attachment schemes that may give rise to these states [171]. In particular, we postulate that states with the same parameterization of the $\mathscr{K}$ matrix are more likely to be robust at the same field, since they differ only in the occupation of composite fermion LLs but not in the nature of the flux attachment. We also expect that states which can be specified with the fewest number of independent entries in the $\mathscr{K}$ matrix are the most likely to occur and focus on these as candidate variational states.

4.2.2 Töke-Jain Fractions

We first consider Toke-Jain states [143]. The simplest construction of the $\mathscr{K}$ matrix is when all elements are equal, i.e. $2k = 2k_1 = 2k_3 = m = m_1 = m_2 = n$ and parametrized by a single parameter, k. This is equivalent to having a single species CF. This leads to the Toke-Jain sequence of states: $\nu = \nu_*/(2k\nu_* + 1)$ [143], yielding the sequence $\frac{1}{3}, \frac{2}{5}, \frac{3}{7}, \frac{4}{9}, \ldots$ for $k = 1$. They are always odd denominator states (except in the limit $\nu_* \to \infty$, for which $\nu \to 1/(2k)$ which corresponds to an even denominator state for a single component system which is a compressible state([95, 145]) and hence are not candidates for EDFQH states.

$(k, 2k, n)$ states

We next consider more general Modak-Mandal-Sengupta (MMS) [145] states with $k = k_1 = k_3$ and $m = m_1 = m_2$, which are labeled by the *triplet* (k, m, n). A simple limit is when $2k = m$ and $n \neq 2k$, so the flux attachment is of the form $(k, 2k, n)$ and specified by two parameters, k and n. For the states with flux attachment $(k, 2k, n)$ we have $k = k_1 = k_3$, $m = 2k$ and $n \neq 2k$ and Eqs. 4.28-4.31 take the simpler form

$$\begin{pmatrix} 1 + q_0\nu_* & q_1\nu_C & 0 & 0 \\ q_0\nu_C & 1 + \nu_* q_1 & 0 & 0 \\ q_0\nu_F & q_1\nu_N & 1 & 0 \\ q_0\nu_N & q_1\nu_F & 0 & 1 \end{pmatrix} \begin{pmatrix} 1 \\ C \\ F \\ N \end{pmatrix} = \frac{1}{\nu} \begin{pmatrix} \nu_* \\ \nu_C \\ \nu_F \\ \nu_N \end{pmatrix}, \tag{4.37}$$

with

$$q_0 = k + \frac{n}{2}, \qquad q_1 = k - \frac{n}{2}. \tag{4.38}$$

(k,m,n)	$(\nu_1,\nu_2,\nu_3,\nu_4)$	(C,F,N)	Other fractions
(1,2,1)	(1, 0, 1, 0) (1, 0, 0, 1) (0, 1, 1, 0) (0, 1, 0, 1)	(0, 1, 0) (0, 0, 1) (0, 0, -1) (0, -1, 0)	$\mathbf{\frac{1}{3}}$, $\mathbf{\frac{2}{5}}$, $\mathbf{\frac{3}{7}}$, $\mathbf{\frac{4}{9}}$ $\frac{7}{13}$, $\mathbf{\frac{5}{9}}$, $\mathbf{\frac{4}{7}}$, $\frac{5}{11}$
(1,1,2)	(1, 1, 0, 0) (0, 0, 1, 1) (1, 1, 1, 0) (1, 1, 0, 1) (1, 0, 1, 1) (0, 1, 1, 1) (1, 1, 2, 0) (1, 1, 0, 2) (1, 1, 1, 2) (1, 1, 2, 1) (1, 2, 1, 1) (2, 1, 1, 1) (1, 1, 0, 3) (1, 1, 3, 0) (0, 3, 1, 1) (3, 0, 1, 1)	(1, 0, 0) (-1, 0, 0) (1, 0, 0) (1, 0, 0) (-1, 0, 0) (-1, 0, 0) (1, 0, 0) (1, 0, 0) (1, 0, 0) (1, 0, 0) (-1, 0, 0) (-1, 0, 0) (1, 0, 0) (1, 0, 0) (-1, 0, 0) (-1, 0, 0)	$\mathbf{\frac{1}{3}}$, $\mathbf{\frac{2}{5}}$, $\mathbf{\frac{3}{7}}$, $\mathbf{\frac{4}{9}}$ $\frac{7}{13}$, $\mathbf{\frac{5}{9}}$, $\mathbf{\frac{4}{7}}$, $\frac{5}{11}$

Table 4.1: Parameters for possible $\nu = \frac{1}{2}$ states. Other fractions that can occur for the same (k,m,n) are indicated. Fractions observed in Ref. [171] are indicated in **bold**.

These equations can be solved using Eq. 4.35. The order parameters are given by

$$C = \frac{\nu_C}{\nu_* + \left(k-\frac{n}{2}\right)\left({\nu_*}^2 - \nu_C^2\right)}, \tag{4.39}$$

$$F = \frac{\nu_F + \left(k-\frac{n}{2}\right)\left(\nu_* \nu_F - \nu_N \nu_C\right)}{\nu_* + \left(k-\frac{n}{2}\right)\left({\nu_*}^2 - \nu_C^2\right)}, \tag{4.40}$$

$$N = \frac{\nu_N + \left(k-\frac{n}{2}\right)\left(\nu_* \nu_N - \nu_F \nu_C\right)}{\nu_* + \left(k-\frac{n}{2}\right)\left({\nu_*}^2 - \nu_C^2\right)}. \tag{4.41}$$

We use slightly different notation, but these expressions are equivalent to Eq. (12) in Ref. [145] and the allowed fractions for such states are

$$\nu = \frac{\nu_* + (k-n/2)\left(\nu_*^2 - \nu_C^2\right)}{1 + 2\,k\;\nu_* + (k^2 - n^2/4)\left(\nu_*^2 - \nu_C^2\right)}. \tag{4.42}$$

4.2.3 $(k,m,2k)$ states

A second class of two parameter MMS states can be obtained by assuming $2k = n$ and $m \neq 2k$ in which case the flux attachment is of the form $(k,m,2k)$. The states with flux

ν	(k,m,n)	$(\nu_1,\nu_2,\nu_3,\nu_4)$	(C,F,N)
1/3	(1,2,1)	(1,0,0,0)	(1,1,1)
1/3	(1,1,2)	(1,0,0,0)	(1,1,1)
2/5	(1,2,1)	(2,0,0,0)	(1,1,1)
2/5	(1,1,2)	(2,0,0,0)	(1,1,1)
3/7	(1,2,1)	(0,0,2,1)	(-1,1/3,-1/3)
3/7	(1,1,2)	(1,0,2,0)	(-1/3,1,-1/3)
4/9	(1,2,1)	(3,1,0,0)	(1,1/2,1/2)
4/9	(1,1,2)	(3,0,1,0)	(1/2,1,1/2)
7/13	(1,2,1)	(2,0,1,0)	(1/7,1,1/7)
7/13	(1,1,2)	(2,1,0,0)	(1,1/7,1/7)
5/9	(1,2,1)	(3,0,1,0)	(1/5,1,1/5)
5/9	(1,1,2)	(3,1,0,0)	(1,1/5,1/5)
4/7	(1,2,1)	(1,1,1,1)	(0,0,0)
4/7	(1,2,1)	(1,1,1,1)	(0,0,0)
4/7	(1,1,2)	(1,1,1,1)	(0,0,0)
5/11	(1,2,1)	(3,2,0,0)	(1,1/5,1/5)
5/11	(1,1,2)	(3,0,2,0)	(1/5,1,1/5)

Table 4.2: Parameters for other fractions that have the same (k,m,n) as the $\nu = 1/2$ states in Table 4.1.

attachment $(k,m,2k)$ are those for which $2k = 2k_1 = 2k_3$, $n = 2k$ and $m \neq 2k$. In this case we can write:

$$\begin{aligned} \frac{\nu_*}{\nu} &= (1+q_0\nu_*) + Cq_1\nu_C + Fq_2\nu_F + Nq_2\nu_N, \quad \frac{\nu_C}{\nu} = q_0\nu_C + (1+q_1\nu_*)C + Fq_2\nu_N + Nq_2\nu_F, \\ \frac{\nu_F}{\nu} &= q_0\nu_F + q_1\nu_N C + F(1+q_2\nu_*) + Nq_2\nu_C, \quad \frac{\nu_N}{\nu} = q_0\nu_N + q_1\nu_F C + Fq_2\nu_C + N(1+q_2\nu_*), \end{aligned} \tag{4.43}$$

with

$$q_0 = \frac{3k}{2} + \frac{m}{4}, \quad q_1 = \frac{m}{4} - \frac{k}{2} = -q_2.$$

We find that the EDFQH state at $\nu = \frac{1}{2}$ can be described in terms of these two types of flux attachments, but they are insufficient to describe the EDFQH state at $\nu = \frac{1}{4}$.

There are many different triplets (k,m,n) which can give rise to EDFQH states at $\nu = \frac{1}{2}$. However, if we apply the condition that these triplets should also give rise to the fractions $\nu = \frac{1}{3}, \frac{2}{5}, \frac{3}{7}, \frac{4}{9}$, then we find that this restricts us to $(k,2k,n)$ states with $k = 1$ and $n = 1$, i.e. (1,2,1) states and $(k,m,2k)$ states with $k = 1$ and $m = 1$, i.e. (1,1,2) states. For the (1,2,1) combination we would also expect to see incompressible states at

$\nu = \frac{7}{13}, \frac{5}{9}, \frac{4}{7}$, and $\frac{5}{11}$ and similarly for (1,1,2). The $\nu = \frac{5}{9}$ and $\frac{4}{7}$ states were observed by Zibrov *et al.* [171] but were weaker at the fields where the $\nu = \frac{1}{2}$ state was observed. The twenty states that fit these criteria are listed in Table 4.1 and the other fractions that were observed or have the same set of (k,m,n) values is given in Table 4.2. The (1,1,2) states all have $C \neq 0$, $N = 0$, $F = 0$ while the (1,2,1) states all have $C = 0$ and either N or F non-zero.

(k,m,n)	$(\nu_1, \nu_2, \nu_3, \nu_4)$	(C,F,N)	Other fractions
(2,4,3)	(1, 0, 1, 0) (1, 0, 0, 1) (0, 1, 1, 0) (0, 1, 0, 1)	(0, 1, 0) (0, 0, 1) (0, 0, -1) (0, -1, 0)	$\mathbf{\frac{1}{5}}, \mathbf{\frac{2}{9}}, \mathbf{\frac{3}{13}}$
(2,3,4)	(1, 1, 0, 0) (0, 0, 1, 1) (1, 1, 1, 0) (1, 1, 0, 1) (1, 0, 1, 1) (0, 1, 1, 1)	(1, 0, 0) (-1, 0, 0) (1, 0, 0) (1, 0, 0) (-1, 0, 0) (-1, 0, 0)	$\mathbf{\frac{1}{5}}, \mathbf{\frac{2}{9}}, \mathbf{\frac{3}{13}}, \mathbf{\frac{3}{11}}$
(3,6,1)	(1, 0, 1, 0) (1, 0, 0, 1) (0, 1, 1, 0) (0, 1, 0, 1)	(0, 1, 0) (0, 0, 1) (0, 0, -1) (0, -1, 0)	$\frac{1}{7}, \frac{2}{13}$

Table 4.3: Parameters for possible $(k,2k,n)$ and $(k,m,2k)$ $\nu = \frac{1}{4}$ states. Fractions observed in Ref. [171] are indicated in **bold**.

For the incompressible state at $\nu = \frac{1}{4}$ we first considered states with flux attachment in the form $(k,2k,n)$ and $(k,m,2k)$ and found possibilities with $(k,m,n) =$ (2,4,3), (2,3,4) or (3,6,1) as listed in Table 4.3 and the corresponding odd denominator fractions are listed in Table 4.4. For $k = 2$ it is easy to find $(k,2k,n)$ states at the fractions $\nu =$

ν	(k,m,n)	$(\nu_1, \nu_2, \nu_3, \nu_4)$	(C,F,N)
1/5	(2,4,3)	(1,0,0,0)	(1,1,1)
1/5	(2,3,4)	(1,0,0,0)	(1,1,1)
2/9	(2,4,3)	(1,0,0,0)	(1,1,1)
2/9	(2,3,4)	(1,0,0,0)	(1,1,1)
3/13	(2,4,3)	(0,0,2,1)	(-1,1/3,-1/3)
3/13	(2,3,4)	(1,0,2,0)	(-1/3,1,-1/3)
3/11	(2,3,4)	(2,2,0,1)	(5/3,1/5,-1/5)
1/7	(3,6,1)	(1,0,0,0)	(1,1,1)
2/13	(3,6,1)	(2,0,0,0)	(1,1,1)

Table 4.4: Parameters for other fractions that have the same (k,m,n) as the $\nu = 1/4$ state in Table 4.3.

$\frac{1}{5}, \frac{2}{9}, \frac{3}{13}, \frac{4}{9}$, which are seen in Ref. [171], while for $k=3$ and $n=1$ one finds the fractions $\nu=\frac{1}{7}$ and $\frac{2}{13}$ which are not seen in Ref. [171], instead of $\nu=\frac{1}{5}$ and $\frac{2}{9}$. However, neither of the combinations $(k,2k,n)$ or $(k,m,2k)$ above support states at the experimentally observed fraction $\nu=\frac{2}{7}$.

Hence, we consider more general MMS states for which $m\neq 2k$ and $n\neq 2k$, which depend on the three parameters (k,m,n).

4.2.4 (k,m,n) states

For general MMS states with flux attachment (k,m,n) we have three parameters, k, $m\neq 2k$ and $n\neq 2k$. In this case we can write

$$\frac{\nu_*}{\nu} = (1+q_0)\nu_* + Cq_1\nu_C + Fq_2\nu_F + Nq_2\nu_N, \tag{4.44}$$
$$\frac{\nu_C}{\nu} = q_0\nu_C + (1+q_1\nu_*)C + Fq_2\nu_N + Nq_2\nu_F, \tag{4.45}$$
$$\frac{\nu_F}{\nu} = q_0\nu_F + q_1\nu_N C + F(1+q_2\nu_*) + Nq_2\nu_C, \tag{4.46}$$
$$\frac{\nu_N}{\nu} = q_0\nu_N + q_1\nu_F C + Fq_2\nu_C + N(1+q_2\nu_*), \tag{4.47}$$

where

$$q_0=\frac{k}{2}+\frac{m}{4}+\frac{n}{2},\quad q_1=\frac{k}{2}+\frac{m}{4}-\frac{n}{2},\quad q_2=\frac{k}{2}-\frac{m}{4}.$$

The set of equations 4.44- 4.47 can be recast in matrix form as,

$$\begin{pmatrix} 1+q_0\nu^* & q_1\nu_C & q_2\nu_F & q_2\nu_N \\ q_0\nu_C & 1+\nu_* q_1 & q_2\nu_N & q_2\nu_F \\ q_0\nu_F & q_1\nu_N & 1+q_2\nu_* & q_2\nu_C \\ q_0\nu_N & q_1\nu_F & 1+q_2\nu_C & 1+q_2\nu_* \end{pmatrix}\begin{pmatrix} 1 \\ C \\ F \\ N \end{pmatrix} = \frac{1}{\nu}\begin{pmatrix} \nu^* \\ \nu_C \\ \nu_F \\ \nu_N \end{pmatrix}. \tag{4.48}$$

We solved Eq. 4.48 for the filling fraction and order parameters but were not able to find compact analytic forms for the order parameter solutions.

Noting that the $k=2$ states appear to be more promising for $\nu=\frac{1}{4}$ than the $k=3$ states, we found the following combinations in addition to $(2,4,3)$ and $(2,3,4)$ that can give rise to a $\nu=\frac{1}{4}$ EDFQH state: $(2,0,3)$, $(2,1,3)$, $(2,2,3)$, $(2,3,0)$, $(2,3,1)$, $(2,3,2)$, and $(2,3,3)$. When we investigate the above combinations of (k,m,n) to see which combinations also allow for FQHE states at $\nu=\frac{1}{5}$ and $\nu=\frac{2}{7}$, three prominent candidates emerge: $(2,2,3)$, $(2,3,2)$ and $(2,3,3)$. All three combinations can also have $\nu=\frac{2}{9}$ states, but only the $(2,3,3)$ combination also allows for a $\nu=\frac{3}{11}$ state. Given that the $\nu=\frac{3}{11}$ state disappears at fields at which the $\nu=\frac{1}{4}$ state is observed, we eliminate

(k,m,n)	$(\nu_1,\nu_2,\nu_3,\nu_4)$	(C,F,N)	Other fractions
(2, 3, 2)	(1, 1, 0, 0) (0, 0, 1, 1)	(1, 0, 0) (-1, 0, 0)	$\frac{1}{5}, \frac{2}{9}, \frac{3}{13}, \frac{2}{7}, \frac{4}{9}$
(2, 2, 3)	(1, 0, 1, 0) (1, 0, 0, 1) (0, 1, 1, 0) (0, 1, 0, 1)	(0, 1, 0) (0, 0, 1) (0, 0, -1) (0, -1, 0)	$\frac{1}{5}, \frac{2}{9}, \frac{3}{13}, \frac{2}{7}, \frac{4}{9}$

Table 4.5: Parameters for candidate $\nu = \frac{1}{4}$ states. Other fractions that can occur for the same (k,m,n) are indicated. Fractions observed in Ref. [171] are indicated in **bold**.

ν	(k,m,n)	$(\nu_1,\nu_2,\nu_3,\nu_4)$	(C,F,N)
1/5	(2,3,2)	(1,0,0,0)	(1,1,1)
1/5	(2,2,3)	(1,0,0,0)	(1,1,1)
2/9	(2,3,2)	(2,0,0,0)	(1,1,1)
2/9	(2,2,3)	(2,0,0,0)	(1,1,1)
3/13	(2,3,2)	(3,0,0,0)	(1,1,1)
3/13	(2,2,3)	(3,0,0,0)	(1,1,1)
4/9	(2,3,2)	(2,0,2,0)	(0,1,0)
4/9	(2,2,3)	(2,2,0,0)	(1,0,0)
2/7	(2,3,2)	(1,0,1,0)	(0,1,0)
2/7	(2,2,3)	(1,1,0,0)	(1,0,0)

Table 4.6: Parameters for other fractions that have the same (k,m,n) as the $\nu = 1/4$ state in Table 4.5.

the $(2,3,3)$ combination, leaving $(2,2,3)$ and $(2,3,2)$ as competing flux attachment schemes. The parameters for these candidate $\nu = \frac{1}{4}$ states are listed in Table 4.5 and the parameters for the corresponding odd denominator fractions are given in Table 4.6.

The (2,3,2) combination has $C \neq 0$, with $F = 0$, $N = 0$, while the (2,2,3) combination has $C = 0$ and allows for either $F \neq 0$ or $N \neq 0$. We observed that the $\nu = \frac{2}{7}$ state is quite robust when the $\nu = \frac{1}{4}$ state forms and differs from the $\nu = \frac{1}{5}$ and $\frac{2}{9}$ states in that only one order parameter is non-zero when it occurs. In contrast, the $\nu = \frac{1}{5}$ and $\nu = \frac{2}{9}$ states have $|C| = |N| = |F| = 1$, and appear to be weaker at the fields where the $\nu = \frac{1}{4}$ EDFQH is observed, suggesting similarities in the broken symmetry states for $\nu = \frac{1}{4}$ and $\frac{2}{7}$.

4.3 Conclusion

Based on the idea that fractions that coexist with EDFQH states at the same magnetic field are likely to have the same $\mathscr{K}$ matrix, but different fillings of Dirac composite fermion LLs, we suggest that the likely candidate variational wavefunctions for $\nu = \frac{1}{2}$ have $(k,m,n) = (1,1,2)$ or $(1,2,1)$ and those for $\nu = \frac{1}{4}$ have (k,m,n) as (2,2,3) or

(2,3,2). Even within this limited set of flux attachments there is a degeneracy associated with the pattern of symmetry breaking orders present in the states, as shown in Tables 4.1 and 4.5. In order to discriminate further, we need information about the nature of the broken symmetries in the various EDFQH states. Note that C and N are CSB orders and therefore cause strong LL mixing. As a result, the onset of CDW and AFM orders for composite Dirac fermions may cause the system to lower its energy by pushing filled LLs of composite Dirac fermions further down in energy. Hence we expect any FQH state with $C \neq 0$ or $N \neq 0$ to be energetically superior to those with $F \neq 0$. Such states can be expected to arise in graphene due to electron-electron interactions. The actual pattern of symmetry breaking depends on the relative strength of various finite range components of the Coulomb interaction.

Zibrov *et al*. [171] noted that there was a sublattice gap in their experiments, the size of which was correlated with the magnetic field at which EDFQH states were seen. They proposed that the EDFQH states are associated with a phase transition from a partially sublattice polarized (PSP) to a canted antiferromagnet (CAF) phase. Within the variational states we consider this would correspond to a transition from a state with $C \neq 0$ to one with spin ordering. A more general variational state than we have considered here might be achieved by taking linear combinations of states of the form of Eq. (4.36) with the same (k, m, n) but different $(\nu_1, \nu_2, \nu_3, \nu_4)$. These might give ways to realize PSP or CAF states. On the other hand, experiments by Amet *et al.* [59] reported that the FQHE states in the $n = 0$ LL do not show appreciable change in a tilted magnetic field, leading them to conclude that the state is spin polarized, which would favour $F \neq 0$. However, as noted in Ref. [130] the order parameters in $\nu = 0$ states (believed to be a CAF) can be relatively insensitive to even quite strong parallel fields, and so it may be possible to have both $F \simeq 0$ and relatively little sensitivity to tilted fields.

We suggest that measurement is the best way to resolve the ambiguity of the nature of the broken symmetry in the EDFQH states. In the case of CDW order, sublattice resolved STM measurements could determine the presence of non-zero C in EDFQH states, and the spin ordering (either F or N) could be probed with spin resolved STM. Such information could pare down the possible states quite significantly. Additionally, studies of edge states via tunnelling measurements could provide additional constraints on possible states [171]. Investigation of the excitation spectra for different possible states might also provide ways to discriminate between different states. The recent construction of a multicomponent Abelian Chern-Simons theory in a functional integral approach [146] is a step in this direction. This is the approach taken in Chapter 5.

Finally, we note that the multicomponent states we consider here are considerably more complex in their flux attachment than the standard sequence of FQHE states that

have been proposed for monolayer graphene but actually show many of the standard fractions. This observation raises questions about the nature of states that have been observed in graphene previously [56, 57, 59] and whether these do indeed belong to families with the simplest flux attachment. We also note an interesting observation about the states we have identified. The flux attachments for the states at $\nu = \frac{1}{4}$ are related to those found for $\nu = \frac{1}{2}$ by $j \to j+1$ for $j = k, m, n$ (although the patterns of symmetry breaking are not the same in going from one set of flux attachments to the other).

In summary, we propose candidate wavefunctions for the recently observed incompressible EDFQH states at $\nu = \frac{1}{2}$ and $\nu = \frac{1}{4}$. The possibilities we uncover indicate that the lowest LL in graphene may harbour even more richness in possible electron states than previously anticipated. We urge additional experimental efforts to uncover the nature of these unusual states which may help to pin down the patterns of broken symmetry states in graphene.

Chapter 5

Collective Excitations

In chapter 4 we proposed a set of variational wavefunctions for the incompressible states at $\nu = 1/2, 1/4$ within the multi-component flux attachment scheme. The proposed set of wavefunctions left the nature of the underlying symmetry breaking ambiguous. In this chapter[1] we investigate the excitation spectra for different possible states as a means to discriminate between different states.

Interest in understanding collective excitations in FQH liquids dates back to mid-1980s. Girvin, MacDonald and Platzman (GMP) [183, 184] studied the collective excitations of the FQH liquid within a single mode approximation (SMA) in analogy with Feynman's theory of superfluid helium [185]. They observed a gap in the spectrum at zero wave vector due to the incompressibility of the FQH liquid. GMP also observed a minimum in the excitation spectra which they named magnetoroton in analogy to rotons in theory of superfluid helium. Lopez and Fradkin showed how a system of electrons coupled to a Chern-Simons gauge field is equivalent to a system of composite fermions [168]. Employing a random phase approximation method they were able to arrive at expressions for the electromagnetic response of these states for finite wave vector, $\vec{q}$, and frequency, ω, [186]. Halperin, Lee and Read (HLR) [95] extended their methods to study the FQH state at $\nu = \frac{1}{2}$ and Simon and Halperin [169] further developed this approach by taking into account the corrections due to mass renormalization that the Chern-Simons term induces. These results were consistent with experiments involving using inelastic light scattering [187] and observation of geometric resonances in the cyclotron orbits of composite fermions (CFs) using surface acoustic waves [170]. The methods developed by Fradkin and Lopez [188] has been applied to the case of graphene and expressions for the components of the electromagnetic response tensor

[1] Most of this chapter is based on the publication: S. Narayanan and M. P. Kennett, Phys. Rev. B, **106**, 165119 (2022).

were obtained [146]. However these calculations did not take into account any form of symmetry breaking orders, originally emphasized in Ref. [153].

We are primarily interested in studying the collective excitations of FQH states for which the filling fraction lies between $0 < \nu < 1$. For calculational convenience we focus on the following symmetry breaking orders: out of plane antiferromagnetism, charge density wave and ferromagnetism, since these are easily accommodated in the Chern-Simons theory we employ [145, 176]. We work in the zeroth Landau level (ZLL) where the sublattice and valley degrees of freedom coincide. The flux attachment scheme, described in Sec. 4.2, determines the order parameters Eq. 4.18. Our aim is to understand how the collective excitations change in the presence of the order parameters. This is potentially a path to gain insight into the nature of symmetry breaking present in the ZLL in graphene.

5.1 Model

Starting from the extended Hubbard model on the honeycomb lattice, and applying the Hartree-Fock approximation [119] gives rise to a low energy Hamiltonian, in sublattice space, including CSB orders m_α and ferromagnetic order f_α of

$$H_\alpha^\xi = \xi_\alpha \hbar v_F \left(\Pi_1 \sigma_1 + \Pi_2 \sigma_2\right) + m_\alpha \sigma_3 + f_\alpha \sigma_0, \tag{5.1}$$

where $\Pi_i = p_i + eA_i; i = 1, 2$, with p_i the momentum operator and A_i the vector potential. The index $\alpha = 1, 2, 3, 4$ labels components of the spin and valley degrees of freedom (also called flavours or species) as $1 \equiv K\uparrow$, $2 \equiv K\downarrow$, $3 \equiv K'\uparrow$ and $4 \equiv K'\downarrow$. K and K' are the two inequivalent Brillouin-zone (BZ) points where the valence band touches the conduction band in reciprocal lattice space. The sigma matrices act in the 2×2 sublattice space and $\xi_\alpha = \pm$ correspond to the $+(K)$ and $-(K')$ valleys respectively. The Hamiltonian Eq. 5.1 acts on the spinor $\Psi_\alpha = (u_\alpha, v_\alpha)^T$ where $u_\alpha(v_\alpha)$ is the amplitude on the $A(B)$ sublattice of graphene's honeycomb lattice.

In Eq. 5.1 the m_α are a combination of chiral symmetry breaking orders defined as: $m_1 = C + N; m_2 = C - N; m_3 = -(C + N)$; and $m_4 = -(C - N)$ where C is the charge density wave order and N is easy-axis Neel anti-ferromagnetic order. The ferromagnetic order (F) enters Eq. 5.1 through f_α, defined as: $f_1 = F; f_2 = -F; f_3 = F$; and $f_4 = -F$.

Equation 5.1 describes interacting electrons in graphene in the presence of a magnetic field at the mean field level. A system of electrons in a magnetic field can be equivalently described by a system of composite fermions (CFs) in an effective magnetic field [83]. We consider four different species or flavours of composite fermions, corresponding to the different values of α as defined above. We begin by introducing

the transformation in Eq. 4.6

$$\Phi_\alpha = \mathscr{K}_{\alpha\beta} \int d\vec{r}' \arg(\vec{r} - \vec{r}')\rho_\beta(\vec{r}'), \tag{5.2}$$

where the matrix $\mathscr{K}$ was defined in Eq. 4.7. For our calculations we consider the elements of $\mathscr{K}$ with the simplification $k_i = k$, $m_i = m$ and $n_i = n$ which are labelled by the triplet (k, m, n) as in Sec. 4.2.4.

The derivative terms in the Hamiltonian transform as

$$\Psi^\dagger_\alpha(\pm\sigma_1\Pi_1 - \sigma_2\Pi_2)\Psi_\alpha \to \psi^\dagger_\alpha(\pm\sigma_1\tilde{\Pi}_1 - \sigma_2\tilde{\Pi}_2)\psi_\alpha,$$

where $\tilde{\Pi}_i = \Pi_i - a^\alpha_i$, with the Chern-Simons field a^α_i defined as

$$a^\alpha = \mathscr{K}_{\alpha\beta} \int d\vec{r}' g(\vec{r} - \vec{r}')\rho_\beta(\vec{r}'); \quad g(\vec{r}) = \frac{\hat{z} \times \vec{r}}{r^2}.$$

Here ρ_α corresponds to the density of composite fermion species of type α. In terms of these densities we can define our order paramaters given by Eq. 4.18.

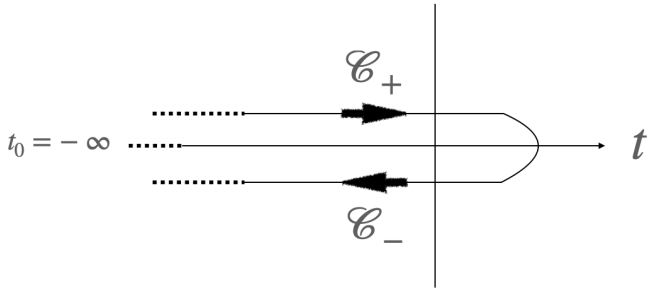

Figure 5.1: Schwinger-Keldysh closed contour with forward time branch ($\mathscr{C}_+$) and backward time branch ($\mathscr{C}_-$). We set the reference time $t_0 = -\infty$.

The composite fermion Hamiltonian is thus

$$H^\xi_\alpha = \xi_\alpha v_F(\tilde{\Pi}^\alpha_1\sigma_1 + \tilde{\Pi}^\alpha_2\sigma_2) + m_\alpha\sigma_3 + f_\alpha\sigma_0, \tag{5.3}$$

where $\Pi^\alpha_i = p_i + eA_i + a^\alpha_i$, with α again labelling the species.

Following Fräßdorf [146], we now employ the Schwinger-Keldysh technique [189–192] to develop a field theoretic description of the multi-species composite fermions coupled to four statistical $U(1)$ gauge fields, a^α. In the Schwinger-Keldysh technique the time argument is promoted from a real variable to a complex variable corresponding to a contour-time and the correlation functions are defined as path-ordered products of the fields on the Schwinger-Keldysh contour. Since we work with an equilibrium system

we take the reference time, t_0 on the contour to be in the infinite past, thereby reducing the kinetic equation solutions to well known equilibrium distributions. The Schwinger-Keldysh technique leaves open the option to extend our theory to a finite temperature and non-equilibrium scenarios.

5.2 Effective action

The generating functional for the Hamiltonian defined in Eq. 5.1 is given by

$$Z[\psi_\alpha, A_\mu, \mathscr{A}_\mu^\alpha, a_\mu^\alpha] = \int \mathscr{D}\psi^\dagger \mathscr{D}\psi e^{iS[\psi, e(A_\mu + \mathscr{A}_\mu^\alpha) + a_\mu^\alpha]}, \tag{5.4}$$

where the external vector potential, $A_\mu + \mathscr{A}_\mu^\alpha$, is composed of two terms: a piece A_μ corresponding to the perpendicular magnetic field and a small fluctuating term with vanishing average, $\mathscr{A}_\mu^\alpha$, which is used to probe the electromagnetic response of the system.

The action S can be written as

$$S = S_D + S_{CS}, \tag{5.5}$$

where S_D is the composite fermion action corresponding to the Hamiltonian in Eq. 5.3:

$$S_D[\psi, A_\mu + \mathscr{A}_\mu^\alpha + a_\mu^\alpha] = \int_{C,\vec{r}} \psi^{\dagger,\alpha} \hat{G}^{-1}_{0,\alpha\beta} \psi^\beta, \tag{5.6}$$

with

$$\int_{C,\vec{r}} \equiv \int_C dt \int d^2 r, \tag{5.7}$$

and C is the Schwinger-Keldysh contour along which the integration is performed. The matrix $\hat{G}_0^{-1}$ is the inverse contour-time propagator which is diagonal in the species index:

$$\hat{G}_0^{-1} = \mathrm{diag}(G^{-1}_{0,K\uparrow}, G^{-1}_{0,K\downarrow}, G^{-1}_{0,K'\uparrow}, G^{-1}_{0,K'\downarrow}), \tag{5.8}$$

with

$$G^{-1}_{0,\alpha}(x,y) = \delta_C(x-y)(i\sigma^\mu_\alpha \mathscr{D}^\alpha_\mu - \mu_\alpha + m_\alpha \sigma_3 + f_\alpha \sigma_0). \tag{5.9}$$

We note that we have already included interaction terms at the mean field level, which leads to order parameters C and N (that combine to form m_α) and F. Here $\delta_C(x-y) = \delta_C(x_0 - y_0)\delta(\vec{x} - \vec{y})$ is the contour-time delta function and $\sigma^\mu_\alpha = (\sigma_0, \kappa_\alpha v_F \sigma_1, \kappa_\alpha v_F \sigma_2)$

and m_α, f_α have been defined above. The gauge covariant derivative

$$\mathscr{D}^\alpha_\mu = \partial_\mu + ieA_\mu + ie\mathscr{A}^\alpha_\mu + ia^\alpha_\mu,$$

contains the fields $A_\mu + \mathscr{A}^\alpha_\mu$ and the statistical gauge field a^α_μ.

S_{CS} is the Chern-Simons action which describes the dynamics of the statistical gauge field a^α_μ and has the form

$$S_{CS} = \frac{1}{2}(\mathscr{K})^{-1}_{\alpha\beta} \int_{C,\vec{r}} \epsilon^{\mu\nu\lambda} a^\alpha_\mu \partial_\nu a^\beta_\lambda. \tag{5.10}$$

We integrate out the fermionic fields ψ from the action S in Eq. 5.5 to obtain an effective action in terms of the gauge fields only,

$$S_{\text{eff}}[e(A_\mu + \mathscr{A}^\alpha_\mu), a^\alpha_\mu] = -i\text{Tr}\ \ln G_0^{-1}\left[e(A_\mu + \mathscr{A}^\alpha_\mu), a^\alpha_\mu\right] + S_{CS}\left[a^\alpha_\mu\right]. \tag{5.11}$$

We find the saddle point configuration of the path integral for the statistical gauge fields a^α_μ and then perform an expansion of the effective action in terms of fluctuations around this mean field solution. Following Fradkin and Lopez [168] we search for a solution that leads to a vanishing charge carrier current and a non-zero, time independent charge carrier density, ρ_α, which is given by

$$\rho_\alpha = -(\mathscr{K})^{-1}_{\alpha\beta}\mathscr{B}^\beta, \tag{5.12}$$

where $\mathscr{B}^\beta$ is a uniform field due to the statistical gauge field experienced by a CF of species β. Inverting this relation gives us

$$\mathscr{B}^\beta = -\rho_\alpha \mathscr{K}^{\alpha\beta}. \tag{5.13}$$

The effect of this field is to reduce/enhance (depending on the sign of charge carriers present in the sample) the original magnetic field so that a CF of species α experiences an effective magnetic field given by

$$B^\alpha_{\text{eff}} = B + \mathscr{B}^\alpha = B - \rho_\beta \mathscr{K}^{\alpha\beta}. \tag{5.14}$$

Here ρ is the total electron density and ν is the filling fraction for the electrons. From Eq. 5.14 we get a relationship [145] between the composite fermion filling fraction ν_α

for species α, the density ρ_α and the flux attachment matrix of

$$\frac{\rho_\alpha}{\nu_\alpha} = \frac{\rho}{\nu} - \mathscr{K}^{\alpha\beta}\rho_\beta. \tag{5.15}$$

We now represent the effective action in Eq. 5.11 in a more convenient form by performing a Keldysh rotation. The contour illustrated in Fig. 5.1 consists of a forward ($\mathscr{C}_+$) and a backward ($\mathscr{C}_-$) piece, and the fields on the respective pieces of the contour may be be written as $\psi_\pm$, $a_\pm$. We transform to a new set of double fields $\psi_{c,q}$ and $a_{c,q}$ which are symmetric and antisymmetric linear combinations of the $\pm$ double fields with, e.g. for ψ:

$$\psi_c = \frac{1}{\sqrt{2}}(\psi_+ + \psi_-), \quad \psi_q = \frac{1}{\sqrt{2}}(\psi_+ + \psi_-). \tag{5.16}$$

The labels c, q correspond to classical and quantum components respectively [193]. The net result is that the derivatives of the action with respect to the gauge fields are now performed with respect to the quantum components [191].

The gauge fields, a^α, can be viewed as being comprised of a mean field part ($\bar{a}^\alpha$) and a fluctuation part (Δa^α), $a^\alpha = \bar{a}^\alpha + \Delta a^\alpha$, and we expand the effective action in terms of the fluctuations up to the second order in Δa. Terms linear in fluctuations vanish and we get

$$\begin{aligned} S_{\text{eff}}[\mathscr{A}^\alpha_\mu, a^\alpha_\mu] = \int_{xy} &\Big[(\Delta a_c)^\alpha_\mu + (\mathscr{A}_c)^\alpha_\mu \;\; (\Delta a_q)^\alpha_\mu + (\mathscr{A}_q)^\alpha_\mu\Big](x) \begin{bmatrix} 0 & (\Pi^A)^{\mu\nu}_{\alpha\beta} \\ (\Pi^R)^{\mu\nu}_{\alpha\beta} & (\Pi^K)^{\mu\nu}_{\alpha\beta} \end{bmatrix}(x,y) \\ &\begin{bmatrix} (\Delta a_c)^\beta_\nu + (\mathscr{A}_c)^\beta_\nu) \\ (\Delta a_q)^\beta_\nu + (\mathscr{A}_q)^\beta_\nu) \end{bmatrix}(y) \\ &+\Big[(\Delta a_c)^\alpha_\mu \;\; (\Delta a_q)^\alpha_\mu)\Big](x) \begin{bmatrix} 0 & (C^A)^{\mu\nu}_{\alpha\beta} \\ (C^R)^{\mu\nu}_{\alpha\beta} & (C^K)^{\mu\nu}_{\alpha\beta} \end{bmatrix}(x,y) \begin{bmatrix} (\Delta a_c)^\beta_\nu \\ (\Delta a_q)^\beta_\nu \end{bmatrix}(y), \end{aligned}$$

which can be written in a more compact form as :

$$\begin{aligned} S_{\text{eff}}[\mathscr{A}^\alpha_\mu, \mathbf{a}^\alpha_\mu] = \int_{xy} &\Big[(\mathbf{\Delta a})^\alpha_\mu + (\mathscr{A})^\alpha_\mu)\Big]^{\mathbf{T}}(x)\mathbf{\Pi}^{\mu\nu}_{\alpha\beta}(x,y)\Big[(\mathbf{\Delta a})^\beta_\nu + (\mathscr{A})^\beta_\nu\Big](y) \\ &+ (\mathbf{\Delta a})^\alpha_\mu(x)\mathbf{C}^{\mu\nu}_{\alpha\beta}(x,y)(\mathbf{\Delta a})^\beta_\nu(y). \end{aligned} \tag{5.17}$$

Here the fields $\mathscr{A}_\mu^\alpha$ and $\mathbf{a}_\mu^\alpha$ are two component fields in Keldysh space

$$\mathscr{A} = \begin{pmatrix} \mathscr{A}^c \\ \mathscr{A}^q \end{pmatrix},$$

and similarly for the fields $\mathbf{a}_\alpha^\mu$. The polarization tensor $\mathbf{\Pi}$ and the Chern-Simons tensor $\mathbf{C}$ are 2×2 matrices with advanced (A), retarded (R) and Keldysh (K) components:

$$\mathbf{C}_{\alpha\beta}^{\mu\nu} = \begin{pmatrix} 0 & (C^A)_{\alpha\beta}^{\mu\nu} \\ (C^R)_{\alpha\beta}^{\mu\nu} & (C^K)_{\alpha\beta}^{\mu\nu} \end{pmatrix}. \tag{5.18}$$

We use bold font to indicate that a quantity has classical (c) and quantum (q) components if a vector, or Advanced (A), Retarded (R) and Keldysh (K) components if a 2×2 matrix. As the system is in equilibrium, in the linear response regime, the different components of $\mathbf{\Pi}$ satisfy the bosonic fluctuation-dissipation theorem. The polarization tensor $\mathbf{\Pi}$ is given by

$$\mathbf{\Pi}_{\alpha\beta}^{\mu\nu} = -\frac{i}{2}\frac{\delta^2}{\delta \mathbf{a}_\nu^\beta \delta \mathbf{a}_\mu^\alpha}\ \mathrm{Tr}\ \ln\ \hat{\mathbf{G}}_{\mathbf{0}}^{-1}[e\mathbf{A}_\mu + \mathbf{a}_\mu^\alpha]\Big|_{\mathbf{a}=\bar{\mathbf{a}}}, \tag{5.19}$$

where $\mathbf{A}_\mu$ is the electromagnetic field and $\hat{\mathbf{G}}_{\mathbf{0}}^{-1}$ is the inverse time propagator mapped onto the Keldysh basis. Since the propagators are diagonal in the species index α, the polarization tensor is also diagonal, $\mathbf{\Pi}_{\alpha\beta}^{\mu\nu} = \mathbf{\Pi}_{\alpha\beta}^{\mu\nu}\delta^{\alpha\beta}$. To determine the collective excitation spectra we only need consider the retarded (R) components of the polarization tensor given in Appendix A.

The Chern-Simons tensor has the following form

$$C_{\alpha\beta}^{\mu\nu} = (\mathscr{K})_{\alpha\beta}^{-1}\epsilon^{\mu\nu\lambda}\partial_\lambda. \tag{5.20}$$

The polarization tensor and the Chern-Simons tensor are transverse. As a consequence of this the polarization tensor can be decomposed into scalars $\mathbf{\Pi^0}$, $\mathbf{\Pi^1}$ and $\mathbf{\Pi^2}$ [168] as follows:

$$\begin{aligned}
\mathbf{\Pi}_{\alpha\beta}^{00}(\omega,\mathbf{q}) &= -q^2\mathbf{\Pi}_{\alpha\beta}^0, && (5.21)\\
\mathbf{\Pi}_{\alpha\beta}^{0i}(\omega,\mathbf{q}) &= -\omega q^i\mathbf{\Pi}_{\alpha\beta}^0(\omega,\mathbf{q}) + i\epsilon^{0ij}q_j\mathbf{\Pi}_{\alpha\beta}^1(\omega,\mathbf{q}), && (5.22)\\
\mathbf{\Pi}_{\alpha\beta}^{i0}(\omega,\mathbf{q}) &= -\omega q^i\mathbf{\Pi}_{\alpha\beta}^0(\omega,\mathbf{q}) - i\epsilon^{0ij}q_j\mathbf{\Pi}_{\alpha\beta}^1(\omega,\mathbf{q}), && (5.23)\\
\mathbf{\Pi}_{\alpha\beta}^{ij}(\omega,\mathbf{q}) &= -\omega^2\delta^{ij}\mathbf{\Pi}_{\alpha\beta}^0(\omega,\mathbf{q}) + i\epsilon^{0ij}\omega\mathbf{\Pi}_{\alpha\beta}^1(\omega,\mathbf{q}) \\
&\quad +(\delta^{ij}q^2 - q^iq^j)\mathbf{\Pi}_{\alpha\beta}^2(\omega,\mathbf{q}). && (5.24)
\end{aligned}$$

5.3 Electromagnetic response tensor

In order to obtain the electromagnetic response tensor we integrate over the statistical gauge fields. Due to the transverse nature of the polarization and Chern-Simons tensor the inverse of both is ill defined and so is the inverse of the sum of these two tensors, $(\mathbf{\Pi}+\mathbf{C})^{-1}$, which appears when we perform the integration over the statistical gauge fields.

In order to overcome this problem one can employ the Fadeev-Poppov method [194]. The result of this is a gauge fixed generating functional of the form

$$\mathscr{Z}_{\mathrm{GF}}[\mathscr{A}_{\mu}^{\alpha}]=\int(\mathscr{D}\Delta a)\;\; e^{i(S_{\mathrm{eff}}[\mathscr{A},\Delta a]+S_{\mathrm{GF}}[\Delta a])}, \tag{5.25}$$

where the gauge fixing action has the form

$$S_{\mathrm{GF}}=\left(\frac{1}{2\eta}\right)\int_{\mathscr{C},x}(\partial_{\mu}\Delta a^{\mu})^{2}=\frac{1}{2}\int_{\mathscr{C},x}\Delta a^{\mu}\mathscr{G}_{\mu\nu}\Delta a^{\nu}, \tag{5.26}$$

where η is a real valued parameter which we can set to be $\eta=1$ [194]. Since the electromagnetic tensor is a physical quantity the choice of gauge should not matter and hence all references to the parameter η drop out in the end. Now we can perform the integral over the gauge fields since the addition of $\mathscr{G}$ makes the sum $\mathbf{\Pi}+\mathscr{G}+\mathbf{C}$ invertible. The object that we obtain as a consequence of performing the integral is the electromagnetic response tensor which has the form

$$\mathbf{K}=\mathbf{\Pi}-\mathbf{\Pi}(\mathbf{\Pi}+\mathscr{G}+\mathbf{C})^{-1}\mathbf{\Pi}. \tag{5.27}$$

The electromagnetic tensor can be expressed, similarly to the polarization and Chern-Simons tensors, in Keldysh space as a 2×2 matrix with advanced (A), retarded (R) and Keldysh (K) components:

$$\mathbf{K}=\begin{pmatrix}0 & (K^{A})^{\mu\nu}_{\alpha\beta}\\ (K^{R})^{\mu\nu}_{\alpha\beta} & (K^{K})^{\mu\nu}_{\alpha\beta}\end{pmatrix}. \tag{5.28}$$

The Keldysh component is related to the advanced and retarded components through the bosonic fluctuation-dissipation theorem:

$$K^{K}_{\omega,\mathbf{q}}=\coth\left(\frac{\omega}{2T}\right)(K^{R}_{\omega,\mathbf{q}}-K^{A}_{\omega,\mathbf{q}}). \tag{5.29}$$

The electromagnetic response tensor is also transverse and hence admits a decomposition, similar to the polarization tensor, in terms of scalar kernels, K_0, K_1 and K_2

which can be written as[2]

$$K_0^R(\omega,\mathbf{q}) = -(\mathscr{K}^{-1})^2\frac{\Pi_0^R(\omega,\mathbf{q})}{D^R(\omega,\mathbf{q})}, \tag{5.30}$$

$$K_1^R(\omega,\mathbf{q}) = \mathscr{K}^{-1}+(\mathscr{K}^{-1})^2\frac{(\mathscr{K}^{-1}+\Pi_1^R(\omega,\mathbf{q}))}{D^R(\omega,\mathbf{q})}, \tag{5.31}$$

$$K_2^R(\omega,\mathbf{q}) = (\mathscr{K}^{-1})^2\frac{\Pi_2^R(\omega,\mathbf{q})}{D^R(\omega,\mathbf{q})}. \tag{5.32}$$

Since the polarization tensor is diagonal in the species index α, it commutes with $\mathscr{K}^{-1}$. Here $D^{R/A}$ is the denominator matrix which has the form

$$D^{R/A} = \omega^2(\Pi_0^{R/A})^2-(\mathscr{K}^{-1}+\Pi_1^{R/A})^2+q^2(\Pi_0^{R/A}\Pi_2^{R/A}). \tag{5.33}$$

The retarded and advanced kernels are Hermitian conjugates of each other. Full expressions for Π_0, Π_1, Π_2 are given in Appendix F. The denominator matrix D is of central importance to our work. The zeros of the determinant of the denominator matrix gives us the location of poles for the electromagnetic response tensor.

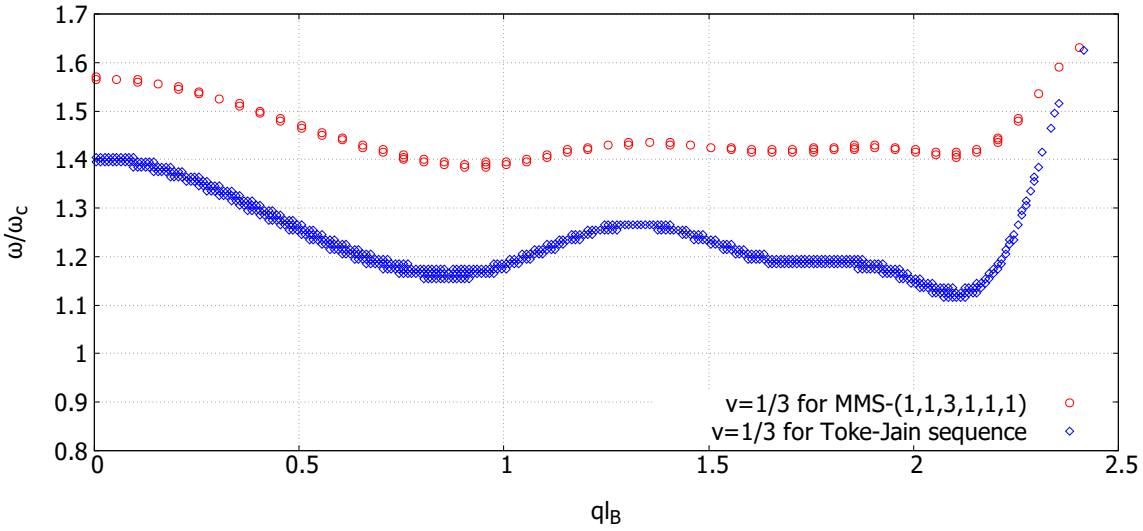

Figure 5.2: Location of poles as a function of $\frac{\omega}{\omega_c}$ and ql_B for $\nu = 1/3$ for the Toke-Jain sequence (black) and the MMS state for $(k,m,n) = (1,1,3)$ (red). Here $\omega_c = \sqrt{2}\frac{v_F}{l_B}$

[2]Details of calculations are in Appendix E.

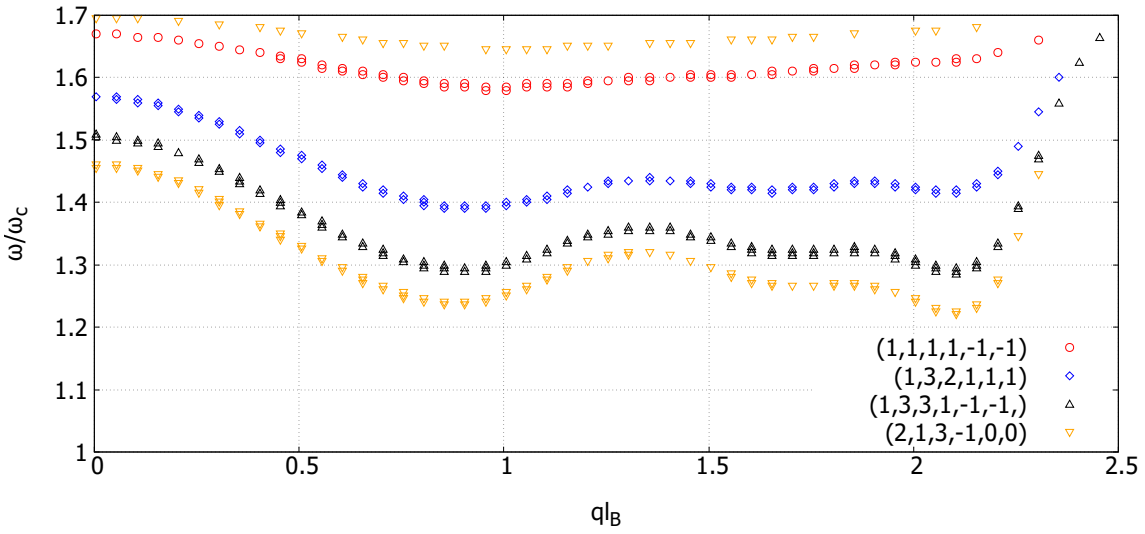

Figure 5.3: Location of poles as a function of $\frac{\omega}{\omega_c}$ and ql_B for $\nu = 1/3$ for the parameter set defined in the text (k, m, n, C, N, F). $(1,1,1,1,-1,-1)$ (red), $(1,3,2,1,1,1)$ (blue), $(1,3,3,1,-1,-1)$ (black) and $(2,1,3,-1,0,0)$ (orange).

5.4 Numerical Results

In this section we find the poles of the electromagnetic response tensor numerically so as to determine the collective excitation spectra of various FQH states in graphene. Specifically, we calculate the zeros of the determinant of the denominator matrix $D^{R/A}$ given in Eq. 5.33. We calculate the excitation spectra for flux attachment schemes at several different filling fractions ν.

Different flux attachment schemes are encoded in the matrix elements $\mathscr{K}_{\alpha\beta}$. Using the parametrization presented in Eq. 5.3, the simplest case is when the same number of flux quanta, $2k$, is attached to all the species [143, 145]. This is the same as considering a single species with $2k$ flux quanta attached to it. For this case the filling fractions of FQH states are given by $\nu = \frac{\nu^*}{2k\nu^*+1}$ with $\nu^* = \nu_1 + \nu_2 + \nu_3 + \nu_4$, which is known as the Töke-Jain sequence [143]. Here ν_α, $\alpha = 1,2,3,4$, are the filling fractions of the individual species. Hence the Töke-Jain sequence can be characterized by the set of parameters (ν^*, k). Following Refs. [145, 176], we also consider the following simplification of $\mathscr{K}$: $k_i = k$, $m_i = m$ and $n_i = n$ for all i, which we refer to as the Modak-Mandal-Sengupta (MMS) states. This allows us to label MMS flux attachment schemes by the triplet (k, m, n). In order to specify a FQH state with a given filling ν, we also need to specify fillings ν_α for the composite fermion Landau levels. Once ν_α, ν and (k, m, n) are specified this determines the values of the order parameters C, N and F [145, 176]. We characterize the states we consider by the flux attachment parameters (k, m, n) determined from the $\mathscr{K}$ matrix. In our numerical calculations we truncated

the number of Landau levels (labelled by n and n′) included in the calculation of D to $N_c = 10$ in Eq. F.2 in order to cut computational time. We confirmed that our results were not sensitive to this choice of cut-off.

For each parameter set we calculate the collective modes and plot their angular frequency $\frac{\omega}{\omega_c}$ against ql_B where $\omega_c = \sqrt{2}v_F/l_B$ is the cyclotron frequency with v_F being the Fermi velocity and l_B being the magnetic length. We characterize each dispersion curve by the following parameters, ω_g: the energy gap as $q \to 0$; q^i_{rm}: the position of the i^{th} magnetoroton minimum; and Δ^i_r: the energy at the position of the i^{th} magnetoroton minimum. We observe the following generic features in the dispersion curves for the lowest energy collective mode: i) a gap as $q \to 0$ and ii) minima for $ql_B \sim 1$, and $ql_B \sim 2.1$, which we attribute as a magnetoroton minima, similar to those seen for non-relativistic FQH states. Numerous states also have an additional minimum or shoulder for $ql_B \sim 1.7$. The sharp rise in the dispersion seen near $ql_B \sim 2.5$ marks the right edge of the sequence of magnetoroton minima and the dispersion flattens for larger values of ql_B. [3] For higher energy collective modes, the dispersion is relatively flat in comparison to the lowest energy mode.

The general structure of the collective mode spectrum has qualitative similarities to the collective modes observed in non-relativistic FQH systems [169, 183, 184]. Recently Golkar *et al.* [195] made estimates based on quantized shape deformations of the composite fermion Fermi surface at $\nu = 1/2$. We are not aware of similar arguments for the FQH states in graphene, but this would appear to be an interesting direction for future study.

In Fig. 5.2 we compare the dispersion curves for two different $\nu = 1/3$ states, the Töke-Jain state for the parameter set $(\nu^* = 1, k = 1)$ and the MMS state for the parameter set $(k = 1, m = 1, n = 3)$. We notice that the MMS state has a higher gap as $q \to 0$ and has a higher magnetoroton energy as compared to the Töke-Jain state. In the rest of the results we focus on MMS states motivated by their relevance for EDFQH states [176].

We consider several different MMS $\nu = 1/3$ states and observe that: i) the roton energy is lowest for the state with order parameters $(C, F, N) = (1, -1, -1)$ and $(k, m, n) = (1, 1, 1)$; and ii) as we increase k, m or n the energy of the roton, Δ_r, decreases. In addition, we also observe the appearance of a second minimum around $ql_B \sim 2.1$ and what is sometimes a shoulder and sometimes a local minimum at around $ql_B \sim 1.7$. Numerical values are tabulated in Table 5.1. The minima deepen with increasing values of k, m, and n.

[3] See Appendix G for a plot to this end

k	m	n	C	N	F	ω_g/ω_c	$q^1_{rm}l_B$	$q^2_{rm}l_B$	$q^3_{rm}l_B$	Δ^1_r/ω_c	Δ^2_r/ω_c	Δ^3_r/ω_c
1	1	1	1	-1	-1	1.67	0.99	-	-	1.58	-	-
1	3	2	1	1	1	1.57	0.91	1.65	2.09	1.39	1.42	1.42
1	3	3	1	-1	-1	1.51	0.90	1.73	2.10	1.29	1.32	1.29
2	1	3	-1	0	0	1.46	0.89	1.74	2.11	1.24	1.26	1.22

Table 5.1: Dispersion parameters for selected $\nu = 1/3$ states. ω_g is the gap at $q \to 0$, the $q^i_{rm}l_B$ are the positions of magnetoroton minima and Δ_i/ω_c are the energies of the corresponding rotons.

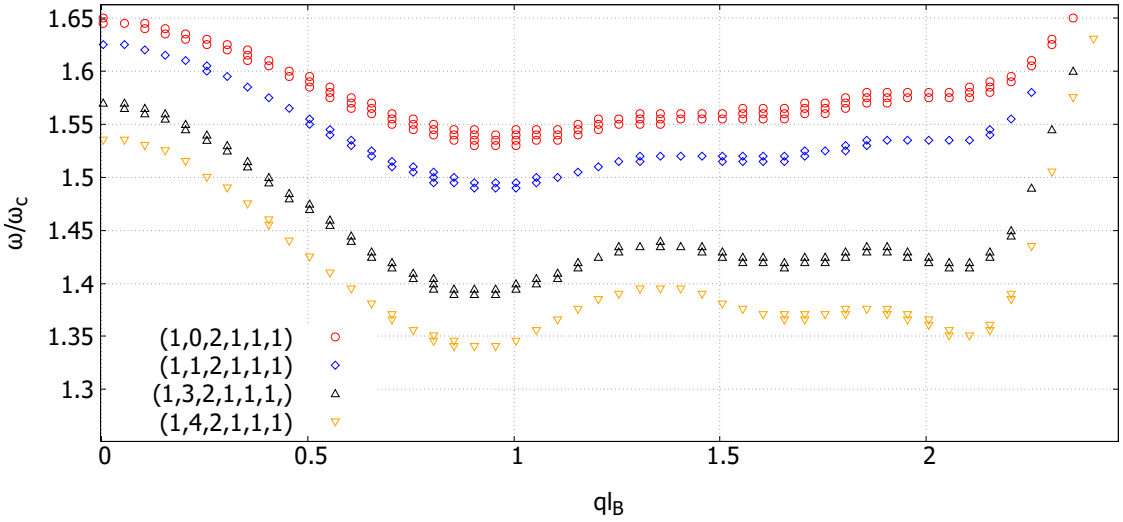

Figure 5.4: Dispersion curves for $\nu = 1/3$ varying the parameter m. The parameter set defined in the text (k, m, n, C, N, F). $(1, 0, 2, 1, 1, 1)$ (red), $(1, 1, 2, 1, 1, 1)$ (blue), $(1, 3, 2, 1, 1, 1)$ (black), $(1, 4, 2, 1, 1, 1)$ (orange).

In Fig. 5.4 we show the variation of the position of the poles and the roton energy as we change m in the triplet (k, m, n). As before, the states we studied are parameterized by the set of parameters (k, m, n, C, F, N). We fixed all the parameters except m. The results are summarized in Table 5.2.

In Fig. 5.5. we show the dispersions for several different $\nu = 1/3$ MMS states with k and m fixed, but varying n. The results are summarized in Table 5.3.

Figures 5.4 and 5.5 lead to the following observations: i) the gap at $q \to 0$ decreases as we go from a low $m(n)$ value to a higher $m(n)$ value; ii) the position of the first roton minimum shifts towards slightly lower q as we go from lower $m(n)$ to higher values of $m(n)$; iii) the position of the second and third roton minima shifts to slightly higher q as we go from lower $m(n)$ to higher values; iv) the roton energies Δ^i_r decrease as we go from lower $m(n)$ to higher values for $i = 1, 2, 3$. In Tables 5.2 and 5.3 we confirm that the observations i)-iv) hold as we go from lower $m(n)$ values to higher $m(n)$ values.

k	m	n	C	N	F	ω_g/ω_c	$q^1_{rm}l_B$	$q^2_{rm}l_B$	$q^3_{rm}l_B$	Δ^1_r/ω_c	Δ^2_r/ω_c	Δ^3_r/ω_c
1	0	2	1	1	1	1.65	0.98	1.66	2.08	1.53	1.56	1.58
1	1	2	1	1	1	1.62	0.97	1.60	2.09	1.49	1.52	1.53
1	3	2	1	1	1	1.57	0.91	1.65	2.09	1.39	1.42	1.42
1	4	2	1	1	1	1.54	0.89	1.69	2.10	1.34	1.37	1.35

Table 5.2: Parameters for $\nu = 1/3$ states varying m. All parameters have the same meaning as in Table I.

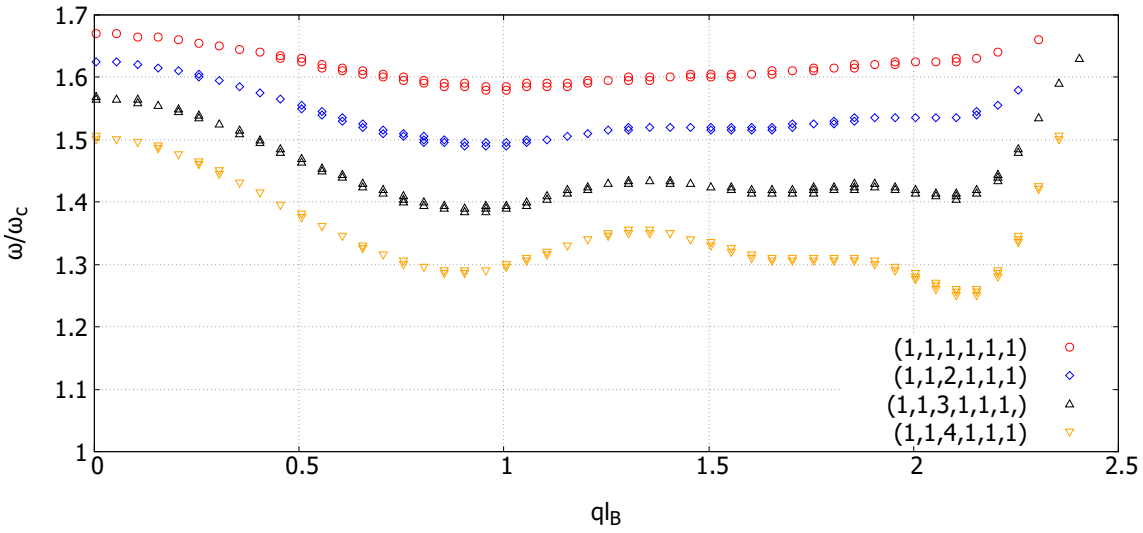

Figure 5.5: Dispersion curves for $\nu = 1/3$ varying the parameter n. The parameter set defined in the text is (k, m, n, C, N, F). $(1,1,1,1,1,1)$ (black), $(1,1,2,1,1,1)$ (red), $(1,1,3,1,1,1)$ (blue), $(1,1,4,1,1,1)$ (orange).

k	m	n	C	N	F	ω_g/ω_c	$q^1_{rm}l_B$	$q^2_{rm}l_B$	$q^3_{rm}l_B$	Δ^1_r/ω_c	Δ^2_r/ω_c	Δ^3_r/ω_c
1	1	1	1	1	1	1.67	0.99	-	-	1.58	-	-
1	1	2	1	1	1	1.62	0.97	1.60	2.09	1.49	1.52	1.53
1	1	3	1	1	1	1.57	0.93	1.69	2.10	1.38	1.42	1.40
1	1	4	1	1	1	1.50	0.90	1.68	2.13	1.29	1.31	1.25

Table 5.3: Parameters for $\nu = 1/3$ states varying n. All parameters have the same meaning as in Table I.

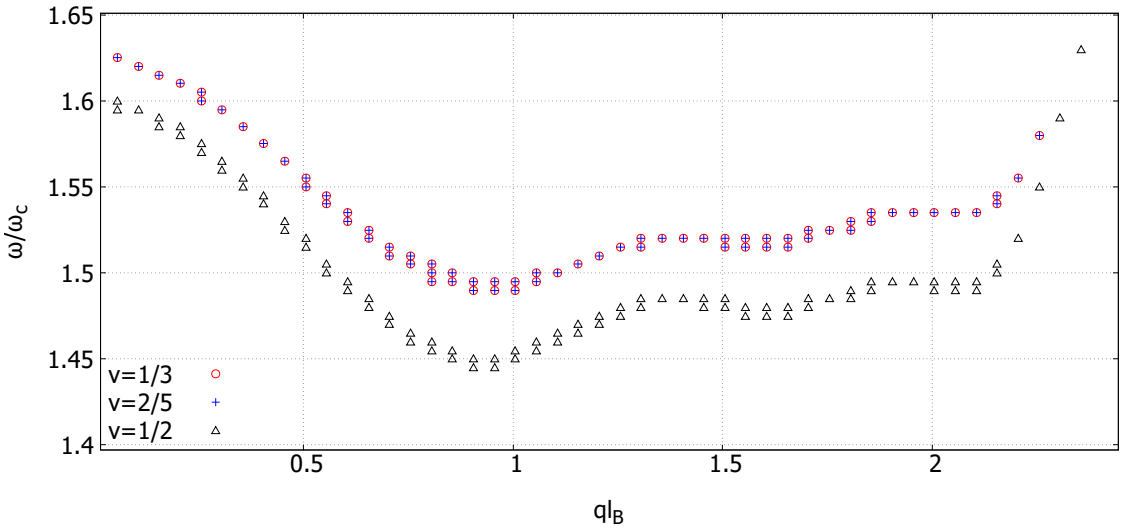

Figure 5.6: Dispersion curves for $\nu = 1/3$ (1,1,2,1,1,1), $\nu = 2/5$ (1,1,2,1,-1,-1) and $\nu = 1/2$ (1,1,2,1,0,0). For this plot (k, m, n) is the same for all three fractions while (C, F, N) varies.

In addition to comparing the effect of different values of m and n on the collective mode spectrum for a given fraction, we also make a comparison of the collective mode spectra for several different incompressible fractions: $\nu = 1/3$, $\nu = 2/5$ and $\nu = 1/2$. Unlike the single component case it is possible to have an incompressible FQH state for $\nu = 1/2$ in a multicomponent quantum Hall system such as graphene [145, 171, 176]. The relevant dispersion curves are plotted in Figs. 5.6 and 5.7.

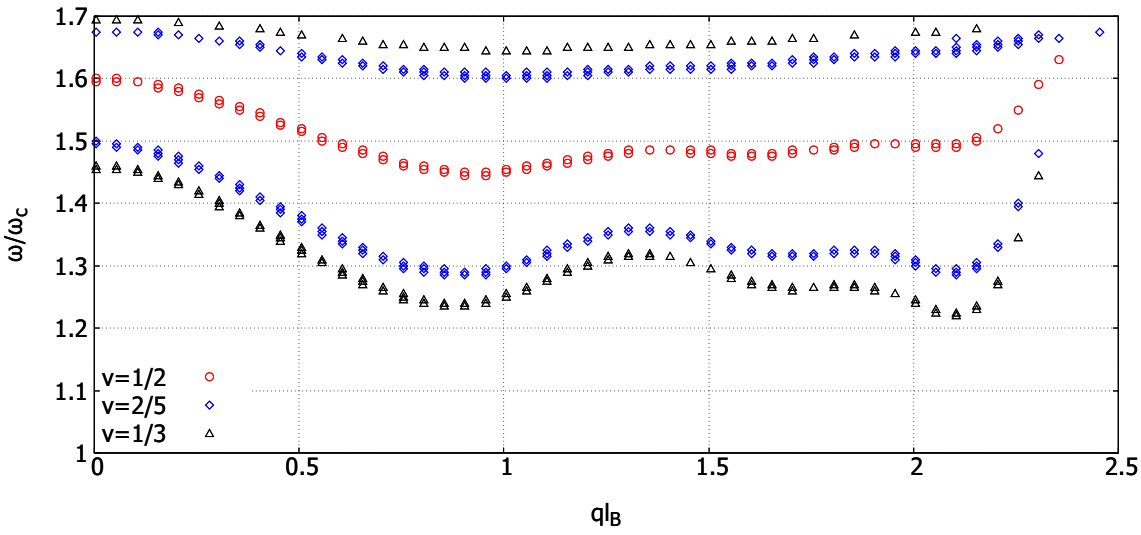

Figure 5.7: Dispersion curves for $\nu = 1/2$ (1,1,2,1,0,0), $\nu = 1/3$ (2,1,2,1,0,0) and $\nu = 2/5$ (2,0,3,1,0,0). For this plot (C, F, N) is the same for all three fractions while (k, m, n) varies.

ν	k	m	n	C	N	F	ω_g/ω_c	$q^1_{rm}l_B$	$q^2_{rm}l_B$	$q^3_{rm}l_B$	Δ^1_r/ω_c	Δ^2_r/ω_c	Δ^3_r/ω_c
1/3	1	1	2	1	1	1	1.62	0.97	1.60	2.06	1.49	1.52	1.53
2/5	1	1	2	1	-1	-1	1.62	0.97	1.60	2.06	1.49	1.52	1.53
1/2	1	1	2	1	0	0	1.59	0.92	1.63	2.07	1.45	1.48	1.49

Table 5.4: $\nu = 1/3$, $\nu = 1/2$ and $\nu = 2/5$ for fixed (k,m,n). All parameters have the same meaning as in Table I.

ν	k	m	n	C	N	F	ω_g/ω_c	$q^1_{rm}l_B$	$q^2_{rm}l_B$	$q^3_{rm}l_B$	Δ^1_r/ω_c	Δ^2_r/ω_c	Δ^3_r/ω_c
1/2	1	1	2	1	0	0	1.59	0.92	1.63	2.07	1.45	1.48	1.49
2/5	2	0	3	1	0	0	1.49	0.91	1.71	2.11	1.29	1.32	1.29
1/3	2	1	3	1	0	0	1.46	0.89	1.70	2.10	1.24	1.26	1.22

Table 5.5: $\nu = 1/3$, $\nu = 1/2$ and $\nu = 2/5$ for fixed (C,F,N). All parameters have the same meaning as in Table I.

For the spectra in Fig. 5.6 we consider the simplest flux attachment, (k,m,n), that is consistent with all three of these states. We found that for this case different CF-LLs are occupied, translating to different order parameter combinations, (C,F,N). The $\nu = 1/3$ and the $\nu = 2/5$ state have the same spectra and a higher gap, ω_g than the $\nu = 1/2$ states. For the spectra in Fig. 5.7 we consider CF-LL fillings (equivalently combinations of CSB orders) that are the same for all three FQH states. In this case the flux attachment parameters (k,m,n) differ in each case. We observe that in this case the $\nu = 1/2$ state is the most stable followed by the $\nu = 2/5$ and then the $\nu = 1/3$ state. The results are summarized in Tables 5.4 and 5.5.

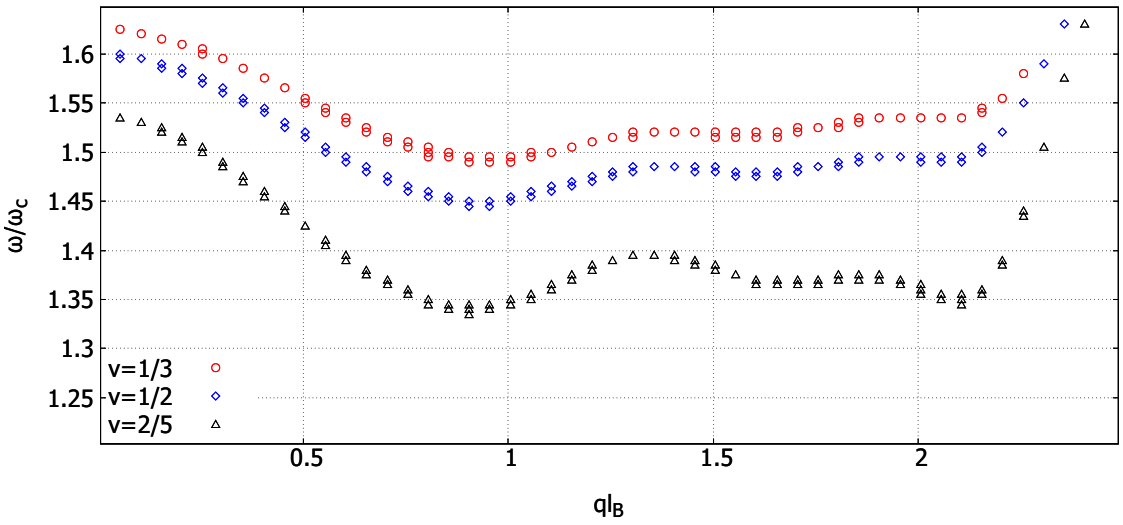

Figure 5.8: Dispersion curves for $\nu = 1/3$ (1,1,2,1,1,1), $\nu = 2/5$ (1,1,2,1,0,0) and $\nu = 1/2$ (1,4,2,1,1,1).

5.5 Conclusion

We primarily studied the $\nu = 1/3$ FQH state, considering various flux attachment schemes parameterized by $\mathscr{K}$. We considered the collective excitations for two classes of variational states - the Töke-Jain sequence [143], parameterized by (ν^*,k) and the MMS sequence [145, 176], parameterized by (k,m,n). We found that the MMS states displayed a larger $q \to 0$ gap, ω_g, and a larger magnetoroton gap than the Töke-Jain states for the variational states we considered. For the MMS states we considered, we found that increasing k, m or n generally reduced ω_g and the magnetoroton gap.

Within the framework of the Chern-Simons theory that we use to obtain the collective excitation spectrum, the larger gaps we find for MMS states with low values of (k,m,n) suggest that these are likely to be the most stable FQH states. However, there is the caveat that as a mean-field like theory, the Chern-Simons approach will almost certainly over-estimate energy gaps and it is unknown whether fluctuations beyond mean field theory will differ between Töke-Jain and MMS states, although we see no a priori reason why they should be significantly different in the two cases.

We compared the excitation spectra for MMS states for several different fractions, $\nu = 1/3$, $2/5$ and $1/2$. The true nature of the ground states for these fractions are not currently known [171, 176]. Hence we considered a variety of variational ground states of the MMS type that give rise to incompressible states at these fractions. We compared excitations for states with the same flux attachment scheme (fixed (k,m,n)), but different composite fermion LL fillings (corresponding to differing order parameters (C,F,N)). We also compared excitations for states with the same order parameters (C,F,N) but different flux attachment schemes. The ordering of the states in terms of which had the largest gap ω_g is different in the two cases. Experimental observations (Fig. S14a in Ref. [176]) show the $\nu = 1/3$ and $\nu = 1/2$ states persisting to a temperature of $T = 2.0$ K, while the $\nu = 2/5$ state is no longer present at that temperature. Our calculation of the collective mode spectra do not take into account temperature dependence of the order parameters C, F and N and so it is not possible to make a direct comparison between our results and experiment. However, we do give an example of states which lead to the same ordering in ω_g as the stability of the experimental states in Fig. 5.8.

In addition to the energy scales associated with the collective excitations, the position of the magnetoroton minimum is also a quantity of interest. Previous work [169, 195–197] has elaborated on the position of the magnetoroton minimum for fractions in the Jain sequence, $\nu = s/(2s+1)$, and it was found that for low values of s the minimum was located around $ql_B \sim 1$. Ref. [196] calculated the positons of minima for $n = 0,1$ LLs in graphene. This is in agreement with our observations in Sec. V, although we find

that for both Töke-Jain and MMS states, there may be secondary and tertiary minima for $ql_B \sim 1.7$ and $ql_B \sim 2$ respectively.

In our calculations here we have shed some light on collective excitations for certain classes of FQH states in graphene. The approach we have taken is restricted to order parameters that can be written in terms of just spin and valley degrees of freedom, such as CDW, Néel AFM and ferromagnetic order, For more general orders that may require an eight component Dirac fermion description, such as in-plane antiferromagnetism [130] or partially sublattice polarized (PSP) order [176], we are unable to calculate the collective excitation spectra. This is because for those more general orders, the order parameter leads to a problem which is mathematically equivalent to one in which one is trying to calculate the collective excitations in a system where there is tunnelling between two separate FQH systems. We are not aware of any succesful attempts to use Chern-Simons approaches to calculate collective excitation spectra in FQH systems with tunnelling between layers. Whilst there is a hope that collective excitations might allow different patterns of symmetry breaking to be distinguished, our results show that at least for the types of symmetry breaking we considered, there are not strong qualitative differences in the dispersions that depend on the symmetry breaking order. Figures 5.6 and 5.7 demonstrate that the flux attachment scheme has more impact on the dispersion than the order parameters we considered. It would be interesting to see if other patterns of symmetry breaking also lead to similar collective excitations. Additionally, including the effects of quantum fluctuations beyond mean field theory would be an interesting avenue to explore in future work.

Chapter 6

Summary and Outlook

The integer quantum Hall effect in graphene is different from the conventional IQHE in semiconductors (e.g. GaAs) owing to the relativistic nature of the electrons in graphene. In graphene the orbital wavefunctions (or form factors) for the zeroth Landau level (ZLL) are identical to the wavefunctions for the lowest Landau level in semiconductor systems. Hence the FQHE in graphene in the ZLL is expected to be similar to the FQHE in semiconductor systems. Thus the particular form of the LLs in graphene does not play a role in the FQHE in graphene [198]. The differences in the FQHE arise due to the SU(4) symmetry of the Landau levels in graphene and the symmetry breaking associated with this SU(4) symmetry. The SU(4) symmetry lends to a multicomponent description of FQH states in graphene [143, 149] which have been observed in experiments [55, 56]. Even denominator states for single component systems are compressible [95, 170] and the same might be expected to be the case in graphene. On the other hand, due to its SU(4) symmetric Landau levels graphene constitutes a multicomponent system and hence supports an even denominator FQH state observed recently in experiments [171] which was argued to be associated with a transition in the underlying isospin order [199]. There have been several theoretical proposals in addition to our work [176] that have attempted to explain the EDFQH states in graphene [200, 201].

In this thesis we have studied the fractional quantum Hall effect in graphene in the presence of chiral symmetry breaking orders : charge density wave (C), easy-axis Neél antiferromagnetic order (N) and ferromagnetic order (F). We proposed candidate variational wavefunctions for EDFQH states at $\nu = \frac{1}{2}$ and $\nu = \frac{1}{4}$ observed in experiments [171, 199]. Subsequently Indra *et al.* [200] studied the ground state energies of various variational wavefunctions that we proposed and several other that we did not propose by including the Coulomb interactions and they observed that for the $\nu = 1/2$ state the parameter set that had the lowest energy was the MMS state with $(k, m, n) = (1, 1, 2)$ which is one of the states we suggested (in Table 4.1). In addition, they also found that parameter set for states with the lowest energy for the $\nu = 1/2$ state was related to the

parameter set of lowest energy states for the $\nu = 1/4$ state by the relation $j \to j+1$ for $j = k, m, n$ which is consistent with our results [176]. We also found that within these set of flux attachment there is a degeneracy associated with the pattern of symmetry breaking present in these states.

In an attempt to develop tools to distinguish between different broken symmetry states we studied the excitation spectra of the FQH states within the formalism developed in Ref. [146]. We primarily studied the $\nu = 1/3$ FQH state, considering various flux attachment schemes parametrized by flux attachment matrix $\mathscr{K}$. We studied the collective excitations for the Töke-Jain states and the MMS states. We found that the MMS states had a larger direct gap ($q \to 0$), ω_g, and a larger magnetoroton gap, Δ, than the Töke-Jain states. Thereafter, focusing on MMS states we found that the gaps, ω_g, Δ, were larger for lower values of k, m and n. The positions of the minima considered were found to be in agreement with previous work which elaborated on the postion of magnetoroton minimum for fractions in the Jain sequence, $\nu = s/(2s+1)$ [169, 195–197]. We also compared the excitation spectra for $\nu = 1/3$, $2/5$ and $1/2$ states and provided examples of parameters that could explain the relative stability of these states observed in experiments. Although the pattern of symmetry breaking does have some impact, the excitation spectra are largely dominated by the flux attachment scheme.

The work presented in this thesis leads to possible research directions for the future. The Schiwnger-Keldysh method developed in Ref. [146] and used to study the collective excitations in this thesis can be extended to include temperature dependence of FQH states, effects of disorder on the FQH states and applied to out of equilibrium dynamics in the FQH states considered here. In the context of traditional FQHE, Halperin, Lee and Read [95] argued that gauge fluctuations of the Chern-Simons gauge field leads to corrections in the effective mass, m^*, that describes low energy excitations. In the case of graphene with massless Dirac fermions there is no obvious analogy that can be made. Going beyond the mean field theory used in the thesis to include the effects of gauge fluctuations will thus be an interesting area of investigation. The multicomponent flux attachment scheme could be used to study the FQHE in multilayer graphene systems like bilayer graphene, twisted bilayer graphene or multilayer graphene systems in general.

Finally, we did not find a clear way to distinguish the pattern of symmetry breaking using collective excitations. A limitation of our approach is that we are restricted to order parameters that are diagonal in the valley + spin subspace namely the C, F, and N orders. More general orders like canted anti-ferromagnetic (CAF) order or partially sublattice polarized (PSP) order that have been proposed for quantum Hall states in the zeroth Landau level are non-diagonal in the valley + spin subspace. In Ref. [138] the authors observed a continuous field-tuned phase transition from a valley ordered

state to a inter-valley coherent state with a Kekulé distortion of the electronic density at $\nu = 0$. A Kekulé type order would also be non-diagonal in the valley + spin subspace. The problem with including the off-diagonal orders is mathematically equivalent to the one with tunneling between two separate FQH systems. This problem has not been resolved and a future resolution to this problem will benefit the multicomponent system considered in this thesis which can then be extended to include interlayer tunneling in multilayered systems.

Bibliography

[1] A. H. Castro Neto, F. Guinea, and N. M. R. Peres, Phys. World **19**, 33 (2006).

[2] R. Saito, G. Dresselhaus, and M. S. Dresselhaus, *Physical Properties of Carbon Nanotubes* (Imperial College Press, London, 1998).

[3] J. C. Charlier, X. Blase, and S. Roche, Rev. Mod. Phys. **79**, 677 (2007).

[4] W. Andreoni, *The Physics of Fullerene-Based and Fullerene-Related Materials* (Springer, Berlin, 2000).

[5] K. S. Novoselov, A. K. Geim, S. V. Morozov, D. Jiang, Y. Zhang, S. V. Dubonos, I. V. Gregorieva, and A. A. Firsov, Science **306**, 666 (2004).

[6] A. K. Geim and A. H. MacDonald, Phys. Today **60**, 35 (2007).

[7] A. H. Castro Neto, F. Guinea, N. M. R. Peres, K. S. Novoselov, and A. K. Geim, Rev. Mod. Phys. **81**, 109 (2009).

[8] M. I. Katsnelson, K. S. Novoselov, and A. K. Geim, Nat. Phys. **2**, 620 (2006).

[9] M. I. Katsnelson and K. S. Novoselov, Solid State. Commun. **143**, 3 (2007).

[10] F. Giannazzo, R. Dagher, E. Schiliro, S. E. Panasci, G. Greco, G. Nicotra, F. Roccaforte, S. Agnello, J. Brault, Y. Cordier, and A. Michon, Nanotechnology **32**, 015705 (2020).

[11] Y. Li, K. Tantiwanichapan, A. K. Swan, and R. Paiella, Nanophotonics **9**, 1901 (2020).

[12] S. Goenka, V. Sant, and S. Sant, J. Control. Release **173**, 75 (2014).

[13] E. Yoo and H. Zhou, ACS Nano **5**, 3020 (2011).

[14] Y. Wang, L. Wang, T. Yang, X. Li, X. Zang, M. Zhu, W. Kunlin, W. Dehai, and H. Zhu, Adv. Funct. Mater. **24**, 4666 (2014).

[15] T. Xie, L. Zhang, Y. Wang, and X. Wang, Ceram. Int. **45**, 2516 (2019).

[16] S. H. Aboutalebi, J. Rouhollah, D. Esrafilzadeh, M. Salari, Z. Gholamvand, S. A. Yamini, K. Konstantinov, R. L. Sheperd, J. Chen, S. E. Moulton, P. C. Innis, A. I. Minett, J. M. Raza, and G. G. Wallace, ACS Nano **8**, 2456 (2014).

[17] Y. Xu, M. G. Schwab, A. J. Strudwick, I. Hennig, X. Feng, and Z. W. Klaus, Adv. Energy Mater. **3**, 1035 (2013).

[18] P. Kuzhir, N. Volynets, S. Maksimenko, T. Kaplas, and Y. Svirko, J. Nanosci. Nanotechnol. **13**, 5864 (2013).

[19] Y. Cao, V. Fatemi, A. Demir, S. Fang, S. L. Tomarken, J. Y. Luo, J. D. Sanchez-Yamagishi, K. Watanabe, T. Taniguchi, E. Kaxiras, R. C. Ashoori, and P. Jarillo-Herrero, Nature **556**, 80 (2018).

[20] Y. Cao, V. Fatemi, S. Fang, K. Watanabe, T. Taniguchi, E. Kaxiras, and P. Jarillo-Herrero, Nature **556**, 43 (2018).

[21] X. Lu, P. Stepanov, W. Yang, M. Xie, M. A. Aamir, I. Das, C. Urgell, K. Watanabe, T. Taniguchi, G. Zhang, A. Bachtold, A. H. MacDonald, and D. E. Efetov, Nature **574**, 653 (2019).

[22] A. Kerelsky, L. J. McGilly, D. M. Kennes, L. Xian, M. Yankowitz, S. Chen, K. Watanabe, T. Taniguchi, J. Hone, C. Dean, A. Rubio, and A. N. Pasupathy, Nature **572**, 95 (2019).

[23] Y. Jiang, X. Lai, K. Watanabe, T. Taniguchi, K. Haule, J. Mao, and E. Y. Andrei, Nature **573**, 91 (2019).

[24] Y. Xie, B. Lian, B. Jäck, X. Liu, C. Chiu, K. Watanabe, T. Taniguchi, B. A. Bernevig, and A. Yazdani, Nature **572**, 101 (2019).

[25] Y. Choi, J. Kemmer, Y. Peng, A. Thomson, H. Arora, R. Polski, Y. Zhang, H. Ren, J. Alicea, G. Refael, F. von Oppen, K. Watanabe, T. Taniguchi, and S. Nadj-Perge, Nat. Phys. **15**, 1174 (2019).

[26] T. J. Peltonen, R. Ojajärvi, and T. T. Heikkilä, Phys. Rev. B **98**, 220504 (2018).

[27] M. Koshino, N. F. Q. Yuan, T. Koretsune, M. Ochi, K. Kuroki, and L. Fu, Phys. Rev. X **8**, 031087 (2018).

[28] H. C. Po, L. Zou, A. Vishwanath, and T. Senthil, Phys. Rev. X **8**, 031089 (2018).

[29] N. F. Q. Yuan and L. Fu, Phys. Rev. B **98**, 045103 (2018).

[30] C. Xu and L. Balents, Phys. Rev. Lett. **121**, 087001 (2018).

[31] J. Kang and O. Vafek, Phys. Rev. X **8**, 031088 (2018).

[32] J. F. Dodaro, S. A. Kivelson, Y. Schattner, X. Q. Sun, and C. P. Wang, Phys. Rev. B **98**, 075154 (2018).

[33] B. Padhi, C. Setty, and P. W. Phillips, Nano. Lett. **18**, 6175 (2018).

[34] X. Y. Xu, K. T. Law, and P. A. Lee, Phys. Rev. B **98**, 121406 (2018).

[35] F. Wu, A. H. MacDonald, and I. Martin, Phys. Rev. Lett. **121**, 257001 (2018).

[36] F. Guinea and N. R. Walet, Phys. Rev. B **99**, 205134 (2019).

[37] V. R. Shaginyan, A. Z. Msezane, V. A. Stephanovich, G. S. Japaridze, and E. V. Kirichenko, Phys. Scripta **94**, 065801 (2019).

[38] J. Wakabayshi and S. Kawaji, J. Phys. Soc. Jpn. **44**, 1839 (1978).

[39] T. Ando, Y. Matsumoto, and Y. Uemura, J. Phys. Soc. Jpn. **39**, 279 (1975).

[40] K. von Klitzing, G. Dorda, and M. Pepper, Phys. Rev. Lett. **45**, 494 (1980).

[41] T. Chakraborty and P. Pietilainen, *The Fractional Quantum Hall Effect* (Springer, New York, 1988).

[42] S. D. Sarma and A. Pinczuk, *Perspectives In Quantum Hall Effects* (John Wiley and Sons Inc., New York, 1997).

[43] D. C. Tsui, H. L. Stormer, and A. C. Gossard, Phys. Rev. Lett. **48**, 1559 (1982).

[44] G. S. Boebinger, A. M. Chang, H. L. Störmer, and D. C. Tsui, Phys. Rev. Lett. **55**, 1606 (1985).

[45] S. Kawaji, J. Wakabayashi, J. Yoshino, and H. Sakaki, J. Phys. Soc. Jpn. **53**, 1915 (1984).

[46] A. M. Chang, M. A. Paalanen, D. C. Tsui, H. L. Störmer, and J. C. M. Hwang, Phys. Rev. B **28**, 6113 (1983).

[47] G. Ebert, K. von Klitzing, J. C. Maan, G. Remenyi, C. Probst, G. Weimann, and W. Schlapp, J. Phys. C **17**, L775 (1984).

[48] R. B. Laughlin, Phys. Rev. Lett. **50**, 1395 (1983).

[49] V. P. Gusynin and S. G. Sharapov, Phys. Rev. Lett. **95**, 146801 (2005).

[50] N. M. R. Peres, F. Guinea, and A. H. Castro Neto, Phys. Rev. B **73**, 125411 (2006).

[51] K. S. Novoselov, A. K. Geim, S. V. Morozov, D. Jiang, M. I. Katsnelson, I. V. Grigorieva, S. V. Dubonos, and A. A. Firsov, Nature **438**, 197 (2005).

[52] Y. Y. W. Zhang, H. L. Tan, H. L. Stormer, and P. Kim, Nature **438**, 201 (2005).

[53] I. Skachko, X. Du, F. Duerr, A. Luican, D. A. Abanin, L. S. Levitov, and E. Y. Andrei, Philos. Trans. R. Soc. A **368**, 5403 (2010).

[54] X. Du, I. Skachko, F. Duerr, A. Luican, and E. Y. Andrei, Nature (London) **462**, 192 (2009).

[55] C. Dean, A. Young, P. Cadden-Zimansky, L. Wang, H. Ren, K. Watanabe, T. Taniguchi, P. Kim, J. Hone, and K. Shepard, Nat. Phys. **7**, 693 (2011).

[56] B. E. Feldman, B. Krauss, J. H. Smet, and A. Yacoby, Science **337**, 1196 (2012).

[57] B. E. Feldman, A. J. Levin, D. A. Krauss, B. annd Abanin, B. I. Halperin, J. H. Smet, and A. Yacoby, Phys. Rev. Lett. **111**, 076802 (2013).

[58] K. I. Bolotin, F. Gharari, M. D. Shulman, H. L. Stormer, and P. Kim, Nature (London) **462**, 196 (2009).

[59] F. Amet, A. J. Bestwick, J. R. Williams, L. Balicas, K. Watanbe, T. Taniguchi, and D. Godlhaber-Gordon, Nat. Commun. **6**, 5838 (2015).

[60] T. Ando, A. B. Fowler, and F. Stern, Rev. Mod. Phys. **54**, 437 (1982).

[61] D. C. Tsui and A. C. Gossard, Appl. Phys. Lett. **38**, 550 (1981).

[62] M. A. Paalanen, D. C. Tsui, and A. C. Gossard, Phys. Rev. B **25**, 5566 (1982).

[63] G. Ebert, K. von Klitzing, C. Probst, and K. Ploog, Solid State Comm. **44**, 95 (1982).

[64] R. J. Nicholas, K. von Klitzing, and T. Englert, Solid Stae Comm. **34**, 51 (1980).

[65] Y. Guldner, J. P. Hirtz, J. P. Vieren, P. Voisin, M. Voos, and M. Razhegi, Physique Lett. **43**, L613 (1982).

[66] Y. Guldner, J. P. Vieren, M. Voos, F. Delahaye, D. Dominiguez, J. P. Hirtz, and M. Razhegi, Phys. Rev. B **33**, 3990 (1986).

[67] W. P. Kirk, P. S. Kobiela, R. A. Schiebel, and M. A. Reed, J. Vac. Sci. Tech. **A4**, 2132 (1986).

[68] E. E. Mendez, L. Esaki, and L. L. Chang, Phys. Rev. Lett. **55**, 2216 (1985).

[69] F. F. Fang, Surf. Sci. **305**, 301 (1983).

[70] D. Tong, electronic preprint arXiv:1606.06687 (2016).

[71] D. C. Tsui, H. L. Stormer, and A. C. Gossard, Rev. Mod. Phys. **71**, S298 (1991).

[72] S. A. Trugman and S. Kivelson, Phys. Rev. B **31**, 5280 (1985).

[73] F. D. M. Haldane, Phys. Rev. Lett. **51**, 605 (1983).

[74] B. I. Halperin, Phys. Rev. Lett. **52**, 1583 (1984).

[75] R. de Picciotto, M. Reznikov, M. Heiblum, V. Umansky, G. Bunin, and D. Mahalu, Nature **389**, 162 (1997).

[76] S. M. Girvin and R. E. Prange, *The Quantum Hall Effect* (Springer, New York, 1990).

[77] S. H. Simon, E. H. Rezayi, and N. R. Cooper, Phys. Rev. B **75**, 195306 (2007).

[78] S. Kivelson, C. Kallin, D. P. Arovas, and J. R. Schrieffer, Phys. Rev. B **36**, 1620 (1987).

[79] A. H. MacDonald and U. E. Ekenberg, Phys. Rev. B **39**, 5959 (1989).

[80] S. R. Eric Yang, A. H. MacDonald, and D. Yoshioka, Phys. Rev. B **41**, 1290 (1990).

[81] Z. Ezawa, *Quantum Hall Effects: Field Theoretical Approach and Related Topics* (World Scientific Publishing Company, Singapore, 2008).

[82] R. B. Laughlin, Surf. Sci. **141**, 11 (1984).

[83] J. K. Jain, Phys. Rev. Lett. **63**, 199 (1989).

[84] N. Read, Phys. Rev. Lett. **65**, 1502 (1990).

[85] F. Wilczek, Phys. Rev. Lett. **49**, 957 (1982).

[86] R. B. Laughlin, Phys. Rev. Lett. **60**, 2677 (1988).

[87] R. B. Laughlin, Phys. Rev. B **23**, 5632 (1981).

[88] B. I. Halperin, Phys. Rev. B **25**, 2185 (1982).

[89] J. K. Jain, *Composite Fermions* (Cambridge University Press, New york, 2007).

[90] E. Witten, electronic preprint arXiv:1510.07698 (2015).

[91] G. V. Dunne, electronic preprint arXiv:hep-th/9902115 (1999).

[92] S. M. Girvin and A. H. MacDonald, Phys. Rev. Lett. **58**, 1252 (1987).

[93] N. Read, Phys. Rev. Lett. **62**, 86 (1989).

[94] A. Lopez and E. Fradkin, Phys. Rev. B **44**, 5246 (1991).

[95] B. I. Halperin, P. A. Lee, and N. Read, Phys. Rev. B **47**, 7312 (1997).

[96] R. Shankar and G. Murthy, Phys. Rev. Lett. **79**, 4437 (1997).

[97] X.-G. Wen, Adv. Phys. **44**, 405 (1995).

[98] X. G. Wen and A. Zee, Phys. Rev. B **46**, 2290 (1992).

[99] P. R. Wallace, Phys. Rev. **71**, 622 (1947).

[100] G. W. Semenoff, Phys. Rev. Lett. **53**, 2449 (1984).

[101] B. Roy, *Aspects of interacting electrons on graphene honeycomb lattice*, Ph.D. thesis, Simon Fraser University (2011).

[102] F. Bassani and G. Pastori Parravicini, *Electronic States and Optical Transitions in Solid* (Pegamon, New York, 1975).

[103] J. González, F. Guinea, and M. A. H. Vozmediano, Nucl. Phys. B **424**, 595 (1994).

[104] D. C. Elias, R. V. Gorbachev, A. S. Mayorov, S. V. Morozov, A. A. Zhukov, P. Blake, L. A. Ponomarenko, I. V. Grigorieva, K. S. Novoselov, F. Guinea, and A. K. Geim, Nat. Phys. **7**, 701 (2011).

[105] I. Herbut, Phys. Rev. Lett. **97**, 146401 (2006).

[106] M. O. Goerbig, Rev. Mod. Phys. **83**, 1193 (2011).

[107] S. C. Zhang, T. H. Hansson, and S. Kivelson, Phys. Rev. Lett. **62**, 82 (1989).

[108] Y. Zhang, Z. Jiang, J. P. Small, M. S. Purewal, Y. W. Tan, M. Fazlollahi, J. D. Chudow, J. A. Jaszczak, H. L. Stormer, and P. Kim, Phys. Rev. Lett. **96**, 136806 (2006).

[109] Z. Jiang, Y. Zhang, H. L. Stormer, and P. Kim, Phys. Rev. Lett. **99**, 106802 (2007).

[110] D. V. Khveshchenko, Phys. Rev. Lett. **87**, 246802 (2001).

[111] H. Leal and D. V. Khveshchenko, Nucl. Phys. B **687**, 323 (2004).

[112] I. Herbut, V. Juričič, and B. Roy, Phys. Rev. B **79**, 085116 (2009).

[113] K. Yang, S. D. Sarma, and A. H. MacDonald, Phys. Rev. B **74**, 075423 (2006).

[114] M. O. Goerbig, R. Moessner, and B. Doucot, Phys. Rev. B **74**, 161407 (R) (2006).

[115] J. N. Fuchs and P. Lederer, Phys. Rev. Lett. **98**, 016803 (2007).

[116] V. P. Gusynin, V. A. Miransky, S. G. Sharapov, and I. A. Shovkovy, Phys. Rev. B **74**, 195429 (2006).

[117] K. Nomura and A. H. MacDonald, Phys. Rev. Lett. **96**, 256602 (2006).

[118] I. Herbut, Phys. Rev. B **76**, 085432 (2007).

[119] I. Herbut, Phys. Rev. B **75**, 165411 (2007).

[120] J. Jung and A. H. MacDonald, Phys. Rev. B **80**, 235417 (2009).

[121] G. W. Semenoff and F. Zhou, J. High Energy Phys. **07**, 037 (2011).

[122] Y. Barlas, K. Yang, and A. H. MacDonald, Nanotechnology **23**, 052001 (2012).

[123] M. Kharitonov, Phys. Rev. B **85**, 155439 (2012).

[124] J. Alicea and M. P. A. Fisher, Phys. Rev. B **74**, 075422 (2006).

[125] E. V. Gorbar, V. P. Gusynin, V. A. Miransky, and I. A. Shovkovy, Phys. Rev. B **78**, 085437 (2008).

[126] E. V. Gorbar, V. P. Gusynin, and V. A. Miransky, Low Temp. Phys. **34**, 790 (2008).

[127] K. Yang, Solid State. Commun. **143**, 27 (2007).

[128] V. A. Miransky and I. A. Shovkovy, Physics Reports **576**, 1 (2015).

[129] V. P. Gusynin, V. A. Miransky, and I. A. Shovkovy, Phys. Rev. Lett. **73**, 3499 (1994).

[130] B. Roy, M. P. Kennett, and S. D. Sarma, Phys. Rev. B **90**, 201409 (R) (2014).

[131] E. V. Gorbar, V. P. Gusynin, V. A. Miransky, and I. A. Shovkovy, Phys. Rev. B **66**, 045108 (2002).

[132] D. A. Abanin, B. E. Feldman, A. Yacoby, and B. I. Halperin, Phys. Rev. B **88**, 115407 (2013).

[133] G. L. Yu, R. Jalil, B. Belle, A. S. Mayorov, P. Blake, F. Schedin, S. V. Morozov, L. A. Ponomarenko, F. Chiappini, S. Wiedmann, U. Zeitler, M. I. Katsnelson, A. K. Geim, K. S. Novoselov, and D. C. Elias, Proc. Natl. Acad. Sci. USA **110**, 3282 (2013).

[134] A. F. Young, C. R. Dean, L. Wang, H. Ren, P. Cadeen-Zimansky, K. Watanabe, T. Taniguchi, J. Hone, K. L. Shepard, and P. Kim, Nat. Phys. **8**, 550 (2012).

[135] H. Chen, M. R. C. Fitzpatrick, S. Narayanan, B. Roy, and M. P. Kennett, Phys. Rev. B **102**, 205401 (2020).

[136] A. F. Young, J. D. Sanchez-Yamagishi, B. Hunt, S. K. Choi, K. Watanabe, T. Taniguchi, R. C. Ashoori, and P. Jarillo-Herrero, Nature (London) **505**, 528 (2014).

[137] S. Li, Y. Zhang, L. Yin, and L. He, Phys. Rev. B **100**, 085437 (2019).

[138] X. Li, G. Farahi, C. Chiu, Z. Papic, K. Watanabe, T. Taniguchi, M. P. Zalatel, and A. Yazdani, Science **375**, 321 (2022).

[139] A. Coissard, D. Wander, H. Vignaud, A. G. Grushin, C. Repellin, K. Watanabe, T. Taniguchi, F. Gay, C. B. Winkleman, H. Courtois, H. Sellier, and B. Sacépe, Nature **605**, 51 (2022).

[140] A. Das, R. K. Kaul, and G. Murthy, Phys. Rev. Lett. **128**, 106803 (2022).

[141] S. J. De, A. Das, S. Rao, R. K. Kaul, and G. Murthy, Phys. Rev. B **107**, 125422 (2023).

[142] A. C. Balram, C. Töke, A. Wójs, and J. K. Jain, Phys. Rev. B **92**, 075410 (2015).

[143] C. Töke and J. K. Jain, Phys. Rev. B **75**, 245440 (2007).

[144] C. Töke, P. E. Lammert, V. H. Crespi, and J. K. Jain, Phys. Rev. B **74**, 235417 (2006).

[145] S. Modak, S. S. Mandal, and K. Sengupta, Phys. Rev. B **84**, 165118 (2011).

[146] C. Fräßdorf, Phys. Rev. B **97**, 115123 (2018).

[147] M. R. Peterson and C. Nayak, Phys. Rev. Lett **113**, 086401 (2014).

[148] R. de Gail, R. N., and M. O. Goerbig, Phys. Rev. B **77**, 165310 (2008).

[149] M. O. Goerbig and N. Regnault, Phys. Rev. B **75**, 241405 (2007).

[150] Z. Papić, M. O. Goerbig, and N. Regnault, Solid State Commun. **149**, 1056 (2009).

[151] V. Scarola and J. K. Jain, Phys. Rev. B **64**, 085613 (2001).

[152] W. Beugeling, M. O. Goerbig, and C. M. Smith, Phys. Rev. B **81**, 195303 (2010).

[153] D. V. Khveshchenko, Phys. Rev. B **75**, 153405 (2007).

[154] K. Yang, S. Das Sarma, and A. H. MacDonald, Phys. Rev. B **74**, 075423 (2006).

[155] I. Sodemann and A. H. MacDonald, Phys. Rev. Lett. **112**, 126804 (2014).

[156] N. Shibata and K. Nomura, J. Phys. Soc. Jpn. **78**, 104708 (2009).

[157] M. O. Goerbig, R. Moessner, and B. Doucot, Phys. Rev. B **74**, 161407(R) (2006).

[158] R. Tao and Y. S. Wu, Phys. Rev. B **31**, 6859 (1985).

[159] G. Fano, F. Ortolani, and E. Tosatti, Il Nuovo Cimento D **9**, 1337 (1987).

[160] R. G. Clark, R. J. Nicholas, and A. Usher, Surf. Sci. **170**, 141 (1986).

[161] R. Willett, J. P. Eisenstein, H. L. Störmer, D. C. Tsui, A. C. Gossard, and J. H. English, Phys. Rev. Lett. **59**, 1776 (1987).

[162] Y. W. Suen, L. W. Engel, M. B. Santos, M. Shayegan, and D. C. Tsui, Phys. Rev. Lett. **68**, 1379 (1992).

[163] J. P. Eisenstein, G. S. Boebinger, L. N. Pfeifer, K. W. West, and S. N. He, Phys. Rev. Lett. **68**, 1383 (1992).

[164] Y. Liu, S. Hasdemir, D. Kamburov, A. L. Graninger, M. Shayegan, L. N. Pfeiffer, K. W. West, K. W. Baldwin, and R. Winkler, Phys. Rev. B **89**, 165313 (2014).

[165] D. R. Luhman, W. Pan, D. C. Tsui, L. N. Pfeiffer, K. W. Baldwin, and K. W. West, Phys. Rev. Lett. **101**, 266804 (2008).

[166] J. Shabani, T. Gokmen, Y. T. Chiu, and M. Shayegan, Phys. Rev. Lett. **103**, 256802 (2009).

[167] S. C. Zhang and V. Kalmeyer, Phys. Rev. B **46**, 9889 (R) (1992).

[168] A. Lopez and E. Fradkin, Phys. Rev. B **44**, 5246 (1991).

[169] S. H. Simon and B. I. Halperin, Phys. Rev. B **48**, 17368 (1993).

[170] R. L. Willett, R. R. Ruel, K. W. West, and L. N. Pfeiffer, Phys. Rev. Lett. **71**, 3846 (1993).

[171] A. A. Zibrov, E. M. Spanton, H. Zhou, C. Kometter, T. Taniguchi, K. Watanabe, and A. F. Young, Nat. Phys. **14**, 930 (2018).

[172] A. A. Zibrov, C. Kometter, H. Zhou, E. M. Spanton, T. Taniguchi, K. Watanabe, M. P. Zaletel, and A. F. Young, Nature **549**, 360 (2017).

[173] J. P. Eisenstein, L. N. Pfeiffer, and K. W. West, Phys. Rev. Lett. **68**, 674 (1992).

[174] J. P. Eisenstein, L. N. Pfeiffer, and K. W. West, Phys. Rev. B **50**, 1760 (1994).

[175] P. Středa, J. Phys. C **15**, L1299 (1982).

[176] S. Narayanan, B. Roy, and M. P. Kennett, Phys. Rev. B **98**, 235411 (2018).

[177] V. M. Apalkov and T. Chakraborty, Phys. Rev. Lett. **97**, 126801 (2006).

[178] B. Feshami and H. A. Fertig, Phys. Rev. B **94**, 245435 (2016).

[179] V. Lukose and R. Shankar, Phys. Rev. B **94**, 085135 (2016).

[180] I. Herbut and B. Roy, Phys. Rev. B **77**, 245438 (2008).

[181] F. Cai, Y. Yu, and Z. Wang, J. Phys.: Condens. Matter **25**, 305601 (2013).

[182] R. Rajaraman, Phys. Rev. B **56**, 6788 (1997).

[183] S. M. Girvin, A. H. MacDonald, and P. M. Platzman, Phys. Rev. Lett. **54**, 581 (1985).

[184] S. M. Girvin, A. H. MacDonald, and P. M. Platzman, Phys. Rev. B **33**, 2481 (1986).

[185] R. P. Feynman, *Statistical Mechanics: A Set of Lectures* (Westview Press, USA, 1998).

[186] Y. H. Chen, F. Wilczek, E. Witten, and B. I. Halperin, Int. J. Mod. Phys. **3**, 1001 (1989).

[187] A. Pinczuk, B. S. Dennis, L. N. Pfeiffer, and K. West, Phys. Rev. Lett. **70**, 3983 (1993).

[188] A. Lopez and E. Fradkin, Phys. Rev. B **47**, 7080 (1993).

[189] J. Schwinger, J. Math. Phys. **2**, 407 (1961).

[190] L. V. Keldysh, Sov. Phys. JETP **20**, 1018 (1965), [Zh. Eksp. Teor. Fiz. **47**, 1515 (1964)].

[191] K. c. Chou, Z. .-b. Su, B. .-l. Hao, and L. Yu, Phys. Rep. **118**, 1 (1985).

[192] A. Kamenev, *Field Theory of Non-Equilibrium Systems* (Cambridge University Press, 2011).

[193] L. F. Cugliandolo and G. Lozano, Phys. Rev. B **59**, 915 (1999).

[194] M. E. Peskin and D. V. Schroeder, *An Introduction to Quantum Field Theory* (Westview Press, 1995).

[195] S. Golkar, D. X. Nguyen, M. M. Roberts, and D. T. Son, Phys. Rev. Lett. **117**, 216403 (2016).

[196] A. C. Balram and S. Pu, Eur. Phys. J. B **90**, 124 (2017).

[197] C. Wang, N. R. Cooper, B. I. Halperin, and A. Stern, Phys. Rev. X **7**, 031029 (2017).

[198] M. O. Goerbig, electronic preprint arXiv:2207.03322 (2022).

[199] H. Zhou, C. Huang, N. Wei, T. Taniguchi, K. Watanabe, M. P. Zaletel, Z. Papić, A. H. MacDonald, and A. F. Young, Phys. Rev. X **12**, 021060 (2022).

[200] M. Indra and D. Majumder, electronic preprint arXiv:2206.08647 (2022).

[201] Y.-H. Wu, Phys. Rev. B **106**, 155132 (2022).

[202] C. Fräßdorf and J. E. M. Mosig, Phys. Rev. B **95**, 125412 (2017).

[203] J. Rammer, *Quantum Field Theory of Non-Equilibrium Systems* (Cambridge University Press, UK, 2007).

[204] S. Narayanan and M. P. Kennett, Phys. Rev. B **106**, 165119 (2022).

Appendix A

Eigenstates of electrons in a magnetic field in the symmetric gauge

In the symmetric gauge the vector potential, $\mathbf{A}$, that gives rise to a magnetic field, $\mathbf{B} = B\hat{\mathbf{z}}$ is

$$\mathbf{A} = -\frac{1}{2}\mathbf{r} \times \mathbf{B} = \frac{1}{2}(-yB\hat{\mathbf{x}} + xB\hat{\mathbf{y}}). \tag{A.1}$$

The symmetric gauge breaks translation symmetry in both x and y directions but preserves rotational symmetry about the origin and hence angular momentum is a good quantum number. We can define a new set of operators

$$\tilde{\boldsymbol{\pi}} = \mathbf{p} - e\mathbf{A}. \tag{A.2}$$

Unlike the gauge invariant momentum operators in Eq. 2.11 these operators are not gauge invariant. The operators $\tilde{\pi}_i;\ \ i = x, y$ satisfy commutation relations

$$\begin{aligned} &\left[\tilde{\pi}_x, \tilde{\pi}_y\right] = ie\hbar B;\ \ [\pi_x, \tilde{\pi}_x] = 2ie\hbar\frac{\partial A_x}{\partial x};\ \ \left[\pi_y, \tilde{\pi}_y\right] = 2ie\hbar\frac{\partial A_y}{\partial y}; \\ &\left[\pi_x, \tilde{\pi}_y\right] = \left[\pi_y, \tilde{\pi}_x\right] = ie\hbar\left(\frac{\partial A_x}{\partial x} + \frac{\partial A_x}{\partial x}\right). \end{aligned} \tag{A.3}$$

In the symmetric gauge all the commutators except for the first one vanish

$$[\pi_i, \tilde{\pi}_j] = 0. \tag{A.4}$$

This allows us to define a new set of raising and lowering operators of the form

$$b = \frac{1}{\sqrt{2e\hbar B}}(\tilde{\pi}_x + i\tilde{\pi}_y); \quad b^\dagger = \frac{1}{\sqrt{2e\hbar B}}(\tilde{\pi}_x - i\tilde{\pi}_y). \tag{A.5}$$

These operators also obey the usual commutation relations of raising and lowering operators; $[b, b^\dagger] = 1$. Along with the raising and lowering operators defined in Eq.

2.13 a general state can be defined as

$$|n,m\rangle = \frac{a^{\dagger n} b^{\dagger m}}{\sqrt{n!m!}} |0,0\rangle \,. \tag{A.6}$$

Introduce complex variables $z = x - iy$ and $\bar{z} = x + iy$ and derivatives $\partial = 1/2(\partial_x + i\partial_y)$ and $\bar{\partial} = 1/2(\partial_x - i\partial_y)$ which obey $\partial z = \bar{\partial}\bar{z} = 1$ and $\partial\bar{z} = \bar{\partial} z = 0$. Using these we can redefine the raising and lowering operators as

$$\begin{aligned} a &= -i\sqrt{2}\left(l_B\bar{\partial} + \frac{z}{4l_B}\right); \quad a^\dagger = -i\sqrt{2}\left(l_B\partial + \frac{\bar{z}}{4l_B}\right); \\ b &= -i\sqrt{2}\left(l_B\partial + \frac{\bar{z}}{4l_B}\right); \quad b^\dagger = -i\sqrt{2}\left(l_B\bar{\partial} - \frac{z}{4l_B}\right). \end{aligned} \tag{A.7}$$

The lowest Landau level wavefunctions are annihilated by operator a and have the form

$$\Psi_{LLL}(z,\bar{z}) = f(z)e^{-|z|^2/4l_B^2}, \tag{A.8}$$

where $f(z)$ is an analytic function.

States with a non-zero value of m, $|0,m\rangle$ can be constructed from the lowest Landau level by acting on the states in Eq. A.8 with the operator $b^\dagger$. A unique state that is annihilated by both a and b is given by

$$\Psi_{LLL,m=0}(z,\bar{z}) = e^{-|z|^2/4l_B^2}. \tag{A.9}$$

States with $m \neq 0$ then have the form

$$\Psi_{LLL,m} \sim \left(\frac{z}{l_B}\right)^m e^{-|z|^2/4l_B^2}. \tag{A.10}$$

These are eigenstates of the angular momentum operator

$$J = \hbar(z\partial - \bar{z}\bar{\partial}), \tag{A.11}$$

and acting on the lowest Landau level states gives

$$J\Psi_{LLL,m} = \hbar m \Psi_{LLL,m}. \tag{A.12}$$

States in higher Landau levels can be constructed by acting with the raising operator $a^\dagger$.

Appendix B

Guiding Centre, Landau Level Form Factor and Pseudopotentials

In an external magnetic field, B, electrons have a cyclotron motion. The position of an electron $\mathbf{r} = (x, y)$ can be decomposed into the guiding centre coordinate $\mathbf{X}$ and a relative coordinate $\mathbf{R}$ as shown in Fig. B.1 and we define $\mathbf{R}$ and $\mathbf{X}$ as

$$R_x = -\frac{P_y}{eB}; \quad R_y = +\frac{P_x}{eB}; \quad X = x - R_x; \quad Y = y - R_y, \tag{B.1}$$

and the relative coordinates and the guiding centre coordinates obey the commutation relations

$$[R_x, R_y] = [X, Y] = -il_B^2. \tag{B.2}$$

The low energy Hamiltonian for a two-particle interaction in the n^{th} Landau level is given by Eq. 2.52 [106]. For an alternate definition of the projected density we first define a projected field operator ψ_n as

$$\psi_n(\mathbf{x}) = \sum_m \langle \mathbf{x}|n, m\rangle \, c_n(m), \tag{B.3}$$

where $|n, m\rangle$ was defined in Eq. A.6 and ψ_n and $c_n(m)$ act only in the n^{th} Landau level with $c_n(m)$ being the electron annihilation operator. Then, the projected density (in momentum space) can be defined as [81]

$$\rho_n(\mathbf{q}) = \frac{1}{2\pi} \sum_m \int d^2x \, \langle n, m|\mathbf{x}\rangle \, e^{i\mathbf{q}\cdot\mathbf{x}} \, \langle \mathbf{x}|n, m'\rangle \, c_n^\dagger(m) c_n(m). \tag{B.4}$$

We can rewrite the position in terms of guiding center $\mathbf{X}$ and relative $\mathbf{R}$ coordinates which commute with each other and simplify the projected density to find

$$\rho_n(\mathbf{q}) = \frac{1}{2\pi} \sum_m \int d^2x \, \langle n| \, e^{i\mathbf{q}\cdot\mathbf{R}} \, |n\rangle \, \langle m| \, e^{i\mathbf{q}\cdot\mathbf{X}} \, |m\rangle \, c_n^\dagger(m) c_n(m), \tag{B.5}$$

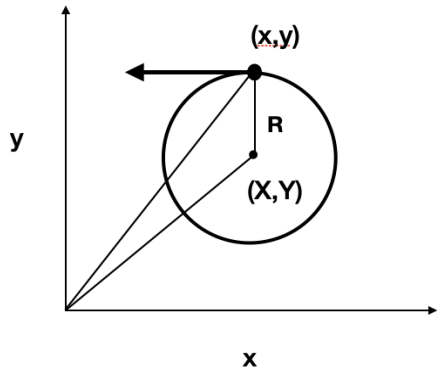

Figure B.1: The coordinate of an electron (x, y) can be decomposed into its guiding centre (X, Y) and its relative coordinate $\mathbf{R}$.

and if we make the following identification

$$F_n(\mathbf{q}) = \langle n|\, e^{i\mathbf{q}\cdot\mathbf{R}}\, |n\rangle\,; \quad \hat{\rho_n}(\mathbf{q}) = \langle m|\, e^{i\mathbf{q}\cdot\mathbf{X}}\, |m\rangle\, c_n^\dagger(m) c_n(m), \tag{B.6}$$

then we arrive at Eq. 2.53 given in the main text. The expression for the form factor in Eq. 2.54 can be derived by noting that $\mathbf{q}\cdot\mathbf{R} = -i\frac{l_B}{\sqrt{2}}(qa^\dagger - q^* a)$ where $a, a^\dagger$ are the Landau level raising and lowering operator. Then using the Haussdorf formula $e^{A+B} = e^A e^B e^{[B,A]/2}$ the form factor becomes

$$F_n(\mathbf{q}) = \frac{1}{n!}\, \langle 0|\, a^n e^{-l_B q a^\dagger/\sqrt{2}} e^{l_B q^* a/\sqrt{2}} (a^\dagger)^n\, |0\rangle\,. \tag{B.7}$$

The general expression for the form factor is then

$$F_{n\neq 0}(\mathbf{q}) = L_n(l_B^2|\mathbf{q}|^2/2) e^{-q^2 l_B^2/4}; \quad F_{n=0}(\mathbf{q}) = e^{-q^2 l_B^2/4}, \tag{B.8}$$

which is the form given in Eq. 2.54.

Appendix C

Cofactors and determinant of matrix M

The determinant of M (Eq. 4.34) and co-factors listed below (along with the various q_i; $i = 0,,1$ defined in Sec. 4.2.1) to determine the allowed fractions and order parameters. The cofactors are as follows

$$
\begin{aligned}
b_{11} &= (1+q_1\nu_*)(1-q_1\nu_*)^2 + 2q_1^3\nu_N\nu_C\nu_F + q_1^2(\nu_F^2+\nu_N^2)(1-q_1\nu_*) - q_1^2\nu_C^2(1+q_1\nu_*),\\
b_{12} &= -q_1\nu_C(1-q_1\nu_*)^2 - 2q_1^2\nu_F\nu_F(1-q_1\nu_*) + q_1^3\nu_C(\nu_C^2-\nu_F^2\nu_N^2),\\
b_{13} &= 2q_1^3\nu_*\nu_C\nu_N + q_1\nu_F(1+q_1\nu_*)(1-q_1\nu_*) - q_1^3\nu_F(\nu_C^2-\nu_F^2\nu_N^2),\\
b_{14} &= q_1\nu_N(1+q_1\nu_*)(1-q_1\nu_*) - q_1^3\nu_N(\nu_C^2+\nu_F^2-\nu_N^2) + 2q_1^3\nu_*\nu_F\nu_C,
\end{aligned}
$$

$$
\begin{aligned}
b_{21} &= -q_0\nu_C(1-q_1\nu_*)^2 - 2q_0q_1\nu_F\nu_N(1-q_1\nu_*) + q_0q_1^2\nu_C(\nu_C^2-\nu_F^2-\nu_N^2),\\
b_{22} &= (1+q_0\nu_*)(1-q_1\nu_*)^2 + q_0q_1^2\nu_F\nu_C\nu_N + q_0q_1(\nu_F^2+\nu_N^2)(1-q_1\nu_*) - q_1^2\nu_C^2(1+q_0\nu_*),\\
b_{23} &= q_1\nu_N(1+q_0\nu_*)(1-q_1\nu_*) - q_0q_1^2\nu_N(\nu_C^2+\nu_F^2-\nu_N^2) - q_0q_1\nu_F\nu_C(1-q_1\nu_*)\\
&\quad + q_1^2\nu_C\nu_F(1+q_0\nu_*),\\
b_{24} &= q_1^2\nu_C\nu_N(1+q_0\nu_*) - q_0q_1\nu_C\nu_N(1-q_1\nu_*) - q_0q_1^2\nu_F(\nu_C^2-\nu_F^2+\nu_N^2)\\
&\quad + q_1\nu_F(1+q_0\nu_*)(1-q_1\nu_*),
\end{aligned}
$$

$$
\begin{aligned}
b_{31} &= -2q_0q_1^2\nu_*\nu_C\nu_N + q_0q_1^2\nu_F(\nu_C^2-\nu_F^2+\nu_N^2) - q_0\nu_F(1+q_1\nu_*)(1-q_1\nu_*),\\
b_{32} &= -q_1\nu_N(1+q_0\nu_*)(1-q_1\nu_*) + q_0q_1^2\nu_N(\nu_C^2+\nu_F^2-\nu_n^2) + q_0q_1\nu_C\nu_F(1-q_1\nu_*)\\
&\quad - q_1^2\nu_C\nu_F(1+q_0\nu_*),\\
b_{33} &= (1+q_0\nu_*)(1+q_1\nu_*)(1-q_1\nu_*) - 2q_0q_1^2\nu_C\nu_F\nu_N + q_0q_1\nu_N^2(1+q_1\nu_*) - q_0q_1\nu_C^2(1-q_1\nu_*)\\
&\quad + q_1^2\nu_F^2(1+q_0\nu_*),\\
b_{34} &= q_1\nu_C(1+q_0\nu_*)(1+q_1\nu_*) - q_0q_1\nu_F\nu_N(1+q_1\nu_*) - q_0q_1^2\nu_C(\nu_c^2-\nu_F^2-\nu_N^2)\\
&\quad - q_1^2\nu_F\nu_N(1+q_0\nu_*),
\end{aligned}
$$

$$
\begin{aligned}
b_{41} &= q_0 q_1^2 \nu_N(\nu_C^2+\nu_F^2-\nu_N^2) - q_0\nu_N(1+q_1\nu_*)(1-q_1\nu_*) - 2q_0q_1^2\nu_*\nu_C\nu_F(1+q_1\nu_*),\\
b_{42} &= -q_1^2\nu_C\nu_N(1+q_0\nu_*) + q_0q_1\nu_C\nu_N(1-q_1\nu_*) + q_0q_1^2\nu_F(\nu_C^2-\nu_F^2+\nu_N^2)\\
&\quad -q_1\nu_F(1+q_0\nu_*)(1-q_1\nu_*),\\
b_{43} &= q_1\nu_C(1+q_0\nu_*)(1+q_1\nu_*) - q_0q_1\nu_F\nu_N(1+q_1\nu_*)\\
&\quad -q_0q_1^2\nu_C(\nu_C^2-\nu_F^2-\nu_N^2) - q_1^2\nu_F\nu_N(1+q_0\nu_*),\\
b_{44} &= (1+q_0\nu_*)(1+q_1\nu_*)(1-q_1\nu_*) - 2q_0q_1^2\nu_C\nu_N\nu_F + q_0q_1\nu_F^2(1+q_1\nu_*)\\
&\quad -q_0q_1\nu_C^2(1-q_1\nu_*) + q_1^2\nu_N^2(1+q_0\nu_*),
\end{aligned}
\tag{C.1}
$$

and the determinant is given by

$$
\begin{aligned}
\det(M) &= (1+q_0\nu_*)(1+q_1\nu_*)(1-q_1\nu_*)^2 + q_1^3\nu_C\nu_F(\nu_F+\nu_N)(1+q_0\nu_*)\\
&\quad +q_1^2(\nu_F^2+\nu_N^2)(1+q_0\nu_*)(1-q_1\nu_*) - q_1^2\nu_C^2(1+q_0\nu_*)(1+q_1\nu_*) - q_0q_1\nu_C^2(1-q_1\nu_*)^2\\
&\quad -4q_0q_1^2\nu_C\nu_F\nu_N(1-q_1\nu_*) + q_0q_1^3(\nu_C^4+\nu_F^4+\nu_N^4) - 2q_0q_1^3\nu_F^2\nu_N^2\\
&\quad +q_0q_1(\nu_F^2-\nu_F\nu_N+\nu_N^2)(1+q_1\nu_*)(1-q_1\nu_*) - 2q_0q_1^3\nu_C^2(\nu_F^2+\nu_N^2)\\
&\quad +q_0q_1^2\nu_C\nu_F\nu_N(1+q_1\nu_*).
\end{aligned}
\tag{C.2}
$$

Appendix D

Schwinger-Keldysh Technique

In this appendix [1] we provide a brief overview of the Green's functions arising in the Schwinger-Keldysh formalism and then discuss the Keldysh rotation to the physical real time representation.

D.0.1 Green's Functions for Schwinger Keldysh Technique

In the Schwinger-Keldysh technique the time arguments are promoted to contour (Schwinger-Keldysh contour [191, 192, 202, 203]) times that lie along a closed time contour starting at some reference point t_0 and extending to $+\infty$ and then returning to the reference point t_0 as shown in Fig. **??**. Operators ($\hat{O}$) in this case are split into two, $\hat{O}_{\pm}$, depending on whether their time argument lies on the forward, $\hat{O}_{+}$, or backward (return) contour, $\hat{O}_{-}$. Time ordering of operators is replaced by path ordering. In path ordering field operators with a "higher" value of contour time are placed to the right of operators with a "lower" contour time as illustrated in Fig. D.1

The single particle Green's function has the form:

$$G(\mathbf{r},t;\mathbf{r}',t') = -i\langle T_{\mathscr{C}}\psi(\mathbf{r},t)\psi^{\dagger}(\mathbf{r}',t')\rangle, \tag{D.1}$$

where $T_{\mathscr{C}}$ is the contour-time ordering operator given by

$$T_{\mathscr{C}}(\psi(\mathbf{r},t)\psi^{\dagger}(\mathbf{r}',t')) = \begin{cases} \psi(\mathbf{r},t)\psi^{\dagger}(\mathbf{r}',t'), & \mathrm{t} \overset{\mathscr{C}}{>} t', \qquad (D.2) \\ \pm\psi^{\dagger}(\mathbf{r}',t')\psi(\mathbf{r},t), & \mathrm{t'} \overset{\mathscr{C}}{>} \mathrm{t} \qquad (D.3) \end{cases}$$

[1] The material in this Apendix is primarily based on Refs. [191, 192, 202, 203].

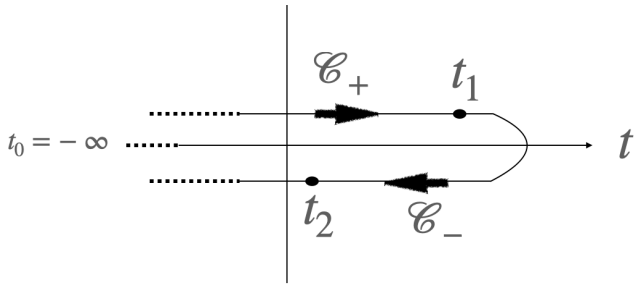

Figure D.1: In path ordering field operators containing contour time t_2 appears to the right of operators containing contour time t_1.

where $t \overset{\mathscr{C}}{\geq} t'$ means that t is further along the contour than t' irrespective of their corresponding numerical values on the real axis. The + sign corresponds to the field operators being boson and the − sign to fermions. In terms of contour ordering we can introduce "greater" and "lesser" Green's functions as

$$G(\mathbf{r},t;\mathbf{r}',t') = \begin{cases} G^<(\mathbf{r},t;\mathbf{r}',t'), & \text{t'} \overset{\mathscr{C}}{>} \text{t}, \quad \text{(D.4)} \\ G^<(\mathbf{r},t;\mathbf{r}',t'), & \text{t} \overset{\mathscr{C}}{>} \text{t'}. \quad \text{(D.5)} \end{cases}$$

For Green's functions that depends on two contour-time variables the time variables can either both belong to the forward contour $\mathscr{C}_+$ or the backward contour C_- or a mix of both. Thus the contour ordered Green's function can be mapped onto a 2×2 matrix in the Schwinger-Keldysh space

$$G(\mathbf{r},t;\mathbf{r}',t') = \begin{pmatrix} G^{++}(\mathbf{r},t;\mathbf{r}',t') & G^{+-}(\mathbf{r},t;\mathbf{r}',t') \\ G^{-+}(\mathbf{r},t;\mathbf{r}',t') & G^{--}(\mathbf{r},t;\mathbf{r}',t') \end{pmatrix} = \begin{pmatrix} G^T(\mathbf{r},t;\mathbf{r}',t') & G^<(\mathbf{r},t;\mathbf{r}',t') \\ G^>(\mathbf{r},t;\mathbf{r}',t') & G^{\tilde{T}}(\mathbf{r},t;\mathbf{r}',t') \end{pmatrix}. \quad \text{(D.6)}$$

The elements of the matrix are the time ordered, lesser, greater and the anti-time ordered Green functions and they are defined as

$$\begin{aligned} G^T(\mathbf{r},t;\mathbf{r}',t') &= -i\langle T\psi(\mathbf{r},t)\psi^\dagger(\mathbf{r}',t')\rangle, & \text{(D.7)} \\ G^<(\mathbf{r},t;\mathbf{r}',t') &= \pm i\langle \psi(\mathbf{r}',t')\psi^\dagger(\mathbf{r},t)\rangle, & \text{(D.8)} \\ G^>(\mathbf{r},t;\mathbf{r}',t') &= -i\langle \psi(\mathbf{r},t)\psi^\dagger(\mathbf{r}',t')\rangle, & \text{(D.9)} \\ G^{\tilde{T}}(\mathbf{r},t;\mathbf{r}',t') &= -i\langle \tilde{T}\psi(\mathbf{r},t)\psi^\dagger(\mathbf{r}',t')\rangle. & \text{(D.10)} \end{aligned}$$

The time ordered and anti-time ordered Green's functions can also be defined in terms of step functions as

$$G^T(\mathbf{r},t;\mathbf{r}',t') = -i\theta(t-t')\langle T\psi(\mathbf{r},t)\psi^\dagger(\mathbf{r}',t')\rangle \pm i\theta(t'-t)\langle \psi(\mathbf{r}',t')\psi^\dagger(\mathbf{r},t)\rangle, \quad \text{(D.11)}$$
$$G^T(\mathbf{r},t;\mathbf{r}',t') = -i\theta(t'-t)\langle T\psi(\mathbf{r},t)\psi^\dagger(\mathbf{r}',t')\rangle \pm i\theta(t-t')\langle \psi(\mathbf{r}',t')\psi^\dagger(\mathbf{r},t)\rangle. \quad \text{(D.12)}$$

The four Green's functions in, Eq. D.6 are not linearly independent and obey the identity

$$G^{++}(\mathbf{r},t;\mathbf{r}',t')+G^{--}(\mathbf{r},t;\mathbf{r}',t')=G^{+-}(\mathbf{r},t;\mathbf{r}',t')+G^{-+}(\mathbf{r},t;\mathbf{r}',t'), \tag{D.13}$$

or

$$G^{T}(\mathbf{r},t;\mathbf{r}',t')+G^{\tilde{T}}(\mathbf{r},t;\mathbf{r}',t')=G^{>}(\mathbf{r},t;\mathbf{r}',t')+G^{<}(\mathbf{r},t;\mathbf{r}',t'). \tag{D.14}$$

D.0.2 Real Time Representation

Equations D.13 and D.14 imply that there exists a transformation to basis with only three, linearly independent, Green's functions. Such a linear transformation is called the real time representation and is given by [191, 192, 202, 203]

$$\tau_1 L\,\hat{G}\,(\tau_1 L)^{-1}=\begin{pmatrix} G^K & G^R \\ G^A & 0 \end{pmatrix}, \tag{D.15}$$

where $\hat{G}$ is the 2×2 matrix form of Green's function in Eq. D.6 written in a compact form. τ_1 and L are given by

$$\tau_1=\begin{pmatrix} 0 & 1 \\ 1 & 0 \end{pmatrix};\quad L=\frac{1}{\sqrt{2}}\begin{pmatrix} 1 & -1 \\ 1 & 1 \end{pmatrix}. \tag{D.16}$$

The Green's functions in Eq. D.15 are called Keldysh, G^K, retarded, G^R and the advanced, G^A respectively. Under the same transformation operators we obtain a new set of double operators $\hat{O}_{cl},\hat{O}_q$ defined by [191, 192, 202, 203]

$$\hat{O}_{cl}=\frac{1}{\sqrt{2}}(\hat{O}_+ +\hat{O}_-);\quad \hat{O}_q=\frac{1}{\sqrt{2}}(\hat{O}_+ -\hat{O}_-), \tag{D.17}$$

where the subscripts cl and q stands for classical and quantum components respectively. The Keldysh, advanced and retarded Green's functions are given by

$$G^R=\frac{1}{2}(G^T-G^<+G^>-G^{\tilde{T}}), \tag{D.18}$$

$$G^A=\frac{1}{2}(G^T+G^<-G^>-G^{\tilde{T}}), \tag{D.19}$$

$$G^K=\frac{1}{2}(G^T+G^<+G^>+G^{\tilde{T}}), \tag{D.20}$$

and they obey the relations

$$(G^R)^\dagger=G^A;\quad (G^K)^\dagger=-G^K, \tag{D.21}$$

as well as the causality relations

$$G^R(\mathbf{r},t;\mathbf{r}',t')=0,\quad \text{if } t<t', \tag{D.22}$$

$$G^A(\mathbf{r},t;\mathbf{r}',t')=0,\quad \text{if } t>t'. \tag{D.23}$$

Appendix E

Components of the Electromagnetic Response Tensor

The expression for the electromagnetic response tensor is given by (restoring the index structure while suppressing the species index of the tensors)

$$\mathbf{K}^{\mu\nu} = \mathbf{\Pi}^{\mu\nu} - \mathbf{\Pi}^{\mu\delta}\left[(\mathbf{M})^{-1}\right]_{\delta\gamma}\mathbf{\Pi}^{\nu\gamma}, \tag{E.1}$$

where $\mu, \nu, \delta, \gamma = 0, 1, 2$ and we have defined $\hat{\mathbf{M}}$ to be

$$\mathbf{M}^{\mu\nu} = \mathbf{\Pi}^{\mu\nu} + \mathbf{C}^{\mu\nu} + \mathbf{G}^{\mu\nu}. \tag{E.2}$$

$\hat{\mathbf{C}}$ and $\hat{\mathbf{G}}$ are :

$$\hat{\mathbf{C}} = \mathscr{K}^{-1}\epsilon^{\mu\nu\lambda}\vec{\partial}_\lambda; \quad \hat{\mathbf{G}} = \frac{1}{2\alpha}(\partial_\mu a^\mu)^2 g^{\mu\nu}, \tag{E.3}$$

where the arrow on the derivative, $\vec{\partial}_\lambda$, in $\hat{\mathbf{C}}$ indicates that the differential operator acts on terms to the left. $\hat{\mathbf{C}}$ is antisymmetric i.e., $\mathbf{C}_{\mu\nu} = 0$ if $\mu = \nu$. $\hat{\mathbf{\Pi}}$ is given by the expression :

$$\begin{aligned}
\mathbf{\Pi}^{00}_{\alpha\beta}(\omega,\mathbf{q}) &= q^2\mathbf{\Pi}^0_{\alpha\beta}, && \text{(E.4)}\\
\mathbf{\Pi}^{01}_{\alpha\beta}(\omega,\mathbf{q}) &= \omega q^1\mathbf{\Pi}^0_{\alpha\beta}(\omega,\mathbf{q}) + iq_2\mathbf{\Pi}^1_{\alpha\beta}(\omega,\mathbf{q}), && \text{(E.5)}\\
\mathbf{\Pi}^{02}_{\alpha\beta}(\omega,\mathbf{q}) &= \omega q^2\mathbf{\Pi}^0_{\alpha\beta}(\omega,\mathbf{q}) - iq_1\mathbf{\Pi}^1_{\alpha\beta}(\omega,\mathbf{q}), && \text{(E.6)}\\
\mathbf{\Pi}^{10}_{\alpha\beta}(\omega,\mathbf{q}) &= \omega q^1\mathbf{\Pi}^0_{\alpha\beta}(\omega,\mathbf{q}) - iq_2\mathbf{\Pi}^1_{\alpha\beta}(\omega,\mathbf{q}), && \text{(E.7)}\\
\mathbf{\Pi}^{11}_{\alpha\beta}(\omega,\mathbf{q}) &= \omega^2\mathbf{\Pi}^0_{\alpha\beta}(\omega,\mathbf{q}) + q_2^2\mathbf{\Pi}^2_{\alpha\beta}(\omega,\mathbf{q}), && \text{(E.8)}\\
\mathbf{\Pi}^{12}_{\alpha\beta}(\omega,\mathbf{q}) &= +i\omega\mathbf{\Pi}^1_{\alpha\beta}(\omega,\mathbf{q}) - q^1q^2\mathbf{\Pi}^2_{\alpha\beta}(\omega,\mathbf{q}), && \text{(E.9)}\\
\mathbf{\Pi}^{20}_{\alpha\beta}(\omega,\mathbf{q}) &= \omega q^2\mathbf{\Pi}^0_{\alpha\beta}(\omega,\mathbf{q}) + iq_1\mathbf{\Pi}^1_{\alpha\beta}(\omega,\mathbf{q}), && \text{(E.10)}\\
\mathbf{\Pi}^{21}_{\alpha\beta}(\omega,\mathbf{q}) &= -i\omega\mathbf{\Pi}^1_{\alpha\beta}(\omega,\mathbf{q}) - q^2q^1\mathbf{\Pi}^2_{\alpha\beta}(\omega,\mathbf{q}), && \text{(E.11)}\\
\mathbf{\Pi}^{22}_{\alpha\beta}(\omega,\mathbf{q}) &= \omega^2\mathbf{\Pi}^0_{\alpha\beta}(\omega,\mathbf{q}) + q_1^2\mathbf{\Pi}^2_{\alpha\beta}(\omega,\mathbf{q}). && \text{(E.12)}\\
& && \text{(E.13)}
\end{aligned}$$

The tensor $\hat{\mathbf{M}}$ has nine components (six are independent) as follows:

$$\mathbf{M}_{00} = -q^2\mathbf{\Pi}^0 + \frac{\omega^2}{\alpha}, \tag{E.14}$$

$$\mathbf{M}^{01} = -\omega q_1\mathbf{\Pi}^0 + iq_2(\mathbf{\Pi}^1 + \mathscr{K}^{-1}) - \frac{\omega q_1}{\alpha}, \tag{E.15}$$

$$\mathbf{M}^{02} = -\omega q_2\mathbf{\Pi}^0 - iq_1(\mathbf{\Pi}^1 + \mathscr{K}^{-1}) - \frac{\omega q_2}{\alpha}, \tag{E.16}$$

$$\mathbf{M}^{10} = -\omega q_1\mathbf{\Pi}^0 - iq_2(\mathbf{\Pi}^1 + \mathscr{K}^{-1}) - \frac{\omega q_1}{\alpha} = (M^{10})^*, \tag{E.17}$$

$$\mathbf{M}^{11} = -\omega^2\mathbf{\Pi}^0 + q_2^2\mathbf{\Pi}^2 + \frac{q_1^2}{\alpha}, \tag{E.18}$$

$$\mathbf{M}^{12} = -q_1q_2\mathbf{\Pi}^2 - i\omega(\mathbf{\Pi}^1 + \mathscr{K}^{-1}) + \frac{q_1q_2}{\alpha}, \tag{E.19}$$

$$\mathbf{M}^{20} = -\omega q_2\mathbf{\Pi}^0 + iq_1(\mathbf{\Pi}^1 + \mathscr{K}^{-1}) - \frac{\omega q_2}{\alpha} = (M^{02})^*, \tag{E.20}$$

$$\mathbf{M}^{21} = -q_1q_2\mathbf{\Pi}^2 + i\omega(\mathbf{\Pi}^1 + \mathscr{K}^{-1}) + \frac{q_1q_2}{\alpha} = (M^{12})^*, \tag{E.21}$$

$$\mathbf{M}^{22} = -\omega^2\mathbf{\Pi}^0 + q_1^2\mathbf{\Pi}^2 + \frac{q_2^2}{\alpha}, \tag{E.22}$$

The determinant of the matrix form of $\hat{\mathbf{M}}$ is

$$\begin{aligned}
\det(\mathrm{M}) = \frac{1}{\alpha^3}\{&[(q_2^2 + \mathbf{\Pi}^2q_1^2\alpha + \mathbf{\Pi}^0\alpha\omega^2)(\mathbf{\Pi}^0q^2q_1^2\alpha - (\mathbf{\Pi}^1 + \mathscr{K}^{-1})^2q_2^2\alpha - \mathbf{\Pi}^0\mathbf{\Pi}^2q^2q_2^2\alpha^2 \\
&+2\mathbf{\Pi}^0q_1^2\alpha\omega^2 + \mathbf{\Pi}^2q_2^2\alpha\omega^2 + \mathbf{\Pi}^2q^2\alpha^2\omega^2 - (\mathbf{\Pi}^0)^2q_1^2\alpha^2\omega^2 + (\mathbf{\Pi}^0)^2\alpha\omega^4)] \\
&[-(q_1q_2 - \mathbf{\Pi}^2q_1q_2\alpha + i\omega(\mathbf{\Pi}^1 + \mathscr{K}^{-1}))(-(-i(\mathbf{\Pi}^1 + \mathscr{K}^{-1})\alpha - q_1\omega + \mathbf{\Pi}^0q_1\alpha\omega) \\
&(-i(\mathbf{\Pi}^1 + \mathscr{K}^{-1})\alpha - q_2\omega + \mathbf{\Pi}^0q_2\alpha\omega) \\
&+(q_1q_2 - \mathbf{\Pi}^2q_1q_2\alpha - i\alpha\omega(\mathbf{\Pi}^1 + \mathscr{K}^{-1}))(\mathbf{\Pi}^0q^2\alpha + \omega^2))] \\
&+[(iq_1\alpha(\mathbf{\Pi}^1 + \mathscr{K}^{-1}) - q_2\omega + \mathbf{\Pi}^0q_2\alpha\omega)((q_1q_2 - \mathbf{\Pi}^2q_1q_2\alpha - i\alpha\omega(\mathbf{\Pi}^1 + \mathscr{K}^{-1})) \\
&(iq_2\alpha(\mathbf{\Pi}^1 + \mathscr{K}^{-1}) - q_1\omega + \mathbf{\Pi}^0q_1\alpha\omega) \\
&-(-i\alpha q_1(\mathbf{\Pi}^1 + \mathscr{K}^{-1} - q_2\omega + \mathbf{\Pi}^0q_2\alpha\omega))(q_1^2 + \mathbf{\Pi}^2q_2^2\alpha + \mathbf{\Pi}^0\alpha\omega^2))]\},
\end{aligned} \tag{E.23}$$

which can be simplified to get the expression

$$\det(\mathrm{M}) = \frac{1}{\alpha}(\mathrm{q}^2 + \omega^2)^2\left[\omega^2(\mathbf{\Pi}^0)^2 + \mathrm{q}^2\mathbf{\Pi}^0\mathbf{\Pi}^2 - (\mathbf{\Pi}^1 + \mathscr{K}^{-1})^2\right]. \tag{E.24}$$

For convenience of notation we define the inverse $\hat{\mathbf{M}}^{-1} = \hat{\mathbf{L}}$ whose components are

$$
\begin{aligned}
\mathbf{L}^{00} &= -\frac{\mathbf{\Pi}^2(q^2)(q^2+\mathbf{\Pi}^0\alpha\omega^2)+\omega^2(\mathbf{\Pi}^0(q^2)-(\mathbf{\Pi}^1+\mathscr{K}^{-1})^2\alpha+(\mathbf{\Pi}^0)^2\alpha\omega^2)}{\alpha\ \det(\mathrm{M})},\\
\mathbf{L}^{01} &= \frac{q_1\alpha\omega((\mathbf{\Pi}^1)^2+(\mathscr{K}^{-1})^2)-iq_2(q^2+\omega^2)(\mathbf{\Pi}^1+\mathscr{K}^{-1})}{\alpha\ \det(\mathrm{M})}\\
&\quad \frac{+2\mathbf{\Pi}^1(\mathscr{K}^{-1})q_1\alpha\omega-q_1(-1+\mathbf{\Pi}^0\alpha)\omega(\mathbf{\Pi}^2q^2+\mathbf{\Pi}^0\omega^2)}{\alpha\ \det(\mathrm{M})},\\
L^{02} &= \frac{q_2\alpha\omega((\mathbf{\Pi}^1)^2+(\mathscr{K}^{-1})^2)-iq1(q^2+\omega^2)(\mathbf{\Pi}^1+\mathscr{K}^{-1})}{\alpha\ \det(\mathrm{M})}\\
&\quad +\frac{2\mathbf{\Pi}^1(\mathscr{K}^{-1})q_2\alpha\omega-q_2(-1+\mathbf{\Pi}^0\alpha)\omega(\mathbf{\Pi}_2q^2+\mathbf{\Pi}_0\omega^2)}{\alpha\ \det(\mathrm{M})},\\
\mathbf{L}^{10} &= \frac{q_1\alpha\omega((\mathbf{\Pi}^1)^2+(\mathscr{K}^{-1})^2)+iq_2(q^2+\omega^2)(\mathbf{\Pi}^1+\mathscr{K}^{-1})}{\alpha\ \det(\mathrm{M})}\\
&\quad +\frac{2\mathbf{\Pi}^1(\mathscr{K}^{-1})q_1\alpha\omega-q_1(-1+\mathbf{\Pi}^0\alpha)\omega(\mathbf{\Pi}^2q^2+\mathbf{\Pi}^0\omega^2)}{\alpha\ \det(\mathrm{M})},\\
\mathbf{L}^{11} &= \frac{(\mathbf{\Pi}^0)^2q_1^2\alpha\omega^2-q_1^2((\mathbf{\Pi}^1+\mathscr{K}^{-1})^2\alpha-\mathbf{\Pi}^2\omega^2)+\mathbf{\Pi}^0(\mathbf{\Pi}^2q_1^2q^2\alpha+q_1^2q_2^2+(q_2^2+\omega^2)^2)}{\alpha\ \det(\mathrm{M})},\\
\mathbf{L}^{12} &= q_1q_2\frac{(-\alpha(\mathbf{\Pi}^1+\mathscr{K}^{-1})^2+i\omega(q^2+\omega^2)(\mathbf{\Pi}^1+\mathscr{K}^{-1})}{\alpha\ \det(\mathrm{M})}\\
&\quad +q_1q_2\frac{\omega^2((\mathbf{\Pi}^0)^2\alpha+\mathbf{\Pi}^2)+\mathbf{\Pi}^0(q^2(-1+\alpha\mathbf{\Pi}^2)-2\omega^2)}{\alpha\ \det(\mathrm{M})},\\
\mathbf{L}^{20} &= \frac{q_2\alpha\omega((\mathbf{\Pi}^1)^2+(\mathscr{K}^{-1})^2)+iq_1(q^2+\omega^2)(\mathbf{\Pi}^1+\mathscr{K}^{-1})}{\alpha\ \det(\mathrm{M})}\\
&\quad +\frac{2\mathbf{\Pi}^1(\mathscr{K}^{-1})q_2\alpha\omega-q_2(-1+\mathbf{\Pi}^0\alpha)\omega(\mathbf{\Pi}^2q^2+\mathbf{\Pi}^0\omega^2)}{\alpha\ \det(\mathrm{M})},\\
\mathbf{L}^{21} &= \frac{q_1q_2\left[-\alpha(\mathbf{\Pi}^1+\mathscr{K}^{-1})^2-i\omega(q^2+\omega^2)(\mathbf{\Pi}^1+\mathscr{K}^{-1})\right]}{\alpha\ \det(\mathrm{M})}\\
&\quad +q_1q_2\frac{\omega^2((\mathbf{\Pi}^0)^2\alpha+\mathbf{\Pi}^2)+\mathbf{\Pi}^0(q^2(-1+\alpha\mathbf{\Pi}^2)-2\omega^2)}{\alpha\ \det(\mathrm{M})},\\
\mathbf{L}^{22} &= \frac{q_2^2((\mathbf{\Pi}^0)^2\alpha\omega^2-\alpha(\mathbf{\Pi}^1+\mathscr{K}_{-1})^2+\mathbf{\Pi}^2\omega^2)+\mathbf{\Pi}^0((q_1^2+\omega^2)^2+q_2^2(q_1^2+\Pi^2q_2^2\alpha(1+q_2^2)))}{\alpha\ \det(\mathrm{M})}.
\end{aligned}
\tag{E.25}
$$

With $\mathbf{L}^{-1}$ we finally have (from Eq. E.1) the components of $\mathbf{K}$:

$$\mathbf{K}^{00} = q^2\left[\frac{-(\mathscr{K}^{-1})^2\mathbf{\Pi}^0}{\mathscr{D}}\right], \tag{E.26}$$

$$\mathbf{K}^{01} = -q_1\omega\left[\frac{-\mathbf{\Pi}^0(\mathscr{K}^{-1})^2}{\mathscr{D}}\right] + iq_2\left[\mathscr{K}^{-1} + \frac{(\mathscr{K}^{-}1)^2(\mathbf{\Pi}^1+\mathscr{K}^{-1})}{\mathscr{D}}\right], \tag{E.27}$$

$$\mathbf{K}^{02} = q_2\omega\left[\frac{-(\mathscr{K}^{-1})^2\mathbf{\Pi}^0}{\mathscr{D}}\right] - iq_1\left[\mathscr{K}^{-1} + \frac{(\mathscr{K}^{-}1)^2(\mathbf{\Pi}^1+\mathscr{K}^{-1})}{\mathscr{D}}\right], \tag{E.28}$$

$$\mathbf{K}^{10} = q_1\omega\left[\frac{-\mathbf{\Pi}^0(\mathscr{K}^{-1})^2}{\mathscr{D}}\right] - iq_2\left[\mathscr{K}^{-1} + \frac{(\mathscr{K}^{-}1)^2(\mathbf{\Pi}^1+\mathscr{K}^{-1})}{\mathscr{D}}\right], \tag{E.29}$$

$$\mathbf{K}^{11} = \omega^2\left[\frac{(-\mathscr{K}^{-1})^2\mathbf{\Pi}^0}{\mathscr{D}}\right] + q_2^2\left[\frac{(\mathscr{K}^{-1})^2\mathbf{\Pi}^2}{\mathscr{D}}\right], \tag{E.30}$$

$$\mathbf{K}^{12} = -q_1q_2\left[\frac{-\mathbf{\Pi}^2(\mathscr{K}^{-1})^2}{\mathscr{D}}\right] - i\omega\left[\mathscr{K}^{-1} + \frac{(\mathscr{K}^{-}1)^2(\mathbf{\Pi}^1+\mathscr{K}^{-1})}{\mathscr{D}}\right], \tag{E.31}$$

$$\mathbf{K}^{20} = q_2\omega\left[\frac{-(\mathscr{K}^{-1})^2\mathbf{\Pi}^0}{\mathscr{D}}\right] + iq_1\left[\mathscr{K}^{-1} + \frac{(\mathscr{K}^{-}1)^2(\mathbf{\Pi}^1+\mathscr{K}^{-1})}{\mathscr{D}}\right], \tag{E.32}$$

$$\mathbf{K}^{21} = -q_1q_2\left[\frac{-\mathbf{\Pi}_2(\mathscr{K}^{-1})^2}{\mathscr{D}}\right] + i\omega\left[\mathscr{K}^{-1} + \frac{(\mathscr{K}^{-}1)^2(\mathbf{\Pi}^1+\mathscr{K}^{-1})}{\mathscr{D}}\right], \tag{E.33}$$

$$\mathbf{K}^{22} = \omega^2\left[\frac{(-\mathscr{K}^{-1})^2\mathbf{\Pi}^0}{\mathscr{D}}\right] + q_1^2\left[\frac{(\mathscr{K}^{-1})^2\mathbf{\Pi}^2}{\mathscr{D}}\right]. \tag{E.34}$$

where $\mathscr{D}$ is the denominator matrix referred to in the text. $\mathscr{D}$ is given by

$$\mathscr{D} = (\mathbf{\Pi}^0)^2\omega^2 + \mathbf{\Pi}^0\mathbf{\Pi}^2q^2 - (\mathbf{\Pi}^1+\mathscr{K}^{-1})^2. \tag{E.35}$$

We define the following terms:

$$\mathbf{K}^0 = -\frac{\mathbf{\Pi}^0(\mathscr{K}^{-1})^2}{\mathscr{D}}, \tag{E.36}$$

$$\mathbf{K}^1 = \mathscr{K}^{-1} + \frac{(\mathscr{K}^{-}1)^2(\mathbf{\Pi}^1+\mathscr{K}^{-1})}{\mathscr{D}}, \tag{E.37}$$

$$\mathbf{K}^2 = -\frac{\mathbf{\Pi}^2(\mathscr{K}^{-1})^2}{\mathscr{D}}. \tag{E.38}$$

In terms of the scalars, $\mathbf{K}_0, \mathbf{K}_1, \mathbf{K}_2$ the electromagnetic tensor can be decomposed and has the same form as the polarization tensor :

$$\mathbf{K}^{00}(\omega,\mathbf{q}) = q^2\mathbf{K}^0, \tag{E.39}$$

$$\mathbf{K}^{0i}(\omega,\mathbf{q}) = \omega q^i\mathbf{K}^0(\omega,\mathbf{q}) + i\epsilon^{0ij}q_j\mathbf{K}^1(\omega,\mathbf{q}), \tag{E.40}$$

$$\mathbf{K}^{i0}(\omega,\mathbf{q}) = \omega q^i\mathbf{K}^0(\omega,\mathbf{q}) - i\epsilon^{0ij}q_j\mathbf{K}^1(\omega,\mathbf{q}), \tag{E.41}$$

$$\mathbf{K}^{ij}(\omega,\mathbf{q}) = \omega^2\delta^{ij}\mathbf{K}^0_{\alpha\beta}(\omega,\mathbf{q}) + i\epsilon^{0ij}\omega\mathbf{K}^1(\omega,\mathbf{q}) + (\delta^{ij}q^2 - q^iq^j)\mathbf{K}^2(\omega,\mathbf{q}). \tag{E.42}$$

Appendix F

Calculation of Polarization Tensor and Denominator matrix

In this appendix we give more details on the calculation of the polarization tensor that we use to find collective modes. We begin with Eq. (5.27) for the electromagnetic response tensor

$$\mathbf{K} = \mathbf{\Pi} - \mathbf{\Pi}(\mathbf{\Pi} + \mathbf{C} + \mathscr{G})^{-1}\mathbf{\Pi}, \tag{F.1}$$

where $\mathbf{\Pi}$ is the polarization tensor, $\mathbf{C}$ is the Chern-Simons tensor and $\mathscr{G}$ is a gauge fixing term added to the Lagrangian to make the inverse term finite. As mentioned in Sec. IV, due to the transverse nature of the polarization tensor it can be decomposed in terms of scalars, Π^0, Π^1 and Π^2, as shown in Eq. 5.21. Here we are interested in the retarded component of the polarization tensor $(\Pi^i)^R$ and for simplicity we have dropped the R.

In the presence of chiral symmetry breaking orders the polarization tensor can be expressed as [146, 204]:

$$\begin{aligned}\Pi^{\mu\nu}_{\alpha}(\omega,\mathbf{q}) &= \frac{1}{32\pi^2 l_\alpha^4}\sum_{n,n'=0}^{\infty}\sum_{\lambda,\lambda'=\pm1}\frac{\mathscr{F}^{\lambda\lambda'}_{n,n'}(T,\mu_\alpha)}{\omega-\lambda\sqrt{n+\Delta_g^2}\,\omega_c^\alpha+\lambda'\sqrt{n'+\Delta_g^2}\,\omega_c^\alpha} \\ &\quad\times\int_{\Delta\mathbf{r}} e^{-i\mathbf{q}\cdot\Delta\mathbf{r}}e^{-\Delta\mathbf{r}^2/l_\alpha^2}\mathrm{Tr}\left[\sigma^\mu_\alpha M^\alpha_n(\lambda\Delta\mathbf{r})\sigma^\nu_\alpha M^\alpha_{n'}(-\lambda'\Delta\mathbf{r}')\right],\end{aligned} \tag{F.2}$$

with

$$\mathscr{F}^{\lambda\lambda'}_{n,n'}(T,\mu_\alpha) = \tanh\left(\frac{\lambda'\sqrt{n'+\Delta_g^2}\,\omega_c^\alpha-\mu_\alpha}{2T}\right)-\tanh\left(\frac{\lambda\sqrt{n+\Delta_g^2}\,\omega_c^\alpha-\mu_\alpha}{2T}\right). \tag{F.3}$$

Here, T is the temperature, Δ_g is the gap arising from linear combinations of m_α and f_α, μ_α is the chemical potential of species α, $\lambda(\lambda') = \pm1$ refers to the conduction (+1)

band or valence (-1) band, $\sigma^{\mu}_{\alpha} = (\sigma_0, \kappa^{\alpha} v_F \sigma_1, \kappa^{\alpha} v_F \sigma_2)$, $\omega_c = \sqrt{2}\frac{v_F}{l_{\alpha}}$ and

$$M^{\alpha}_{n}(\lambda \Delta \mathbf{r}) = \mathscr{P}_{+} L^{0}_{n}\left(\frac{\Delta \mathbf{r}^2}{2 l_{\alpha}}\right) + \mathscr{P}_{-} L^{0}_{n-1}\left(\frac{\Delta \mathbf{r}^2}{2 l_{\alpha}}\right) + i \frac{\lambda \kappa}{\sqrt{2} l_{\alpha}} \frac{\sigma \cdot \Delta \mathbf{r}}{\sqrt{n}} L^{1}_{n-1}\left(\frac{\Delta \mathbf{r}^2}{2 l_{\alpha}}\right), \tag{F.4}$$

where L^{k}_{n} is a generalized Laguerre polynomial and $\mathscr{P}_{\pm}$ are projection operators on the sublattice space defined as:

$$\mathscr{P}_{\pm} = \frac{1}{2}\left[\sigma_0 \pm \text{sign}(e \mathscr{B}^{\text{eff}}_{\alpha}) \sigma_3\right]. \tag{F.5}$$

The scalars Π^0, Π^1 and Π^2 are given by:

$$\begin{aligned} \Pi^{0}_{\alpha}(\omega, \vec{q}) &= \frac{-1}{32\pi^2 l^4_{\alpha} \vec{q}^2} \sum_{n,n'=0}^{\infty} \sum_{\lambda,\lambda'=\pm 1} \frac{\mathscr{F}^{\lambda\lambda'}_{n,n'}(T, \mu_{\alpha})}{\omega - \lambda \sqrt{n + \Delta^2_g}\omega^{\alpha}_{c} + \lambda' \sqrt{n' + \Delta^2_g}\omega^{\alpha}_{c}} \\ &\quad \times \left[I^{0}_{n-1,n'}(\mathscr{Q}_{\alpha}) + I^{0}_{n,n'-1}(\mathscr{Q}_{\alpha}) + \frac{2\lambda\lambda'}{\sqrt{nn'}} I^{1}_{n-1,n'-1}(\mathscr{Q}_{\alpha}) \right], \end{aligned} \tag{F.6}$$

$$\Pi^{1}_{\alpha}(\omega, \vec{q}) = -\frac{v^2_F}{32\pi^2 l^4_{\alpha} \omega} \sum_{n,n'}^{\infty} \sum_{\lambda,\lambda'=\pm 1} \frac{\mathscr{F}^{\lambda\lambda'}_{n,n'}(T, \mu_{\alpha})}{\omega - \lambda \sqrt{n + \Delta^2_g}\omega^{\alpha}_{c} + \lambda' \sqrt{n' + \Delta^2_g}\omega^{\alpha}_{c}} \left[I^{0}_{n-1,n'}(\mathscr{Q}_{\alpha}) - I^{0}_{n,n'-1}(\mathscr{Q}_{\alpha}) \right], \tag{F.7}$$

$$\Pi^{2}_{\alpha}(\omega, \vec{q}) = \frac{v^2_F}{32\pi^2 l^2_{\alpha}} \sum_{n,n'=0}^{\infty} \sum_{\lambda,\lambda'=\pm 1} \frac{\mathscr{F}^{\lambda\lambda'}_{n,n'}(T, \mu_{\alpha})}{\omega - \lambda \sqrt{n + \Delta^2_g}\omega^{\alpha}_{c} + \lambda' \sqrt{n'}\omega^{\alpha}_{c}} \left[\frac{2\lambda\lambda'}{\sqrt{nn'}} \partial^2_{\mathscr{Q}_{\alpha}} \tilde{I}^{1}_{n-1,n'-1}(\mathscr{Q}_{\alpha}) \right]. \tag{F.8}$$

The terms $I^{k}_{n,n'}$ and $\tilde{I}^{k}_{n,n'}$ are given by [146]

$$I^{k}_{n,n'}(\mathscr{Q}_{\alpha}) = 2\pi \ell^2_{\alpha} \mathscr{Q}^{(n_> - n_<)}_{\alpha} e^{-\mathscr{Q}_{\alpha}} \frac{(n_< + k)!}{n_>!} L^{(n_> - n_<)}_{n_<}(\mathscr{Q}_{\alpha}) L^{(n_> - n_<)}_{(n_< + k)}(\mathscr{Q}_{\alpha}), \tag{F.9}$$

$$\tilde{I}^{1}_{n-1,n'-1}(\mathscr{Q}_{\alpha}) = \sum_{m=0}^{n-1} \sum_{m'=0}^{n'-1} I^{0}_{m,m'}(\mathscr{Q}_{\alpha}), \tag{F.10}$$

where $\mathscr{Q}_{\alpha} = q^2 l^2_B/2$, $n_< = \min\{n, n'\}$ and $n_> = \max\{n, n'\}$. Clearly both $\tilde{I}^{k}_{n-1,n'-1}(\mathscr{Q}_{\alpha})$ and $I^{k}_{n,n'}(\mathscr{Q}_{\alpha})$ are symmetric in the indices n and n'.

F.1 Sums of Laguerre Polynomials

To evaluate the scalars, Π^0, Π^1 and Π^2 we have to evaluate sums of the form

$$S^b = \sum_{n,n'=0}^{\infty} \sum_{\lambda,\lambda'=\pm 1} \frac{\tanh\left(\frac{\lambda'\sqrt{n'+\Delta_g^2}\omega_c^\alpha-\mu_\alpha}{2T}\right)-\tanh\left(\frac{\lambda\sqrt{n+\Delta_g^2}\omega_c^\alpha-\mu_\alpha}{2T}\right)}{(\omega\pm i0)-\lambda\sqrt{n+\Delta_g^2}\omega_c^\alpha+\lambda'\sqrt{n'+\Delta_g^2}\omega_c^\alpha} T^{k,b}_{n,n'}, \tag{F.11}$$

and of the form

$$S_1^b = \sum_{n,n'=0}^{\infty} \sum_{\lambda,\lambda'=\pm 1} \frac{2\lambda\lambda'}{\sqrt{nn'}} \frac{\tanh\left(\frac{\lambda'\sqrt{n'+\Delta_g^2}\omega_c^\alpha-\mu_\alpha}{2T}\right)-\tanh\left(\frac{\lambda\sqrt{n+\Delta_g^2}\omega_c^\alpha-\mu_\alpha}{2T}\right)}{(\omega\pm i0)-\lambda\sqrt{n+\Delta_g^2}\omega_c^\alpha+\lambda'\sqrt{n'+\Delta_g^2}\omega_c^\alpha} T^{k,b}_{n,n'}, \tag{F.12}$$

where $b = 0, 1, 2$. The $T^{k,b}_{n,n'}$ are terms involving $I^k_{n,n'}$, $\tilde{I}^k_{n,n'}$ present in Π^b . We have,

$$n_F(\xi) = 1/2\left[1-\tanh\left(\frac{\beta}{2}\xi\right)\right] \Rightarrow \tanh\left(\frac{\beta}{2}\xi\right) = 1-2n_F(\xi),$$

where $n_F(\xi)$ is the Fermi-Dirac distribution and in the limit $T \to 0$, n_F becomes a step function and we can write the sum as

$$S^b = 2\sum_{n,n'=0}^{\infty} \sum_{\lambda,\lambda'=\pm 1} \frac{\Theta(\lambda\sqrt{n+\Delta_g^2}\omega_c^\alpha-\mu_\alpha)-\Theta(\lambda'\sqrt{n'+\Delta_g^2}\omega_c^\alpha-\mu_\alpha)}{(\omega\pm i0)-\lambda\sqrt{n+\Delta_g^2}\omega_c^\alpha+\lambda'\sqrt{n'+\Delta_g^2}\omega_c^\alpha} T^{k,b}_{n,n'}. \tag{F.13}$$

Now, depending on whether λ, λ' is $\pm$ we have 4 different possible terms. The chemical potential can be either positive or negative. We begin with the case for positive chemical potential.

F.1.1 Positive Chemical Potential

Evaluating S^b for $\mu_\alpha > 0$ gives

$$\begin{aligned} S^b \;=\; & 2\sum_{n'=0}^{\beta}\sum_{n=\beta+1}^{\infty} \frac{1}{(\omega\pm i0)-\sqrt{n+\Delta_g^2}\omega_c^\alpha+\sqrt{n'+\Delta_g^2}\omega_c^\alpha} T^{k,b}_{n,n'} \\ & -2\sum_{n=0}^{\beta}\sum_{n'=\beta+1}^{\infty} \frac{1}{(\omega\pm i0)-\sqrt{n+\Delta_g^2}\omega_c^\alpha+\sqrt{n'+\Delta_g^2}\omega_c^\alpha} T^{k,b}_{n,n'} \\ & -2\sum_{n=0}^{\infty}\sum_{n'=\beta+1}^{\infty} \frac{1}{(\omega\pm i0)+\sqrt{n+\Delta_g^2}\omega_c^\alpha+\sqrt{n'+\Delta_g^2}\omega_c^\alpha} T^{k,b}_{n,n'} \\ & +2\sum_{n'=0}^{\beta}\sum_{n=\beta+1}^{\infty} \frac{1}{(\omega\pm i0)-\sqrt{n+\Delta_g^2}\omega_c^\alpha-\sqrt{n'+\Delta_g^2}\omega_c^\alpha} T^{k,b}_{n,n'}, \end{aligned} \tag{F.14}$$

with $\beta = \lfloor \frac{\mu_\alpha^2}{(\omega_c^\alpha)^2} \rfloor$.

F.1.2 Negative Chemical Potential

Evaluating for S^b for $\mu_\alpha < 0$ gives

$$\begin{aligned} S^b &= 2\sum_{n=0}^{\infty}\sum_{n'=\beta+1}^{\infty} \frac{1}{(\omega \pm i0) - \sqrt{n+\Delta_g^2}\omega_c^\alpha - \sqrt{n'+\Delta_g^2}\omega_c^\alpha} T^{k,b}_{n,n'} \\ &\quad -2\sum_{n=0}^{\beta}\sum_{n'=0}^{\infty} \frac{1}{(\omega \pm i0) + \sqrt{n+\Delta_g^2}\omega_c^\alpha + \sqrt{n'+\Delta_g^2}\omega_c^\alpha} T^{k,b}_{n,n'} \\ &\quad +2\sum_{n=0}^{\beta}\sum_{n'=\beta+1}^{\infty} \frac{1}{(\omega \pm i0) + \sqrt{n+\Delta_g^2}\omega_c^\alpha - \sqrt{n'+\Delta_g^2}\omega_c^\alpha} T^{k,b}_{n,n'} \\ &\quad -2\sum_{n'=0}^{\beta}\sum_{n=\beta+1}^{\infty} \frac{1}{(\omega \pm i0) + \sqrt{n+\Delta_g^2}\omega_c^\alpha - \sqrt{n'+\Delta_g^2}\omega_c^\alpha} T^{k,b}_{n,n'}. \end{aligned} \tag{F.15}$$

Since the terms $I^k_{n,n'}$ and $\tilde{I}^k_{n,n'}$ are symmetric in n and n', the expressions for the sums are exactly the same for $\mu_\alpha > 0$ and $\mu_\alpha < 0$ if we exchange n and n' which are just dummy variables. We can hence simplify S^b further by combining the terms carefully to get the final expressions as:

$$\begin{aligned} S^b = &\left[2\sum_{n'=0}^{\beta}\sum_{n=\beta+1}^{\infty} \frac{2\sqrt{n+\Delta_g^2}\omega_c^\alpha \left[(\omega)^2 - (n-n')(\omega_c^\alpha)^2\right]}{\omega^4 - \omega^2(\omega_c^\alpha)^2(n+n'+2\Delta_g^2) + (n-n')^2(\omega_c^\alpha)^4} \right] T^{k,b}_{n,n'} \\ &+ \left[2\sum_{n'=\beta+1}^{\infty}\sum_{n=\beta+1}^{\infty} \frac{2\omega_c^\alpha(\sqrt{n+\Delta_g^2} + \sqrt{n'+\Delta_g^2})}{\omega^2 - (\omega_c^\alpha)^2(\sqrt{n+\Delta_g^2} + \sqrt{n'+\Delta_g^2})^2} \right] T^{k,b}_{n,n'}. \end{aligned} \tag{F.16}$$

Our expression for Π^1 [Eq. (F.6)] then becomes:

$$\Pi^1_\alpha = -\frac{v_F^2}{32\pi^2 l_\alpha^4 \omega} S^1. \tag{F.17}$$

In Π^0 and Π^2 [Eq. (F.6)] and [Eq. (F.8)] respectively, we have a multiplicative factor of $\frac{2\lambda\lambda'}{\sqrt{nn'}}$. Taking into account the multiplicative factor we get the sum, S^b_1, over λ, λ' and n, n' to be:

$$S_1^b = \left[-4\sum_{n=0}^{\infty}\sum_{n'=\beta+1}^{\infty}\frac{1}{\sqrt{nn'}}\frac{\omega_c^\alpha(\sqrt{n+\Delta_g^2}+\sqrt{n'+\Delta_g^2})}{\omega^2-(\sqrt{n+\Delta_g^2}+\sqrt{n'+\Delta_g^2})^2(\omega_c^\alpha)^2}\right]T_{n,n'}^{k,b} + \left[4\sum_{n'=0}^{\beta}\sum_{n=\beta+1}^{\infty}\frac{1}{\sqrt{nn'}}\frac{\omega_c^\alpha(\sqrt{n+\Delta_g^2}-\sqrt{n'+\Delta_g^2})}{\omega^2-(\sqrt{n+\Delta_g^2}-\sqrt{n'+\Delta_g^2})^2(\omega_c^\alpha)^2}\right]T_{n,n'}^{k,b}. \quad \text{(F.18)}$$

With this we can write down the expression for Π^0 as,

$$\Pi_\alpha^0 = -\frac{1}{32\pi^2 l_\alpha^4 q^2}[S^0 + S_1^0]. \quad \text{(F.19)}$$

Similarly, Π_2 is given by,

$$\Pi_\alpha^2 = \frac{v_F^2}{32\pi^2 l_\alpha^2}(S_1^2). \quad \text{(F.20)}$$

Appendix G

Excitation Spectra

The numerical results, Fig. 5.2 - 5.8, exhibit a sharp increase of the energy of the low-lying excitations at the largest wavenumbers shown. We consider larger values of ql_B, in which case we can see that the sharp increase is the right edge of the magnetoroton minima, and for larger values of ql_B the dispersion flattens out. This is illustrated in the Fig. G.1

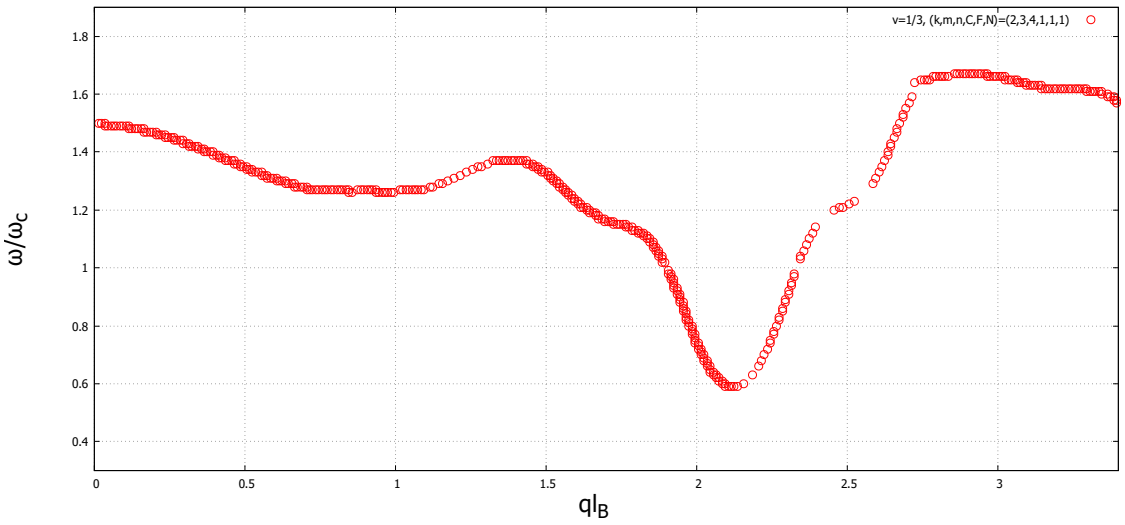

Figure G.1: Location of poles as a function of $\frac{\omega}{\omega_c}$ and ql_B for $\nu = 1/3$ for the parameter set defined in the text $(k, m, n, C, N, F) = (2, 3, 4, 1, 1, 1)$.